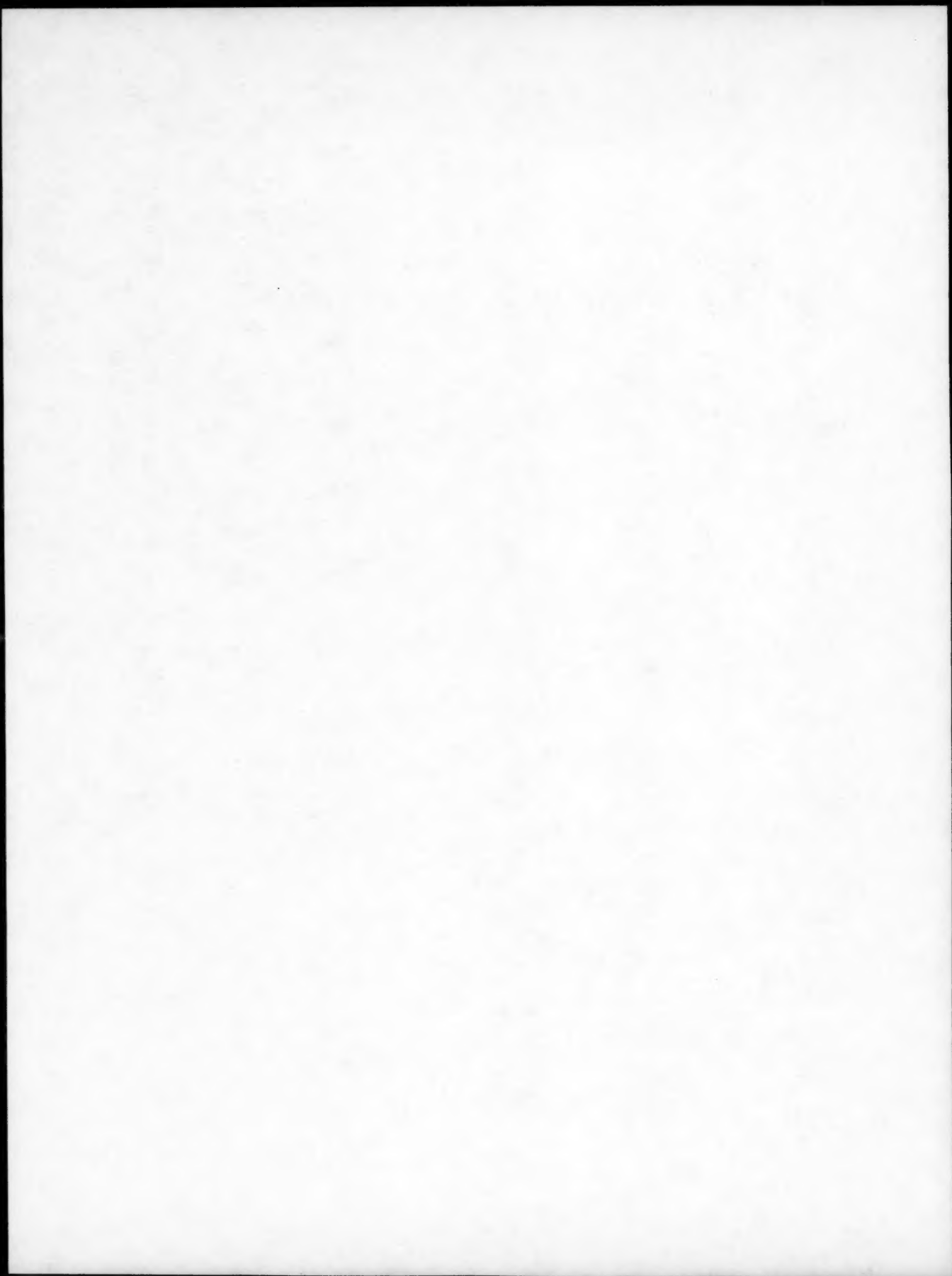


Combined Author Index

- Aaronson, H.I. 427-440A
 Abel Engh, T. 1807-1818A
 Abell, G.C. 83-94B
 Adams, B.L. 177-183A
 1179-1185A
 2611A
 Adler, P.H. 2705-2711A
 Agren, J. 409-416A
 Ahmadzai, H. 303-310B
 Ai, D.K. 571-579B
 Alam, M. 613-616B
 Alavi, A. 543-548A
 Altstetter, C.J. 651-656A
 1187-1192A
 145-152A
 Amemiya, Y. 1973-1980A
 Anand, S. 331-334B
 Andersson, J.-O. 627-636A
 1385-1394A
 47-52B
 Ando, S. 495-504A
 Andresen, P.L. 2665-2669A
 Andrews, J.B. 2645-2650A
 3045-3055A
 Anewalt, M.R. 1645-1656A
 Angers, L.M. 3077-3086A
 Annavarapu, S. 1277-1293A
 Antolovich, S.D. 93-103A
 Anyalebechi, P.N. 227-232B
 Aoki, M. 3077-3086A
 Apelian, D. 213-226B
 Argyropoulos, S.A. 859-870B
 Armstrong, J.H. 473-478A
 Arrott, A.P. 2631-2637A
 Asahi, H. 2171-2177A
 Asaki, Z. 47-52B
 Asaro, R.J. 2179-2206A
 Aust, K.T. 1345-1349A
 1667-1675A
 617-625A
 Austin, L.K. 505-507B
 Awakura, Y. 355-363B
 347-354B
 5-12B
 53-58B
 Ayer, R. 1645-1656A
- Bae, J.C. 2399-2405A
 Baek, K.-K. 1721-1726A
 Baer, D.R. 2005-2011A
 Baifon, J.-P. 2575-2587A
 Baker, C.L. 73-82A
 Baldo, P.M. 2567-2573A
 Baldock, B.R. 375-382B
 Ban-Ya, S. 233-242B
 Banerjee, S. 453-465A
 Banerji, K. 961-971A
 Barbieri, F. 2659-2664A
 2695-2703A
 Barsch, G.R. 761-775A
 Barsous, M.W. 637-644A
 Bartusick, R.D. 563-570B
 Basaviah, M. 2153-2161A
 Baxter, W.J. 2457-2465A
 83-91A
 Beatty, J.H. 1617-1620A
 973-986A
 Bellows, R.S. 479-486A
 Belton, G.R. 959-965B
 Benci, J.E. 837-845A
 Bendersky, L.A. 2893-2900A
 1101-1107A
 Berger, S.A. 571-579B
 Bergman, R.A. 181-186B
 Bernstein, I.M. 2819-2829A
 73-82A
 301-308A
 1437-1443A
 Bhadeshia, H.K.D.H. 669-674A
 1597-1602A
 Bhargava, S. 1205-1211A
 Bhat, M.S. 1751-1760A
 Bhattacharya, R.S. 1372-1374A
 Bianchiello, F.S. 2983-2990A
 Bianchiello, F.S. 1101-1107A
 Biber, H.E. 1603-1608A
 1609-1616A
 Biner, S.B. 829-835A
 Bizen, Y. 383-385A
 Blank, E. 987-998A
 Bobeck, G.E. 2733-2739A
 Boettinger, W.J. 1101-1107A
 Bok, K.A. 1125-1127A
 Bondaryev, E.N. 2407-2413A
 Borofka, J.C. 1841-1847A
 Bose, A. 487-494A
 3100-3103A
 1905-1913A
 2467-2476A
- Bose, D.K. 669-675B
 Bourrell, D.L. 2041-2048A
 1634-1638A
 Bowman, R. 93-103A
 Boyd, J.D. 1221-1234A
 755-764B
 Bradley, J.R. 2013-2025A
 Brakman, C.M. 925-932A
 2415-2426A
 Brannen, J.M. 187-199B
 Brewer, L. 893-917B
 Briant, C.L. 137-143A
 2091-2098A
 2099-2108A
 495-504A
 277-287B
 Brimacombe, J.K. 289-301B
 941-952A
 Brooks, C.R. 409-416A
 Bros, J.P. 2075-2089A
 Brown, C.C. 1425-1427A
 Brown, L.C. 2921-2929A
 Budka, P.Z. 1919-1923A
 Bui, R.T. 171-180B
 Burns, R.J. 1931-1937A
 Burns, W. 477-482B
 Buxbaum, R.E. 1425-1427A
 Byrne, J.G. 1371-1372A
- Cabrera, A.L. 3045-3055A
 Calderon, H.A. 1135-1146A
 Calvo, F.A. 165-170B
 Caram, H.S. 563-570B
 Carlson, O.N. 1429-1435A
 Carpenter, S.H. 473-478A
 Carr, M.J. 3063-3069A
 657-667A
 Cassagne, T.B. 281-292A
 Castillo, R. 2049-2066A
 Caulfield, T. 1841-1847A
 Chai, A.-T. 1895-1899A
 Chan, A.H. 334-336B
 Chan, K.S. 2477-2486A
 Chandier, H.D. 2975-2978A
 Chang, J.W. 1569-1573A
 Chang, Y.A. 441-446A
 Chao, C.G. 1213-1219A
 Charlot, L.A. 2005-2011A
 Chastell, D.J. 1445-1460A
 Chaudhuri, P.C. 547-556B
 Chaudhuri, P.K. 2741-2752A
 Chen, D. 409-416B
 617-622B
 2359-2363A
 Chen, F.-R. 1727-1737A
 Chen, T.-K. 803-817B
 Chen, X.-F. 1319-1334A
 Cheng, C. 73-82A
 Cheng, C. 2567-2573A
 925-932A
 2415-2426A
 Chhabra, R.P. 273-279A
 Chilton, J.P. 709-717B
 Cho, K. 2027-2040A
 Chokshi, A.H. 1621-1624A
 2487-2496A
 Chopra, M.A. 3087-3096A
 Chou, K.-C. 373-376A
 Chou, T.-W. 129-135A
 Chou, Y.T. 1305-1309A
 Chu, C.W. 2639-2643A
 Chu, W.-Y. 1335-1343A
 1067-1073A
 Chung, K. 293-300A
 Chung, Y.W. 337-344A
 Cieslak, M.J. 2319-2331A
 3063-3069A
 35-50A
 657-667A
 319-329B
 893-917B
 763-787A
 1761-1766A
 732-733A
 Clothier, G.W. 493-503B
 Clough, R.B. 1657-1666A
 Collier, J.P. 1657-1666A
 1221-1234A
 Collins, L.E. 329-335A
 Collins, T.H. 967-972B
 Collur, M.M. 709-717B
 Cooke, A.V. 2133-2138A
 Copley, S.M. 709-721A
 Cornie, J.A. 2979-2987A
 Cortie, M.B. 1027-1035A
 Couper, M.J. 2179-2206A
 Couque, H. 517-526A
 Courtney, T.H. 2163-2170A
 Covino, B.S., Jr. 329-335A
 Crall, L.A.
- Curren, P. 1899-1904A
 Curren, P.A. 2665-2669A
 2671-2678A
 2839-2846A
 2645-2650A
- Daeubler, M.A. 301-308A
 Danley, T.J. 2619-2623A
 Dantzig, J.A. 2589-2602A
 Daryl, M.P. 909-913A
 Das, R.P. 331-334B
 Das, S. 1365-1367A
 Das, S.C. 823-830B
 331-334B
 427-432B
 Davenport, W.G. 2867-2874A
 Davis, R.M. 909-913A
 Dayan, D. 169-175A
 de Fontaine, D. 483-491B
 Debroy, T. 613-616B
 851-858B
 967-972B
 2651-2658A
 207-216A
 Desmond, J. 159-167A
 Dewandre, T. 1925-1929A
 Dey, D.N. 514-518B
 2839-2846A
 2847-2853A
 Dhindaw, B.K. 1899-1904A
 2575-2587A
 873-880A
 Dixon, G. 1127-1128A
 Dogan, B. 505-516A
 1221-1234A
 5-12B
 1445-1460A
 Dollar, M. 675-686A
 Dolling, G. 2207-2214A
 Domingo, S. 933-940A
 Donepudi, V.S. 3071-3075A
 Dong, Y. 409-418B
 Dorward, R.C. 1631-1634A
 Dube, R.K. 1205-1211A
 Dubke, M. 581-593B
 595-602B
 2179-2206A
 311-317B
 Dupre, B. 1773-1783A
 Dutkiewicz, J. 1853-1860A
 Dutrizac, J.E. 803-817B
 187-199B
- Edwards, G.R. 95-101B
 Ehrlich, F.R. 329-335A
 Ekimoto, T. 235-242A
 El-Kaddah, N. 765-775B
 831-837B
 787-802B
 El Moujahid, S. 663-668B
 Eliezer, D. 723-730A
 Elliott, J.F. 699-908A
 935-941B
 745-754B
 Engh, T.A. 427-440A
 Enomoto, M. 1807-1818A
 541-546B
 Espinola, A. 663-668B
 Essadiqi, E. 417-426A
 Et-Tabirou, M. 311-317B
 Evans, J.W. 397-408B
- Farooq, S. 1905-1913A
 Farouk, B. 123-226B
 Faucher, B. 505-516A
 Fernando, L.A. 1083-1100A
 Ferro, A.C. 1147-1151A
 Fine, M.E. 1135-1146A
 337-344A
 1051-1059A
 185-191A
 193-198A
 199-205A
 677-684B
 Finlayson, T.R. 1395-1401A
 281-292A
 2067-2074A
 2805-2817A
 1109-1119A
 709-721A
 Finlayson, T.R. 1445-1460A
 2399-2405A
 Fong, C. 2753-2764A
 2765-2773A
 255-259B
- Fleming, H.G. 2607-2074A
 Flemings, M.C. 1109-1119A
 709-721A
 Flewitt, P.E.J. 1445-1460A
 Finn, J.E. 2399-2405A
 Fong, C. 2753-2764A
 2765-2773A
 255-259B
- Fortes, M.A. 1147-1151A
 Franck, R.E. 2363-2366A
 Frank, F.C. 403-408A
 Fras, E. 1367-1369A
 1235-1241A
 709-717B
 731-732A
 23-33A
 1372-1374A
 2215-2224A
 261-268B
 419-425B
 334-336B
 643-648B
 319-329B
 2723-2731A
 2931-2936A
 803-810A
 1269-1275A
 987-998A
- Frolich, S. 1372-1374A
 Fruehan, R.J. 2215-2224A
 261-268B
 419-425B
 334-336B
 643-648B
 319-329B
 2723-2731A
 2931-2936A
 803-810A
 1269-1275A
 987-998A
- Fuerschbach, P.W. 1372-1374A
 Fujita, F.E. 2723-2731A
 2931-2936A
 803-810A
 1269-1275A
 987-998A
- Fukaya, K. 1372-1374A
 Funk, W. 2723-2731A
 2931-2936A
 803-810A
 1269-1275A
 987-998A
- Gambino, M. 409-416A
 Gao, M. 1739-1750A
 Garcia-Zayas, J. 541-546B
 Garrett, G.G. 2979-2987A
 3103-3107A
 Garrison, W.M., Jr. 2989-3003A
 1751-1760A
 623-626B
 Gaune-Escard, M. 409-416A
 2075-2089A
 2901-2909A
 887-892A
 George, E.P. 1319-1334A
 Gerberich, W.W. 487-494A
 German, R.M. 1523-1532A
 3100-3103A
 1905-1913A
 2467-2476A
 839-850B
 885-892B
 311-317B
 1945-1953A
 3067-3096A
 1243-1255A
 823-830B
 2123-2131A
 2153-2161A
- Ghosh, A. 165-170B
 2695-2703A
 1925-1929A
 227-232B
 777-785B
 919-925B
 141-146B
 734-738A
 738-743A
 1895-1899A
 Grimsey, E.J. 243-247B
 Grugel, R.N. 2677-2680A
 Grummon, D.S. 2775-2788A
 Guilemany, J.M. 165-170B
 Gungor, M.N. 2215-2224A
 Gupta, C.K. 669-675B
 Gurland, J. 2027-2040A
 Gustafson, P. 2531-2546A
 2547-2554A
 Guthrie, R.I.L. 507-511B
 Guzik, E. 1235-1241A
 Guzowski, M.M. 385-387A
- Hack, G.A.J. 723A
 Hagni, R.D. 719-729B
 Hahn, G.T. 2067-2074A
 Hahn, R.C. 1945-1953A
 Hahn, Y.B. 871-884B
 Hajra, J.P. 649-654B
 Hamano, R. 1461-1469A
 Hammarlund, G.R. 2619-2623A
 409-418B
 Han, Q. 617-622B
 2989-3003A
 Hansen, G.P. 1889-1894A
 1939-1943A
 Hardy, D.J. 187-199B
 Hardy, S.C. 2713-2721A
 Harprashad, B. 517-526A
 Harvey, D.P., II 1547-1553A
 Hashimoto, M. 2789-2798A
 Hashizume, H. 1973-1980A
 Hassam, S. 409-416A
 2075-2089A
 Hauge, R.H. 1889-1894A
 1939-1943A
 2363-2366A
 217-223A
- Haw, X.C. 217-223A

Headley, T.J. Hellowell, A.	2319-2331A 3097-3100A 1861-1871A	Kato, E. Kattner, U.R. Kaukler, W.F.	511-513B 2389-2397A 2625-2630A	Lewandowski, J.J. Li, B.Q. Li, H.	3005-3011A 397-408B 383-395B	Meubus, P. Meyn, D. Michael, J.R.	927-933B 1626-1631A 953-959A
Hendrickson, A.A. Hendrix, B.C. Higashiyama, H. Hills, C.R. Himbeault, D.D. Hipsley, C.A. Hirabayashi, M. Hirato, T. Hiskey, J.B. Hoch, M. Hoffeiner, W. Holden, T.M. Holt, R.A. Homonnay, Z. Hon, M.H. Hong, J.W. Horikawa, H. Howe, J.M. Howell, P.R. Hsiao, C.-M.	1471-1480A 1841-1847A 2171-2177A 3063-3069A 2109-2113A 3005-3011A 797-801A 355-363B 943-949B 2075-2089A 855-862A 2207-2214A 2207-2214A 259-264A 1213-1219A 121-127A 915-923A 2911-2920A 51-66A 1335-1343A 1067-1073A	Kawahara, M. Kawasaki, Y. Kelly, J.E. Kelly, T.F. Kenyon, J. Kestenbach, H.-J. Khachatryan, A.G. Kikuchi, M. Kim, C. Kim, C.H. Kim, D. Kim, J.-S. Kim, S. Kim, Y.G. Kim, Y.J. Kim, Y.W.	181-186B 505-507B 2589-2602A 2399-2405A 783-787A 387-389A 249-258A 645-650A 1263-1268A 309-317A 973-975B 1721-1726A 999-1007A 2013-2025A 1625-1626A 1849-1852A 2041-2048A 1634-1638A 2359-2363A 677-684B 2567-2573A	Li, P. Li, P.L. Li, Z. Liaw, P.K. Lichter, B.D. Lim, C.Y. Lin, C.I. Lin, D. Lin, H.R. Lin, J.-C. Lindsey, T.F. Lippold, J.C. Liszka, A. Liu, D. Liu, W.J. Liu, Z.	2133-2138A 2139-2151A 887-892A 2445-2455A 2215-2224A 2233-2246A 2677-2680A 281-292A 1625-1626A 685-686B 2225-2231A 1471-1480A 441-446A 249-258A 35-50A 1367-1369A 1667-1675A 1403-1413A 1415-1424A 1121-1125A 527-542A	Miyamoto, Y. Miyazaki, S. Moffat, D.L. Mohamed, F.A. Moitra, A. Moore, J.J. Moreau, R.J. Mori, H. Mori, N. Morik, K. Morli, Y. Morris, J.W., Jr. Morris, P.R. Mortensen, A. Morton, A.J. Mott, G. Mou, Y. Mueller, R.R. Muir, D.M. Mukherjee, A.K.	1269-1275A 915-923A 1677-1686 1687-1694A 2389-2397A 2741-2752A 2847-2855A 1899-1904A 1295-1304A 737-744B 1257-1262A 467-471A 915-923A 793-796A 249-258A 1563-1568A 2611A 709-721A 199-205A 2233-2246A 1695-1701A 1645-1656A 37-45B 821-827A 1621-1624A 453-465A 2921-2929A
Iaccoca, R.G. Ichinose, S. Ignatiev, A. Iguchi, Y. Iino, Y. Iizumi, M. Ijiri, Y. Ilegbusi, O.J. Inoue, A.	2305-2313A 915-923A 2639-2643A 233-242B 2603-2605A 793-796A 2215-2224A 557-562B 383-385A 391-393A 1369-1371A 235-242A 2315-2318A 233-242B 419-425B 643-648B 345-352A 353-357A	Klimek, R.B. Klimker, H. Knorr, D.B. Kobayashi, M. Kobayashi, T. Koch, C.C. Kohali-Aval, J. Kollie, T. Kondo, Y.	1931-1937A 909-913A 1009-1020A 13-24B 25-36B 319-327A 2867-2874A 1481-1490A 2319-2331A 1269-1275A 47-52B	Louat, N. Lui, T.S. Luo, C.P. Luo, H.L. Luthra, K.L. Lynch, D.C.	187-199B 1583-1596A 1955-1963A 1965-1971A 505-507B 345-363B 347-354B 5-12B 53-58B	Mukhopadhyay, P. Mukunthan, K. Murgas, L. Murray, J.L. Murthy, A. Murthy, B.V.R. Murty, K.L. Muto, S.	2921-2929A 259-264A 243-247A 765-775B 514-518B 1243-1255A 2723-2731A 2931-2936A
Ishii, F. Ito, K.	419-425B 643-648B	Koo, Y.C. Koontz, J.S. Korevaar, B.M.	1345-1349A 1179-1185A 925-932A	Mackinnon, D.J. Magdowski, R.M. Magnin, P.	187-199B 1583-1596A 1955-1963A 1965-1971A 505-507B		
Izumi, O.	345-352A 353-357A	Korth, G.E. Koss, D.A. Kou, S.	2399-2405A 1767-1773A 1849-1852A 1075-1082A	Majima, H.	345-363B 347-354B 5-12B 53-58B		
Jackson, A.G. Jacob, K.T.	23-33A 465-470B 269-275B 459-463B	Kouli, A.K. Koursaris, A. Krauss, G. Krishna Murthy, G.G.	2049-2066A 2287-2298A 579-589A 839-850B 885-892B	Makabe, C. Makino, H. Makita, T. Malcolm, R.C. Marchand, N.J. Marder, A.R. Margolin, H.	1257-1262A 2603-2606A 793-796A 731-732A 2575-2587A 1193-1203A 1163-1171A 1575-1581A 591-601A 1727-1737A 2503-2512A 1311-1317A 1899-1894A 1939-1943A 627-641B 95-101B 345-352A 353-357A 355-363B 5-12A	Nachtrab, W.T. Nagamori, M. Nagasaka, T. Nagasawa, A. Nagy, S. Nair, K.U. Nakagawa, T. Nakai, Y. Nakajima, H. Nakajima, Y. Nakanishi, N. Nakase, K. Nam, S.W. Nandapurkar, P. Narendmath, K.R.	1305-1309A 547-556B 233-242B 793-796A 259-264A 669-675B 265-271A 543-548A 507-511B 2603-2606A 793-796A 2819-2829A 121-127A 3057-3061A 1163-1171A 2503-2512A
Jacobson, T. Jata, K.V.	1883-1888A 847-854A 973-986A 1051-1059A 331-334B 514-518B	Krishnamurthy, S. Krishnan, S. Kruger, R.M. Krumhansl, J.A. Krzyszowski, J.E.	1889-1894A 1939-1943A 2555-2566A 761-775A 1873-1876A	Margrave, J.L.	1899-1894A 1939-1943A 627-641B 95-101B 345-352A 353-357A 355-363B 5-12A	Nazmy, M. Nee, C.C. Nelson, D.V. Nickel, H. Niedringhaus, J.C.	855-862A 1569-1573A 2497-2502A 359-371A 261-268B
Jensen, C.L. Jeong, W.C. Jiang, C.	893-898A 309-317A 734-738A 736-743A 427-432B	Kullen, P.S. Kumar, A. Kundrat, D.M. Kunitomi, K. Kurz, W.	881-885A 1021-1026A 899-908A 1269-1275A 1955-1963A 1965-1971A 377-382A 59-65B	Marschman, S.C. Martinez, L. Martins, G.P. Masahashi, N.	675-686A 643-648B 383-385A 391-393A 1369-1371A 235-242A 2315-2318A 579-589A 507-511B 1703-1709A 1981-1990A	Nie, T.G. Nikbin, K.M. Nilmani, M. Nishijima, M. Nix, W.D. Noda, Y. Norman, P.D. Norman, P.J. Notis, M.R. Núñez, C.	1173-1178A 873-880A 83-94B 2603-2606A 3013-3024A 265-271A 199-205A 1445-1460A 1193-1203A 2937-2944A 933-940A 365-373B 541-546B 511-513B
Jiang, X.H. Jiao, Q. Jimbo, I. Jin, I. Johansen, S.T.	133-140B 623-626B 3107-3109A 745-754B 755-764B	Kusiński, J. Küzeci, E. Kwon, H.	1975-1971A 377-382A 59-65B 2606-2611A	Mashima, M. Massalski, T.B.	507-589A 507-511B 1703-1709A 1981-1990A	Nunoue, S.-Y.	
Johnson, H.H.	2371-2387A 691-707B	Lai, C.-L. Lake, J.S.H. Lan, Y.	1895-1898A 2805-2817A 2225-2231A	Matlock, D.K. Mazumdar, D. Mazumder, J.	579-589A 507-511B 1703-1709A 1981-1990A		
Johnson, J.A. Johnson, M.J. Johnson, D. Jonas, J.J.	1931-1937A 1187-1192A 3071-3075A 417-426A 1403-1413A 1415-1424A 105-120A 23-33A	Landsberg, A. Langdon, T.G. Lange, N. Lange, W.F., III Larbalestier, D.C.	477-482B 2487-2496A 1385-1394A 427-440A 1677-1686A 1687-1694A 2789-2798A 2799-2803A	McAlister, A.J. McCarron, T.J. McCartney, D.G. McClanahan, E.D. McConnell, C. McDermott, B. McDowell, D.L. McIntyre, N.S. McKinney, T.R. McLean, A. McNallan, M.J.	2893-2900A 2067-2074A 385-387A 5-12A 159-167A 2867-2874A 1277-1293A 3071-3075A 83-91A 383-395B 483-491B 2567-2573A		
Jones, H. Jones, J.W. Jones, R.H.	2775-2788A 2005-2011A	Latansision, R.M.	2606-2611A 1677-1686A 1687-1694A 2789-2798A 2799-2803A	Medina, L.F. Mehrabian, R. Mehrotra, S.P.	663-668B 493-503B 839-850B 885-892B 734-738A 889-743A		
Kacar, A.S. Kacar, S.A. Kaczorowski, M. Kain, K.E.	1833-1839A 2847-2855A 1319-1334A 2067-2074A	Lawley, A. Laxmanan, V.	3077-3086A 2651-2658A 2687-2694A 1075-1082A	Mei, Y.	811-816A 2619-2623A 2299-2304A		
Kaiser, D.L. Kajihara, M. Kaiman, Z.H. Kalmelan, H.	935-941B 645-650A 217-223A 13-24B	Le, Y. Lecomte-Beckers, J.	2333-2340A 2341-2348A 2911-2920A 2671-2678A 329-335A 517-526A	Mesli, M.	811-816A 2619-2623A 2299-2304A		
Kammel, R.	25-36B 59-65B 67-72B	Lee, K.B. Lee, L.H. Lee, M.-C. Lee, S.H. Lee, W.J. Lee, W.M.	2606-2611A 217-223A 2115-2117A 2179-2206A 337-344A 255-259B	Mendelson, S. Merkley, D.R. Meshil, M.	811-816A 2619-2623A 2299-2304A		
Kane, J.S.	341-345B 1257-1262A 1833-1839A Kao, H.P. Karagöz, S. Karwacki, E.J. Katagiri, K.	25-36B 59-65B 67-72B 1379-1383A 341-345B 1257-1262A 1833-1839A Kao, H.P. Karagöz, S. Karwacki, E.J. Katagiri, K.	255-259B 789-792A 1703-1709A 105-120A 687-697A 699-708A	Mendelson, S. Merkley, D.R. Meshil, M.	811-816A 2619-2623A 2299-2304A		



Combined Subject Index

- Abatement (pollution)**
See Pollution abatement
- Aberration**
See Distortion
- Absolute viscosity**
See Viscosity
- Absorption (material)**
See also Hydrogen storage
Kinetics of Hydrogen Absorption in Alpha Titanium. 1425-1427A
- Acceleration measurement**
See Accelerometers
- Accelerometers**
Making Acceleration Data More Accessible and Useful to Microgravity Investigators. 2631-2637A
- Acid cleaning**
See Pickling
- Acid leaching**
Kinetics of Nonoxidative Leaching of Galena in Perchloric, Hydrobromic, and Hydrochloric Acid Solutions. 541-548B
- Acid pickling**
See Pickling
- Acids (inorganic)**
See Inorganic acids
- Acoustic emission**
Acoustic Emission Studies of Electron Beam Surface Modification of Aluminum. 493-503B
Determination of Fracture Initiation in Hydride Blisters Using Acoustic Emission. 2247-2257A
- Actinide metal alloys**
See Plutonium base alloys
Uranium base alloys
- Actinide metal compounds**
See Plutonium compounds
- Actinide metals**
See Plutonium
Uranium
- Activated carbon**
The Behavior of Thiourea and Flotation Reagents in Zinc Electrowinning Circuits. 187-199B
- Activated charcoal**
See Activated carbon
- Activation energy**
Kinetics of Domain Growth in Ordered Ni_3Mo . 941-952A
Literature Survey on Diffusivities of Oxygen, Aluminum, and Vanadium in Alpha Titanium, Beta Titanium, and in Rutile. 1121-1125A
Thermodynamics and Kinetics of $\delta \rightarrow \alpha$ Martensitic Transformation in Plutonium Alloys. 2705-2711A
The Thermal Activation Energy for Fatigue of Fe-1Cr-0.5Mo. 2979-2987A
- Activity (chemical)**
The Effect of Temperature on Nickel Solubility in Silica Saturated Fayalite Slags From 1523-1623K. 243-247B
The Sulfur Partition Ratio and the Sulfide Capacity of $\text{Na}_2\text{O}-\text{SiO}_2$ Slags at 1400°C. 334-338B
Water and Solute Activities of the Solution Systems of $\text{H}_2\text{SO}_4-\text{CuSO}_4-\text{H}_2\text{O}$ and $\text{HCl}-\text{CuCl}_2-\text{H}_2\text{O}$. 347-354B
A New Treatment for Determining the Activities From Ternary Miscibility Gap: the O-Cu-Pb System. 373-376A
The Influence of the Ternary Interaction Parameter $\epsilon_{\text{AB}}^{\text{C}}$ on the Activity of Bismuth in Molten Copper. 427-432B
Thermodynamics of Molten Li-Sn Alloys. 637-644A
- Activity (chemical), Alloying effects**
Activity of Carbon in Nickel-Rich Ni-Mo and Ni-W Alloys. 645-650A
- Activity coefficients**
See Activity (chemical)
- Additives**
See Master alloys
- Age hardening**
See Precipitation hardening
- Age hardening steels**
See Precipitation hardening steels
- Agents**
See Catalysts
- Agglomerating**
See Agglomeration
- Agglomeration**
Behavior of Ceramic Particles at the Solid/Liquid Metal Interface in Metal Matrix Composites. 2847-2855A
- Agglomeration, Field effects**
Melting and Solidification in Microgravity of Sintered Aluminum Powder Alloys. 2695-2703A
- Aggregation**
See Agglomeration
- Aging**
See also Aging (artificial)
Quench aging
- The Effect of Aging on the Fracture Behavior of Cu-Al-Ni β Phase Alloys. 1761-1766A
The Tempering of Iron-Carbon Martensite; Dilatometric and Calorimetric Analysis. 2415-2426A
- Aging (artificial)**
Effect of Single Aging on Stress Corrosion Cracking Susceptibility of Inconel X-750 Under PWR Conditions. 1295-1304A
Correlation Among Microstructure, Strength, and Electrical Conductivity of Cu-Ni-Be Alloy. 2279-2285A
On the Morphology of the Modulated Precipitation of Extended Multiplets and Fe_3C_4 Epsilon or Eta Carbide Obtained by Aging and Tempering in Fe-C Martensite. 2901-2909A
Structure and Deformation Behavior of T_1 Precipitate Plates in an Al-2Li-1Cu Alloy. 2311-2320A
Effects of SiC Whiskers and Particles on Precipitation in Aluminum Matrix Composites. 2945-2953A
Structure and Properties of a Near- α Titanium Alloy After β Solution Treatment and Aging at 625°C. 3025-3033A
- Agitation**
See Electromagnetic stirring
- Aircraft components, Materials selection**
Use of Ion Scattering in Characterizing the Surface Oxide of P/M Aluminum Alloy 7091. 1372-1374A
- Aircraft equipment**
See Aircraft components
- Alkali metal compounds**
See Lithium compounds
Sodium compounds
- Alkali metals**
See Cesium
Lithium
Potassium
Sodium
- Alkaline earth metal alloys**
See Strontium
- Alkaline earth metal compounds**
See Calcium compounds
Lime
- Alkaline earth metals**
See Beryllium
Calcium
Magnesium
Strontium
- Alloy plating**
See also Brass plating
Pulsed Electrodeposition of Layered Brass Structures. 1569-1573A
- Alloy powders, Crystal growth**
Thermal Considerations on the Recalescence of Alloy Powders. 687-697A
- Alloy powders, Synthesis**
Formation of Ultra-Fine Amorphous Powders in Fe-M-B (M = Transition Metal) Systems by Chemical Reduction Method and Their Thermal and Magnetic Properties. 2315-2318A
- Alloy steels**
See also Austenitic stainless steels
Carbon manganese steels
Chromium molybdenum steels
Chromium molybdenum vanadium steels
Chromium steels
Duplex stainless steels
Electrical steels
Ferritic stainless steels
High strength low alloy steels
High strength steels
Low alloy steels
Manganese steels
Maraging steels
Molybdenum steels
Nickel chromium molybdenum steels
Nickel chromium steels
Nickel steels
Precipitation hardening steels
Stainless steels
Titanium steels
Vanadium steels
- Alloy steels, Mechanical properties**
Modeling Tensile Deformation of Dual-Phase Steel. 1263-1268A
- Alloying**
See Mechanical alloying
- Alloys**
See Alloy steels
Bearing alloys
Dispersion hardening alloys
Ferrous alloys
Master alloys
Precipitation hardening alloys
Shape memory alloys
Superalloys
- Alodine process**
See Chromating

Alpha annealing

Alpha annealing See Annealing

Alphatizing See Annealing

Alumina See Aluminum oxide

Aluminum, Alloying elements

- The Effect of Varying Aluminum, Titanium, and Niobium Content on the Phase Stability of Inconel 718. 1657-1666A
- Correction to "The Effects of Varying Aluminum, Titanium, and Niobium Content on the Phase Stability of Inconel 718". An Approach to Developing an Alternative Hot Work Die Steel. 1657-1666A
- Fatigue Damage Accumulation in Nickel Modified by Ion Beam Surface Microalloying. 1751-1760A
- A Preliminary Study of the Influence of Separate and Combined Aluminum and Nickel Additions on the Properties of a Secondary Hardening Steel. 2775-2788A
- 3103-3107A

Aluminum, Binary systems

- Calculation of the Titanium—Aluminum Phase Diagram. 243-247A
- The Cata- or Metatectic Reaction—Occurrence and Microstructural Development. 3097-3100A

Aluminum, Casting

- Performance Analysis of the Aluminum Casting Furnace. Mathematical Modeling of Meniscus Profile and Melt Flow in Electromagnetic Casters. 171-180B
- A Simple Fluid Mechanical Model for Planar Flow Casting Melt-Spinning. 397-408B
- 571-579B

Aluminum, Composite materials

- Modeling of Infiltration Kinetics for Liquid Metal Processing of Composites. 95-101B
- Transverse Elastic Moduli of Unidirectional Fiber Composites With Interfacial Debonding. 129-135A

Aluminum, Corrosion

- Effect of Cathodic Charging on the Mechanical Properties of Aluminum. 2299-2304A

Aluminum, Diffusion

- Prediction of Solute Diffusion Coefficients in Liquid Metals. Literature Survey on Diffusivities of Oxygen, Aluminum, and Vanadium in Alpha Titanium, Beta Titanium, and in Rutile. 273-279A
- Thermodynamics of Segregation in Alloys. 1121-1125A
- 2091-2098A

Aluminum, Extraction

- The Mathematical Modeling Revolution in Extractive Metallurgy. 525-540B

Aluminum, Heat treatment

- Acoustic Emission Studies of Electron Beam Surface Modification of Aluminum. 493-503B

Aluminum, Impurities

- The Effects of Mg^{2+} , Mn^{2+} , Zn^{2+} , and Al^{3+} on the Nickel Deposit During Electrowinning From Sulfate Bath. 823-830B

Aluminum, Mechanical properties

- Modeling of the Plastic Anisotropy of Textured Sheet. 105-120A

Aluminum, Melting

- Discussion of "The Role of Boron in the Grain Refinement of Aluminum With Titanium" and Authors' Reply. 385-387A

Aluminum, Powder technology

- Thermal Considerations on the Recalescence of Alloy Powders. 687-697A
- The Evolution of Microcrystalline Structures in Supercooled Metal Powders. 699-708A

Aluminum, Quaternary systems

- Solidus and Solvus Isotherms for Quaternary Al—Li—Cu—Mg Alloys. 1631-1634A

Aluminum, Reactions (chemical)

- Reactivity of Al—2.5% Li Alloy With Water as Studied by the Exploding Wire Technique. 255-259B
- Reaction Mechanism for the CaO —Al and CaO — CaF_2 Desulfurization of Carbon-Saturated Iron. 261-268B

Aluminum, Reduction (chemical)

- The Moreau—Evans Hydrodynamic Model Applied to Actual Hall—Héroult Cells. 737-744B

Aluminum, Solubility

- On the Solubility of Aluminum in Cryolitic Melts. 449-457B

Aluminum, Thermal properties

- Convective Heat-Transfer Measurements in Liquid Metals Under Different Fluid Flow Conditions. 859-870B

Aluminum base alloys, Alloy development

- Materials for Advanced Studies and Devices. 155-164B
- Ductile Al—Cu—V Amorphous Alloys Without Metalloid. 391-393A
- Materials for Advanced Studies and Devices. 749-758A
- Design and Development of an Experimental Wrought Aluminum Alloy for Use at Elevated Temperatures. 1027-1035A

Aluminum base alloys, Casting

- Characterization of the Aging Response of a Melt-Spun Al—Be—Li Alloy Ribbon. 1173-1178A
- Formation of Metal—Metal Type Aluminum-Based Amorphous Alloys. 1369-1371A

Aluminum base alloys, Composite materials

- Modeling of Infiltration Kinetics for Liquid Metal Processing of Composites. 95-101B
- Columnar Dendritic Solidification in a Metal-Matrix Composite. 709-721A
- Some Observations on the Matrix Microstructure of Aluminum—Silicon Alloy—Graphite Particle Composites. 1365-1367A

- Erosion of Fiber Reinforced Al—4% Cu Composites. 1785-1793A
- Directional Solidification of Al—Ni/SiC Composites During Parabolic Trajectories. 1899-1904A
- Correlation of Mechanical and Ultrasonic Properties of Al—SiC Metal-Matrix Composite. 2233-2246A
- Behavior of Ceramic Particles at the Solid/Liquid Metal Interface in Metal Matrix Composites. 2847-2855A
- Effects of SiC Whiskers and Particles on Precipitation in Aluminum Matrix Composites. 2945-2953A
- A Method of Assessing the Reactivity Between SiC and Molten Aluminum. 3107-3109A

Aluminum base alloys, Crystal growth

- On the Formation of Dispersoids During Rapid Solidification of an Al—Fe—Ni Alloy. 1101-1107A

Aluminum base alloys, Crystal lattices

- Electron Diffraction Study of α - and α' -AlFeSi. 893-898A
- A Finite Element Model of a Persistent Slip Band Based Upon Electron Microscopic Evidence. 2457-2465A

Aluminum base alloys, Directional solidification

- Dendritic Solidification of Alloys in Low Gravity. 2671-2676A
- Influence of Microgravity on the Morphology of the Directionally Solidified Front in an AlSi Alloy. 2681-2686A

Aluminum base alloys, Heat treatment

- Acoustic Emission Studies of Electron Beam Surface Modification of Aluminum. 493-503B

Aluminum base alloys, Mechanical properties

- Growth of Slip Bands During Fatigue of 6061-T6 Aluminum. 83-91A
- Fatigue Crack Propagation in Aluminum—Lithium Alloy 2090. I. Long Crack Behavior. 549-561A
- Fatigue Crack Propagation in Aluminum—Lithium Alloy 2090. II. Small Crack Behavior. 563-569A
- On Through Thickness Crystallographic Texture Gradient in Al—Li—Cu—Zr Alloy. 731-732A
- Creep Crack Growth Behavior of Two Al—Li Alloys. 847-854A
- A Topological Study of Superplastic Deformation in an Al—Li Alloy With a Bimodal Grain Size Distribution. 1621-1624A
- Chemical and Metallurgical Aspects of Environmentally Assisted Fatigue Crack Growth in 7075-T651 Aluminum Alloy. 1739-1750A
- The Role of Hydrogen in Corrosion Fatigue of High Purity Al—Zn—Mg Exposed to Water Vapor. 1775-1783A
- Yield Stress as Determined From Hardness Measurements for Mechanically Alloyed Aluminum Base Alloys. 2363-2366A
- The Mechanical Properties of the Superplastic Al—33Cu Eutectic Alloy. 2487-2496A
- Microstructure—Property Relationship in a 2XXX Aluminum Alloy With Magnesium Addition. 2523-2530A
- The Absence of Steady-State Flow During Large Strain Plastic Deformation of Some FCC Metals at Low and Intermediate Temperatures. 3013-3024A

Aluminum base alloys, Melting

- Melting and Solidification in Microgravity of Sintered Aluminum Powder Alloys. 2695-2703A

Aluminum base alloys, Microstructure

- Modeling of Thermomechanical Processing of Heat-Treatable Aluminum Alloys. 617-625A

Aluminum base alloys, Phase transformations

- Phase Transformation During Annealing of Rapidly Solidified Aluminum-Rich Al—Fe—Si Alloys. 2893-2900A

Aluminum base alloys, Phases (state of matter)

- Quasicrystalline Phase in Al—Si—Mn System Prepared by Annealing of Amorphous Phase. 383-385A
- Microstructural Characterization of the Dispersed Phases in Al—Ce—Fe System. 1645-1656A

Aluminum base alloys, Powder technology

- Aluminum—Lithium Powder Metallurgy Alloys With Improved Toughness. 603-615A
- Thermal Considerations on the Recalescence of Alloy Powders. 687-697A
- Use of Ion Scattering in Characterizing the Surface Oxide of P/M Aluminum Alloy 7091. 1372-1374A

Aluminum base alloys, Reactions (chemical)

- Reactivity of Al—2.5% Li Alloy With Water as Studied by the Exploding Wire Technique. 255-259B
- The Reaction Between Solid Iron and Liquid Al—Zn Baths. 1193-1203A

Aluminum base alloys, Solubility

- The Solubility of Hydrogen in Liquid Binary Al—Li Alloys. 227-232B
- Volume Effects and Associations in Liquid Alloys. 465-470B

Aluminum base alloys, Structural hardening

- The Aging Characteristics of an Al—2% Li—3% Cu—0.12% Zr Alloy at 190°C. 51-66A
- Theoretical Investigation of the Precipitation of δ' in Al—Li. 249-258A
- Investigation of Phase Transformation in an Al—0.58 wt. % Fe Alloy by Mossbauer Spectroscopy. 259-264A
- Growth and Coarsening of G.P. Zones in Al—Zn Alloys. 1973-1980A
- Precipitation of Guinier—Preston Zones in Aluminum—Magnesium; a Calorimetric Analysis of Liquid-Quenched and Solid-Quenched Alloys. 2433-2443A
- Structure and Deformation Behavior of T_1 Precipitate Plates in an Al—2Li—1Cu Alloy. 2911-2920A

Aluminum base alloys, Welding

- On the Weldability, Composition, and Hardness of Pulsed and Continuous Nd:YAG Laser Welds in Aluminum Alloys 6061, 5456, and 5086. 319-329B
- Effects of Oxygen and Sulfur on Alloying Element Vaporization Rates During Laser Welding. 967-972B
- Welding Parameters and the Grain Structure of Weld Metal—a Thermodynamic Consideration. 1075-1082A

Aluminum compounds

See also Aluminum oxide

- Aluminum compounds, Crystal lattices**
The Apparent "Five-Fold" Nature of Large T_2 (Al_6Li_3Cu) Crystals. 2875-2884A
Convergent Beam Electron Diffraction Analysis of the T_1 (Al_2CuLi) Phase in $Al-Li-Cu$ Alloys. 2885-2891B
- Aluminum compounds, Mechanical properties**
High Temperature Strength and Ductility of Recrystallized Ni_3Al-Ni_3Mn Alloys. 345-352A
Hydrogen Embrittlement of Pseudobinary $L1_2$ -Type $Ni_3(Al_0.4Mn_0.6)$ Intermetallic Compound. 353-357A
Creep—Fatigue Behavior of Directionally Solidified and Single Crystal Intermetallic $Ni_3Al(B,H)$ at an Intermediate Temperature. 479-486A
The Strength of Ni_3Al Containing Titanium and Boron. 732-733A
- Aluminum compounds, Solubility**
On the Solubility of Aluminum Carbide in Cryolitic Melts. 441-447B
- Aluminum killed steels, Metal working.**
The Variation of Plastic Anisotropy During Straining. A Wrinkling Index for Press Forming. 2805-2817A
2831-2837A
- Aluminum oxide, Composite materials**
Transverse Elastic Moduli of Unidirectional Fiber Composites With Interfacial Debonding. 129-135A
- Aluminum oxide, Reactions (chemical)**
Conditions Affecting the Formation of Chlorinated Carbon Compounds During Carbochlorination. 477-482B
- Amorphous materials**
See also Metallic glasses
- Amorphous materials, Thin films**
Radiation Induced Crystallization of Amorphous Si:H Alloy. 1345-1349A
- Amplifiers**
See Lasers
- Analyzing**
See Areal analysis
Auger electron spectroscopy
Mathematical analysis
Statistical analysis
Stress analysis
Surface analysis (chemical)
Volumetric analysis
X ray diffraction
- Andrade method**
See Crystal growth
- Androforming**
See Stretch forming
- Angles (geometry)**
See Contact angle
- Anisotropy**
See also Elastic anisotropy
Magnetic anisotropy
- Anisotropy, Temperature effects**
Effect of Annealing Temperature on Yield Anisotropy of Zircaloy-4 TREX. 1243-1255A
- Annealing**
See also Bright annealing
Some Fundamental Aspects of Annealing and Pickling Stainless Steels. 1083-1100A
Determination of Dihedral Angle Distributions in Polycrystals: Application to $\alpha + \beta$ Brass. 1147-1151A
Effect of Annealing Temperature on Yield Anisotropy of Zircaloy-4 TREX. 1243-1255A
Intermittent Annealing as a Means of Improving Impact Properties of Plate Steel. 1481-1490A
Amorphous Cr_2Si_3 Thin Films—Morphology and Kinetics of Crystallization. 1991-2003A
Phase Transformation During Annealing of Rapidly Solidified Aluminum-Rich $Al-Fe-Si$ Alloys. 2893-2900A
- Anodic dissolution**
High Frequency Stage I Corrosion Fatigue of Austenitic Stainless Steel (316L). 2753-2764A
- Antidomains**
See Domains
- Antimony**
Grain Boundary Segregation of Sulfur and Antimony in Iron Alloys. 2005-2011A
- Antimony, Alloying additive**
Effect of Antimony on the Creep Fracture of Stainless Steel. 571-577A
- Antimony, Reactions (chemical)**
Speciation and Reduction Potentials of Metal Ions in Concentrated Chloride and Sulfate Solutions Relevant to Processing Base Metal Sulfides. 37-45B
Thermodynamics for Arsenic and Antimony in Copper Matte Converting—Computer Simulation. 547-556B
- Arc welding**
See also Gas tungsten arc welding
Shielded arc welding
Shielded metal arc welding
Consolidation of Metallic Glass Ribbons Using Electric Discharge Welding. 1634-1638A
- Arc welds**
See Welded joints
- Areal analysis**
Calculation of the Product Phase Grain Boundary Area During Solid State Transformations. 2123-2131A
- Argon, Environment**
Sintering Atmosphere Effects on Tensile Properties of Heavy Alloys. 2467-2476A
Near-Threshold Fatigue Crack Growth in Copper and Alpha-Brass: Grain-Size and Environmental Effects. 2575-2587A
- Argon arc welding**
See Gas tungsten arc welding
- Arrhenius activation energy**
See Activation energy
- Arsenic, Reactions (chemical)**
Speciation and Reduction Potentials of Metal Ions in Concentrated Chloride and Sulfate Solutions Relevant to Processing Base Metal Sulfides. 37-45B
Thermodynamics for Arsenic and Antimony in Copper Matte Converting—Computer Simulation. 547-556B
- Artificial aging**
See Aging (artificial)
- Atmospheres**
See Controlled atmospheres
- Atomic diffusion**
See Diffusion
- Atomic properties**
See Atomic structure
- Atomic structure**
Premartensitic Anelasticity in Indium—Thallium Alloys. 789-792A
Electron Diffraction Study of α - and α' -AlFeSi. 893-898A
- Atomization**
See Atomizing
- Atomizing**
Preparation of Iron-, Cobalt- and Nickel-Based Amorphous Alloy Powders by High-Pressure Gas Atomization and Their Structural Relaxation Behavior. 235-242A
Niobium-Alloyed High Speed Steel by Powder Metallurgy. 1395-1401A
- Auger electron spectroscopy**
Scanning Auger Microprobe Study of Hot-Dipped Regular-Spangle Galvanized Steel. I. Surface Composition of As-Produced Sheet. 1603-1608A
- Austempering**
Development of High Toughness in Austempered Type Ductile Cast Iron and Evaluation of Its Properties. 319-327A
Swing Back in Kinetics Near M_s in Hyperreductoid Steels. 447-452A
- Austenite**
See also Retained austenite
Evaluation of the Effects of Segregation on Austenite Grain Boundary Energy in $Fe-C-X$ Alloys. 1807-1818A
- Austenitic stainless steels, Corrosion**
Cracking Kinetics of Two-Phase Stainless Steel Alloys in Hydrogen Gas. 145-152A
Grain Boundary Segregation in Austenitic Stainless Steels and Its Effect on Intergranular Corrosion and Stress Corrosion Cracking. 495-504A
High Frequency Stage I Corrosion Fatigue of Austenitic Stainless Steel (316L). 2753-2764A
Stage I Corrosion Fatigue Crack Crystallography in Austenitic Stainless Steel (316L). 2765-2773A
- Austenitic stainless steels, Heat treatment**
Inhibition of Nitrogen Uptake by SiO_2 Surface Films Formed on Stainless Steel During Annealing in H/N Atmospheres. 3045-3055A
- Austenitic stainless steels, Mechanical properties**
Creep—Fatigue Life Prediction in Terms of Nucleation and Growth of Fatigue Crack and Creep Cavities. 121-127A
On the Effect of Carbide Precipitation During Creep of 304 and 316 Type Stainless Steels. 327-339A
Effect of Antimony on the Creep Fracture of Stainless Steel. 571-577A
Effects of Water Vapor on Hydrogen Induced Slow Crack Growth in Stainless Steels. 651-656A
Biaxial Path Dependence of Deformation Substructure of Type 304 Stainless Steel. 1277-1293A
Mechanistic Similarities Between Hydrogen and Temperature Effects on the Ductile-to-Brittle Transition of a Stainless Steel. 1547-1553A
The Flow Equation and Its Necking Criterion in Austenitic Cryogenic $Fe-Mn-Al-X$ Steels. 1625-1626A
Cleavage-Like Fracture Along Slip Planes in $Fe-18Cr-3Ni-13Mn-0.37N$ Austenitic Stainless Steel at Liquid Helium Temperature. 1626-1631A
- Austenitic stainless steels, Metal working**
The Effect of Grain Size on the Bulk Formability and Tensile Properties of Austenitic Stainless Steel Types 304 and 316. 2287-2298A
- Austenitic stainless steels, Microstructure**
Intercrystalline Structure Distribution in Alloy 304 Stainless Steel. 1179-1185A
The Microstructure and Phase Relationships in Rapidly Solidified Type 304 Stainless Steel Powders. 2399-2405A
Statistical Considerations on Uniform Grain Size. 2937-2944A
- Austenitic stainless steels, Phase transformations**
Nature of the γ and γ' Phases in Austenitic Stainless Steels Cathodically Charged With Hydrogen. 723-730A
Effect of Temperature and Strain Distribution on Martensitic Transformation During Uniaxial Testing of AISI-304 Stainless Steel. 1021-1026A
- Austenitic stainless steels, Welding**
Free Surface Flow and Heat Transfer in Conduction Mode Laser Welding. 851-858B
Effects of Oxygen and Sulfur on Alloying Element Vaporization Rates During Laser Welding. 967-972B

Austenitic stainless steels

- Environmental Cracking of Type 316 Austenitic Stainless Steel Weldments in High Temperature CO₂ Gas. 1445-1460A
- Austenitizing**
The Effects of Austenitizing Temperature on the High Temperature Ductility of Fe—P—S Alloys. 887-892A
Correlations of Microstructure With Dynamic and Quasi-Static Fracture in a Plain Carbon Steel. 2179-2206A
Influence of Austenitizing Temperature on Stress Corrosion in 4330M Steel—the Role of Impurity Segregation in Stress Corrosion Cracking of High Strength Steel. 2225-2231A
The Effect of Austenitizing Temperature on the Fracture Initiation Toughness of As-Quenched HP9-4-20 Steel. 2989-3003A
- Auto oxidation**
See Oxidation
- Autodiffusion**
See Diffusion
- Autogenous smelting**
See Flash smelting
- Automobile components**
See Automotive components
- Automotive components, Materials selection**
Laser Transformation Hardening of Iron—Carbon and Iron—Carbon—Chromium Steels. 2013-2025A
- A15 compounds, Phase transformations**
Electron—Phonon Based Local Mode Descriptions of Displacive Transformations. 177-183A
Pretransformation Phenomena as Revealed by Elastic Waves. 185-191A
- Babbitt**
See Bearing alloys
- Bainite**
Effect of Microstructure on Plane-Strain Fracture Toughness of AISI 4340 Steel. 2513-2521A
- Bainite, High temperature effects**
Bainite Formation in Low Carbon Cr—Ni Steels. 1695-1701A
- Balling**
See Agglomeration
- Banded structure**
Creep Deformation of Ni₃Al—Mo In Situ Composites. 987-998A
- Basic oxygen processes**
See Oxygen steel making
- Basic oxygen steel making**
See Oxygen steel making
- Batch type furnaces**
See Converters
- Baths**
See Metal baths
- BCC metals, Phase transformations**
Computer Study of Tweed as a Precursor to a Martensitic Transformation of a BCC Lattice. 783-787A
- Beams (radiation)**
See Electron beams
- Bearing alloys, Composite materials**
Correlation of Mechanical Properties With Nondestructive Evaluation of Babbitt Metal/Bronze Composite Interface. 2215-2224A
- Beehive kilns**
See Kilns
- Bend properties**
See Bend strength
- Bend strength, Composition effects**
Ductile Al—Cu—V Amorphous Alloys Without Metalloid. 391-393A
- Bendability**
See Formability
- Bending**
Characterization of Residual Stresses in Bent Incoloy-800 Tubing by Neutron Diffraction. 2207-2214A
- Bending strength**
See Bend strength
- Beryllium, Reactions (chemical)**
Mass Spectrometric Study of the Activities of the Fe—Ge System at 1550°C. 511-513B
- Billet, Casting**
Flow Fields in Electromagnetic Stirring of Rectangular Strands With Linear Inductors. II. Computation of Flow Fields in Billets, Blooms, and Slabs of Steel. 595-602B
Initial Development of Thermal and Stress Fields in Continuously Cast Steel Billets. 2589-2602A
- Bimetals, Nondestructive testing**
Correlation of Mechanical Properties With Nondestructive Evaluation of Babbitt Metal/Bronze Composite Interface. 2215-2224A
- Binary systems, Phases (state of matter)**
Formation of Amorphous and Metastable Extended Solid Solutions in Cu—Ti Alloys Using the Triode Sputtering Technique. 5-12A
Calculation of the Titanium—Aluminum Phase Diagram. 243-247A
Magnetic-Induced Tricritical Points in Alloys. 441-446A
High Temperature Thermodynamics of the Cr—Cr₂N—N₂ System. 471-476B
Thermodynamics of the Cr—Mn System Using an Isopiestic Technique. 649-654B
- On the Slopes of Phase Boundaries. 1819-1825A
Densities of Pb—Sn Alloys During Solidification. 2349-2354A
The Stable and Metastable Ti—Nb Phase Diagrams. 2389-2397A
The Cata- or Metatectic Reaction—Occurrence and Microstructural Development. 3097-3100A
- Binary systems, Solubility**
Mass Spectrometric Study of the Activities of the Fe—Ge System at 1550°C. 511-513B
- Binary systems, Thermal properties**
Enthalpies of a Binary Alloy During Solidification. 3057-3061A
- Bismuth, Binary systems**
The Cata- or Metatectic Reaction—Occurrence and Microstructural Development. 3097-3100A
- Bismuth, Impurities**
The Interaction Between Oxygen and Bismuth in Dilute Solution in Copper at 1300°C. 623-626B
- Bismuth, Reactions (chemical)**
Evaluation of the Activity and Molecular Form of Bismuth in Copper Smelting Slags. I. Ternary Silicate Slags. 627-641B
- Bismuth, Ternary systems**
The Influence of the Ternary Interaction Parameter ϵ_{Bi} on the Activity of Bismuth in Molten Copper. 427-432B
- Bismuth base alloys, Directional solidification**
Directional Solidification of Cu—Pb and Bi—Ga Monotectic Alloys Under Normal Gravity and During Parabolic Flight. 2839-2846A
- Bismuth base alloys, Physical properties**
Experimental Measurement and Numerical Computation of Velocity and Turbulence Parameters in a Heated Liquid Metal System. 765-775B
- Bismuth compounds, Powder technology**
Mechanical Alloying of Brittle Materials. 2867-2874A
- Blades**
See Turbine blades
- Blankets (atmospheres)**
See Controlled atmospheres
- Blast furnace slags, Reactions (chemical)**
Thermodynamic Activity of Na₂O in Na₂O—CaO—SiO₂, Na₂O—MgO—SiO₂, and Na₂O—CaO—SiO₂—Al₂O₃ Melts at 1400°C. 655-661B
- Blasts (explosions)**
See Explosions
- Blister copper, Refining**
The Interaction Between Oxygen and Bismuth in Dilute Solution in Copper at 1300°C. 623-626B
- Blistering**
Determination of Fracture Initiation in Hydride Blisters Using Acoustic Emission. 2247-2257A
- Blooms (metal), Casting**
Flow Fields in Electromagnetic Stirring of Rectangular Strands With Linear Inductors. II. Computation of Flow Fields in Billets, Blooms, and Slabs of Steel. 595-602B
- Blunging**
See Mixing
- Body centered cubic metals**
See BCC metals
- Body centered orthorhombic lattice**
See Orthorhombic lattice
- Bohr model**
See Atomic structure
- Boiler scale**
See Scale (corrosion)
- Bomb reduction**
See Reduction (chemical)
- Bonding strength**
Transverse Elastic Moduli of Unidirectional Fiber Composites With Interfacial Debonding. 129-135A
Correlation of Mechanical Properties With Nondestructive Evaluation of Babbitt Metal/Bronze Composite Interface. 2215-2224A
- Boron, Alloying additive**
Discussion of 'The Role of Boron in the Grain Refinement of Aluminum With Titanium' and Authors' Reply. 385-387A
- Boron, Impurities**
The Influence of Boron on the Grain Boundary Chemistry and Microstructure of Ni—16Cr—9Fe—0.03C. 2555-2566A
- BOS process**
See Oxygen steel making
- Boundaries**
See Grain boundaries
Phase boundary
- Boundary layer**
Dislocation Structures in the Strain Localized Region in Fatigued 85/15 Brass. 1257-1262A
- Brass plating**
Pulsed Electrodeposition of Layered Brass Structures. 1569-1573A
- Brasses**
Near-Threshold Fatigue Crack Growth in Copper and Alpha-Brass: Grain-Size and Environmental Effects. 2575-2587A
- Brasses, Diffusion**
Effect of High Pressure on Interdiffusion in Cu—Zn Alloys at Temperatures Near the Melting Point. 467-471A

- Brasses, Extrusion**
Dislocation Structures in the Strain Localized Region in Fatigued 85/15 Brass. 1257-1262A
- Brasses, Heat treatment**
Determination of Dihedral Angle Distributions in Polycrystals: Application to $\alpha + \beta$ Brass. 1147-1151A
- Brasses, Mechanical properties**
Modeling of the Plastic Anisotropy of Textured Sheet. Elastic Interaction Stresses. I. The Influence of Bicrystal Size on Stresses in [213] Iso-Axial 70-30 Alpha-Brass Bicrystals. 105-120A
1727-1737A
- Brasses, Phase transformations**
Electron Diffuse Scattering Studies of Premartensitic Alloys: β' Cu—Zn, β' Ni—Al, In—Ti, and Fe—Ni. 199-205A
Beta-Phase Stability and Martensitic Nucleation in Hume-Rothery Alloys. 207-216A
- Brasses, Structural hardening**
Slip Observations in 70-30 Alpha Brass. 1575-1581A
- Brick kilns**
See Kilns
- Bridgman method**
See Crystal growth
- Bright annealing**
Inhibition of Nitrogen Uptake by SiO₂ Surface Films Formed on Stainless Steel During Annealing in H/N Atmospheres. 3045-3055A
- Brillouin zone**
Modulated Lattice Relaxation in β -Based Premartensitic Phase. 777-781A
- Brittle fracture, Impurity effects**
The Nucleation of High Temperature Brittle Intergranular Fracture in 2.25Cr—1Mo Steel. 3005-3011A
- Brittleness**
See also Temper brittleness
- Brittleness, Cryogenic effects**
Cleavage-Like Fracture Along Slip Planes in Fe—18Cr—3Ni—13Mn—0.37N Austenitic Stainless Steel at Liquid Helium Temperature. 1626-1631A
- Bronzes, Composite materials**
Correlation of Mechanical Properties With Nondestructive Evaluation of Babbitt Metal/Bronze Composite Interface. 2215-2224A
- Bubbles, Diffusion**
Creep Cavity Growth From Tritium-Induced Helium Bubbles in Nickel. 821-827A
- Bubbling**
Bubbling at High Flow Rates in Inviscid and Viscous Liquids (Slags). 83-94B
Fluid Dynamics in Bubble Stirred Ladies. I. Experiments. 745-754B
Fluid Dynamics in Bubble Stirred Ladies. II. Mathematical Modeling. 755-764B
- Bulge forming**
See Bulging
- Bulging, High temperature effects**
Influence of Solidification Structure on Creep Behavior of Nonalloyed Steel at High Temperatures. 2857-2859A
- Burn up**
See Fuel consumption
- Burning**
See Combustion
- Burnout**
See Fuel consumption
- Cadmium base alloys, Phase transformations**
X-Ray Study of the Premartensitic Phenomena in AuCd. 265-271A
- Caesium**
See Cesium
- Cakes (metal)**
See Ingots
- Calcining**
See Roasting
- Calcium, Alloying elements**
Volume Effects and Associations in Liquid Alloys. 465-470B
- Calcium, Extraction**
An Intrinsic-Transport Model for Solid—Solid Reactions Involving a Gaseous Intermediate. 73-81B
Correction to "An Intrinsic-Transport Model for Solid—Solid Reactions Involving a Gaseous Intermediate". 519B
- Calcium compounds**
See also Lime
- Calcium compounds, Crystal growth**
Determination of Standard Free Energies of Formation of Ca₃P₂ and Ca₂Sn at High Temperatures. 433-439B
- Calcium compounds, Reactions (chemical)**
Thermodynamics of Ca—CaF₂ and Ca—CaC₂ Systems for the Dephosphorization of Steel. 643-648B
- Calcium oxide**
See Lime
- Calculating**
See Computation
- Calculation**
See Computation
- Capillarity**
Experimental Study of Thermocapillary Flows in a Thin Liquid Layer With Heat Fluxes Imposed on the Free Surface. 1895-1898A
- Carbides**
See also Silicon carbide
Tungsten carbide
On the Effect of Carbide Precipitation During Creep of 304 and 316 Type Stainless Steels. 387-389A
- Carbides, Crystal growth**
Investigation of Microstructural Changes in a Ferritic Steel Caused by High Temperature Fatigue. 999-1007A
- Carbides, Crystal lattices**
The Influence of Mo₂C Morphology and Distribution on the Fatigue Crack Initiation and Propagation Behavior of Fe—C—Mo Dual-Phase Steels. 973-986A
- Carbides, Solubility**
On the Solubility of Aluminum Carbide in Cryolitic Melts. 441-447B
- Carbon, Alloying elements**
Rate of Nitrogen Desorption From Liquid Iron—Carbon and Iron—Chromium Alloys With Argon. 233-242B
The Prediction of Precipitation Strengthening in Microalloyed Steels. 1471-1480A
- Carbon, Diffusion**
Change in Direction of Carbon Thermotransport in Nb—V System With Alloying. 1429-1435A
- Carbon, Quaternary systems**
A Thermodynamic Evaluation of the C—Cr—Fe—W System. 2547-2554A
- Carbon, Reactions (chemical)**
Conditions Affecting the Formation of Chlorinated Carbon Compounds During Carbochlorination. 477-482B
Activity of Carbon in Nickel-Rich Ni—Mo and Ni—W Alloys. 645-650A
- Carbon, Ternary systems**
A Thermodynamic Evaluation of the Fe—Cr—C System. 627-636A
- Carbon, Trace elements**
Analysis of Nonisothermal Transformation Kinetics; Tempering of Iron—Carbon and Iron—Nitrogen Martensites. 925-932A
- Carbon compounds**
See also Carbides
Carbon dioxide
Tungsten carbide
- Carbon compounds, Physical properties**
Mixing Fuel Particles for Space Combustion Research Using Acoustics. 1931-1937A
- Carbon dioxide, Reactions (chemical)**
On the Interfacial Rate of Reaction of CO₂ With a Calcium Ferrite Melt. 959-965B
- Carbon fibers, Coating**
Coating of Graphite Fibers With Tungsten Carbide Using Solid and Liquid Copper as a Transfer Medium. 2109-2113A
- Carbon fibers, Composite materials**
Transverse Elastic Moduli of Unidirectional Fiber Composites With Interfacial Debonding. 129-135A
- Carbon manganese steels, Mechanical properties**
Effects of Transformed Ferrite Growth on the Tensile Fracture Characteristics of a Dual-Phase Steel. 309-317A
Void Formation During Tensile Testing of Dual Phase Steels. 579-589A
- Carbon steels**
See also Aluminum killed steels
Carbon manganese steels
Killed steels
- Carbon steels, Casting**
Initial Development of Thermal and Stress Fields in Continuously Cast Steel Billets. 2589-2602A
Processing Effects in Spray Casting of Steel Strip. 3077-3086A
- Carbon steels, Cleaning**
Studies on the Determination of Surface Deuterium in AISI 1062, 4037, and 4140 Steels by Secondary Ion Mass Spectrometry. 3071-3075A
- Carbon steels, Crystal growth**
Influence of Rare Earth Metals on the Nucleation and Solidification Behavior of Iron and 1045 Steel. 383-395B
- Carbon steels, Heat treatment**
Intercritical Annealing as a Means of Improving Impact Properties of Plate Steel. 1481-1490A
Laser Transformation Hardening of Iron—Carbon and Iron—Carbon—Chromium Steels. 2013-2025A
The Tempering of Iron—Carbon Martensite; Dilatometric and Calorimetric Analysis. 2415-2428A
- Carbon steels, Mechanical properties**
Investigation of Panel Crack Formation in Steel Ingots. II. Off-Corner Panel Cracks. 289-301B
An Analysis for the Effect of a Grain Size Gradient on Torsional and Tensile Properties. 329-335A
The Law of Mixtures Applied to the Plastic Deformation of Two-Phase Alloys of Coarse Microstructures. 2027-2040A
Correlations of Microstructure With Dynamic and Quasi-Static Fracture in a Plain Carbon Steel. 2179-2206A
The Effect of Alloying Elements and Microstructure on the Strength and Fracture Resistance of Pearlitic Steel. 2819-2829A
Influence of Solidification Structure on Creep Behavior of Nonalloyed Steel at High Temperatures. 2857-2859A
- Carbon steels, Metal working**
The Variation of Plastic Anisotropy During Straining. 2805-2817A

Carbon steels

Carbon steels, Phase transformations

- Effect of Deformation on the Austenite-to-Ferrite Transformation in a Plain Carbon and Two Microalloyed Steels. 417-426A
Swing Back in Kinetics Near M_s in Hypereutectoid Steels. 447-452A
A Theoretical Analysis of the Spinodal Decomposition in Fe-C Martensite During Aging Stage of Tempering. 2427-2432A

Carbon steels, Sorption

- Wear-Enhanced Hydrogen Evolution From Mild Steel. 1721-1726A

Carbon steels, Structural hardening

- A Stress Relaxation Method for Following Carbonitride Precipitation in Austenite at Hot Working Temperatures. 1403-1413A

Carbon steels, Welding

- A Model for the Strength of the As-Deposited Regions of Steel Weld Metals. 1597-1602A

Carbothermic reactions

- An Intrinsic-Transport Model for Solid-Solid Reactions Involving a Gaseous Intermediate. 73-81B
Carbothermic Reduction of Silicon Dioxide—a Thermodynamic Investigation. 249-253B
Correction to "An Intrinsic-Transport Model for Solid-Solid Reactions Involving a Gaseous Intermediate". 519B
An Ionic Diffusion Mechanism of Chromite Reduction. 677-684B
The Effect of Alkali Salt Catalyst on the Carbothermic Reduction of Nickel Oxide. 685-686B

Cast iron

- See also Gray iron
Nodular iron
White iron

Cast iron, Rolling

- The Effect of Triaxial Stress Field on Intermediate Temperature Embrittlement of Ferritic Spheroidal Graphite Cast Irons. 1213-1219A

Casting

- See Continuous casting
Horizontal continuous casting
Melt spinning

Casting defects

- Channel Formation in Pb-Sn, Pb-Sb, and Pb-Sn-Sb Alloy Ingots and Comparison With the System NH_4Cl-H_2O . 1861-1871A
Study of Microporosity Formation in Nickel-Base Superalloys. 2341-2348A
Initial Development of Thermal and Stress Fields in Continuously Cast Steel Billets. 2589-2602A

Castings

- See also Continuous cast shapes
Ingots

Castings, Mechanical properties

- Structure and Mechanical Properties of Unidirectionally Solidified Fe-Cr-C and Fe-Cr-X-C Alloys. 1235-1241A
Tensile Fracture of Coarse-Grained Cast Austenitic Manganese Steels. 2269-2277A

Castings, Microstructure

- Assessment of Service Induced Microstructural Damage and Its Rejuvenation in Turbine Blades. 2049-2066A

Catalysts

- The Effect of Alkali Salt Catalyst on the Carbothermic Reduction of Nickel Oxide. 685-686B

Cathode ray polarographs

- See Polarimeters

Cathodic coatings (oxide)

- See Oxide coatings

Cathodic protection

- Predicting the Kinetics of Hydrogen Generation at the Tips of Corrosion Fatigue Cracks. 1795-1806A

Cavitation

- Creep Cavity Growth From Tritium-Induced Helium Bubbles in Nickel. 821-827A

Cavitation, Deformation effects

- Microstructural Observations in Cyclically Deformed Pb-Sn Solid Solution Alloy. 1437-1443A

Cellular precipitates

- Orowan Strengthening by Mo_2C Fibers and Needle Interphase Precipitates in Fe-C-Mo Dual-Phase Steels. 1617-1620A

Cellular precipitates, Diffusion effects

- Inhibition of Cyclic Grain Boundary Migration Through Cellular Precipitation in Pb-5% Sn Alloy. 2355-2359A

Cementite, Thermal properties

- Gibbs Free Energy of Formation of Cementite, Fe_3C . 2115-2117A

Cerium, Alloying elements

- Discussion of "Microdistribution of Cerium in Steel" and Author's Reply. 723A

Cesium, Binary systems

- On the Slopes of Phase Boundaries. 1819-1825A

Chalcogenides

- See Sulfides

Charring

- See Combustion

Chemical analysis

- See Surface analysis (chemical)
Volumetric analysis

Chemical attack

- See Intergranular corrosion

Chemical cleaning

- See Pickling

Chemical composition

- Discussion of "Microdistribution of Cerium in Steel" and Author's Reply. 723A
Microsegregation in Directionally Solidified Pb-8.4 at.% Au Alloy. 1351-1364A
Use of Ion Scattering in Characterizing the Surface Oxide of P/M Aluminum Alloy 7091. 1372-1374A

Chemical kinetics

- See Reaction kinetics

Chemical processes

- See Reactions (chemical)

Chemical properties

- See Heat of activation
Heat of formation
Heat of reaction

Chemical reactions

- See Reactions (chemical)

Chemical reactors, Design

- Fluid Dynamics in Channel Reactors Stirred by Submerged Gas Injection. 603-612B

Chemical reduction

- See Reduction (chemical)

Chemical tests

- See Surface analysis (chemical)
Volumetric analysis

Chemistry

- See Electrochemistry

Chlorides, Electrical properties

- Electrical Conductivity of Acidic Chloride Solutions. 53-58B

Chlorides, Environment

- Transgranular Stress-Corrosion Cracking of Disordered Cu-25Au in Aqueous Chloride and Sulfate Media. 281-292A

Chlorides, Reactions (chemical)

- Analysis of Dissolution Rate of Metal Oxide in Acidic Chloride Solution in Terms of Water Activity. 505-507B

Chlorides, Solubility

- Water and Solute Activities of the Solution Systems of $H_2SO_4-CuSO_4-H_2O$ and $HCl-CuCl_2-H_2O$. 347-354B

Chlorination

- Conditions Affecting the Formation of Chlorinated Carbon Compounds During Carbochlorination. 477-482B
Studies on the Dry Chlorination of Deep Sea Manganese Nodules. 514-518B
Studies on Oxychlorination of MoS_2 in a Fluid Bed Reactor. 669-675B

Chromate coating

- See Chromating

Chromate coatings, Chemical analysis

- Scanning Auger Microprobe Study of Hot-Dipped Regular-Spangle Galvanized Steel. II. Surface Composition of Chromated Sheet. 1609-1616A

Chromating

- Scanning Auger Microprobe Study of Hot-Dipped Regular-Spangle Galvanized Steel. II. Surface Composition of Chromated Sheet. 1609-1616A

Chromium, Alloying elements

- Rate of Nitrogen Desorption From Liquid Iron-Carbon and Iron-Chromium Alloys With Argon. 233-242B
Laser Transformation Hardening of Iron-Carbon and Iron-Carbon-Chromium Steels. 2013-2025A
The Effect of Alloying Elements and Microstructure on the Strength and Fracture Resistance of Pearlitic Steel. 2819-2829A

Chromium, Binary systems

- High Temperature Thermodynamics of the Cr-Cr₂N-N₂ System. 471-476B
Thermodynamics of the Cr-Mn System Using an Isopiestic Technique. 649-654B

Chromium, Diffusion

- Thermodynamics of Segregation in Alloys. 2091-2098A

Chromium, Extraction

- Vapor Phase Reduction of Chromic Oxide in an Ar-H₂ RF Plasma. 927-933B

Chromium, Quaternary systems

- A Thermodynamic Evaluation of the C-Cr-Fe-W System. 2547-2554A

Chromium, Ternary systems

- A Thermodynamic Evaluation of the Fe-Cr-C System. 627-636A
Phase Relationships in the Fe-Cr-Ni System at Solidification Temperatures. 899-908A
An Experimental Study and a Thermodynamic Evaluation of the Fe-Cr-Mo System. 1385-1394A
An Experimental Study and a Thermodynamic Evaluation of the Cr-Fe-W System. 2531-2546A

Chromium, Thermal properties

- Measurement of Temperature and Emissivity of Specularly Reflecting Glowing Bodies. 1889-1894A

Chromium base alloys, Surface properties

- Surface Tension of Binary Metal-Surface Active Solute Systems Under Conditions Relevant to Welding Metallurgy. 483-491B

Chromium compounds, Microstructure

- Amorphous Cr₂Si₃ Thin Films—Morphology and Kinetics of Crystallization. 1991-2003A

- Chromium molybdenum nickel steels**
See Nickel chromium molybdenum steels
- Chromium molybdenum steels**
See also Chromium molybdenum vanadium steels
Nickel chromium molybdenum steels
- Chromium molybdenum steels, Cleaning**
Studies on the Determination of Surface Deuterium in AISI 1062, 4037, and 4140 Steels by Secondary Ion Mass Spectrometry. 3071-3075A
- Chromium molybdenum steels, Corrosion**
Discussion of "Sulfide Stress Cracking Susceptibility of Nickel Containing Steels" and Authors' Reply. 153A
- Chromium molybdenum steels, Mechanical properties**
Creep—Fatigue Life Prediction in Terms of Nucleation and Growth of Fatigue Crack and Creep Cavities. 121-127A
Creep Crack Growth Simulation Under Transient Stress Fields. 829-835A
Influence of Cyclic to Mean Load Ratio on Creep/Fatigue Crack Growth. 873-880A
The Effect of Tempering Temperature on Near-Threshold Fatigue Crack Behavior in Quenched and Tempered 4140 Steel. 2497-2502A
The Thermal Activation Energy for Fatigue of Fe—1Cr—0.5Mo. 2979-2987A
The Nucleation of High Temperature Brittle Intergranular Fracture in 2.25Cr—1Mo Steel. 3005-3011A
- Chromium molybdenum steels, Metallography**
Quantitative Fractography: a Modern Perspective. 961-971A
- Chromium molybdenum steels, Structural hardening**
A Preliminary Study of the Influence of Separate and Combined Aluminum and Nickel Additions on the Properties of a Secondary Hardening Steel. 3103-3107A
- Chromium molybdenum vanadium steels, Mechanical properties**
Elevated Temperature Creep—Fatigue Crack Propagation in Nickel-Base Alloys and 1Cr—Mo—V Steel. 855-862A
Influence of Cyclic to Mean Load Ratio on Creep/Fatigue Crack Growth. 873-880A
- Chromium molybdenum vanadium steels, Microstructure**
Measuring Creep Damage Using Microradiography. 837-845A
- Chromium nickel molybdenum steels**
See Nickel chromium molybdenum steels
- Chromium nickel steels**
See Nickel chromium steels
- Chromium ores, Reduction (chemical)**
An Ionic Diffusion Mechanism of Chromite Reduction. 677-684B
- Chromium steels**
See also Austenitic stainless steels
Chromium molybdenum steels
Chromium molybdenum vanadium steels
Duplex stainless steels
Ferritic stainless steels
Nickel chromium molybdenum steels
Nickel chromium steels
Stainless steels
- Chromium steels, Heat treatment**
Laser Transformation Hardening of Iron—Carbon and Iron—Carbon—Chromium Steels. 2013-2025A
- Chromium vanadium steels**
See Chromium molybdenum vanadium steels
- Claddings, Microstructure**
Microstructure of Laser Clad Ni—Cr—Al—Hf Alloy on a γ' Strengthened Nickel-Base Superalloy. 1981-1990A
- Cleaning**
See Pickling
- Cleavage, Environmental effects**
The Mechanism of Hydrogen Induced Cleavage in Fe—3% Si Alloy. 1335-1343A
- Clustering**
Volume Effects and Associations in Liquid Alloys. 465-470B
- Coating**
See Alloy plating
Brass plating
Chromating
Hot dip galvanizing
Platinum plating
- Coatings**
See Chromate coatings
Electroplates
Hot dip coatings
Oxide coatings
Protective coatings
Undercoatings
- Cobalt, Alloying elements**
Effects of Cobalt Concentration on the Relative Resistance to Octahedral and Cube Slip in Nickel-Base Superalloys. 2733-2739A
- Cobalt, Extraction**
Reducibility of Laterite Ores. 181-186B
Leaching of Manganese Nodule in Ammoniacal Medium Using Ferrous Sulfate as the Reductant. 331-334B
- Cobalt, Recovering**
Studies on the Dry Chlorination of Deep Sea Manganese Nodules. 514-518B
- Cobalt base alloys, Mechanical properties**
The Absence of Steady-State Flow During Large Strain Plastic Deformation of Some FCC Metals at Low and Intermediate Temperatures. 3013-3024A
- Cobalt base alloys, Phases (state of matter)**
Spinodal Decomposition of a Co—Ti—Nb Alloy. 1703-1709A
- Cobalt base alloys, Powder technology**
Preparation of Iron-, Cobalt- and Nickel-Based Amorphous Alloy Powders by High-Pressure Gas Atomization and Their Structural Relaxation Behavior. 235-242A
Formation of Ultra-Fine Amorphous Powders in Fe—M—B (M = Transition Metal) Systems by Chemical Reduction Method and Their Thermal and Magnetic Properties. 2315-2318A
- Cobalt base alloys, Welding**
Consolidation of Metallic Glass Ribbons Using Electric Discharge Welding. 1634-1638A
- Coefficient of friction**
See Friction
- Cold cracking (welds)**
See Weld defects
- Cold deformation**
See Deformation
- Cold ductility**
See Ductility
- Cold formability**
See Formability
- Cold forming**
See Cold working
- Cold reduction**
See Cold working
- Cold shortness**
See Brittleness
- Cold working**
See also Stretch forming
The Effects of Heat Treatment and Cold Working on the Room-Temperature and Cryogenic Mechanical Properties of Fe—30Mn—9Al—0.9C Steel. 1873-1876A
- Columbium**
See Niobium
- Columbium base alloys**
See Niobium base alloys
- Columbium compounds**
See Niobium compounds
- Columnar structure**
The Nonuniform Distribution of Inclusions in Low-Alloy Steel Weld Deposits. 669-674A
Columnar Dendritic Solidification in a Metal-Matrix Composite. 709-721A
- Combustion**
Mixing Fuel Particles for Space Combustion Research Using Acoustics. 1931-1937A
- Compacting**
See also Hot isostatic pressing
Changes in the Longitudinal Flow and Apparent Plastic Poisson's Ratio of a Porous Metal Strip During Hot Densification Rolling. 1205-1211A
Use of Ion Scattering in Characterizing the Surface Oxide of P/M Aluminum Alloy 7091. 1372-1374A
Densification of Oxide Superconductors by Hot Isostatic Pressing. 1841-1847A
- Compacts**
See Powder compacts
Sintered compacts
- Compliance (elasticity)**
See Modulus of elasticity
- Composite materials**
See also Bimetals
Fiber composites
Particulate composites
Whisker composites
Materials for Advanced Studies and Devices. 155-164B
Materials for Advanced Studies and Devices. 749-758A
- Composite materials, Crystal growth**
Directional Solidification of Al—Ni/SiC Composites During Parabolic Trajectories. 1899-1904A
- Composite materials, Fabrication**
Modeling of Infiltration Kinetics for Liquid Metal Processing of Composites. 95-101B
- Composite materials, Mechanical properties**
Creep Deformation of Ni₃Al—Mo In Situ Composites. 987-998A
- Composite materials, Microstructure**
Some Observations on the Matrix Microstructure of Aluminum—Silicon Alloy—Graphite Particle Composites. 1365-1367A
- Compositions**
See Chemical composition
- Compression strength**
See Compressive strength
- Compressive modulus**
See Modulus of elasticity
- Compressive strength, Microstructural effects**
The Strength of Ni₃Al Containing Titanium and Boron. 732-733A

Compressive yield strength

Compressive yield strength

See Compressive strength

Computation

Equilibria Between the Rare Earth Elements, Oxygen and Sulfur, in Molten Iron. 409-418B

Computer programs

Biaxial Path Dependence of Deformation Substructure of Type 304 Stainless Steel. 1277-1293A
Fractal Analysis of a Nucleation and Growth Process. 1371-1372A

Computer simulation

Thermodynamics for Arsenic and Antimony in Copper Matte Converting—Computer Simulation. 547-556B
Computer Study of Tweed as a Precursor to a Martensitic Transformation of a BCC Lattice. 783-787A
A Computer Simulation on Tensile Strength of Metal Matrix Composites Reinforced With Surface-Damaged Fibers. 1491-1497A

Computing

See Computation

Concast

See Continuous casting

Concentrates (ores), Electrical properties

Measurements of Dielectric Properties for Particulate Sphalerite Samples and Zinc Concentrates. 13-24B

Concentrates (ores), Oxidation

Correlation Between Dielectric Properties and Aqueous Oxidation Rate for Pulverized Sphalerites and Zinc Concentrates. 25-36B

Concentration (stress)

See Stress concentration

Condensation resins

See Silicone resins

Conducting sheet analog

See Heat transmission

Conductivity

See Resistivity

Conductivity (electrical)

See Resistivity

Constitutional diagrams

See Phase diagrams

Consumption

See Energy consumption
Fuel consumption

Contact angle

Determination of Dihedral Angle Distributions in Polycrystals: Application to $\alpha + \beta$ Brass. 1147-1151A
The Wetting Characteristics and Surface Tension of Some Nickel-Based Alloys on Yttria, Hafnia, Alumina, and Zirconia Substrates. 1833-1839A

Contact testing

See Ultrasonic testing

Continuous cast shapes, Mechanical properties

Influence of Solidification Structure on Creep Behavior of Nonalloyed Steel at High Temperatures. 2857-2859A

Continuous casting

See also Horizontal continuous casting
Mathematical Modeling of Meniscus Profile and Melt Flow in Electromagnetic Casters. 397-408B
Flow Fields in Electromagnetic Stirring of Rectangular Strands With Linear Inductors. I. Theory and Experiments With Cold Models. 581-593B
Flow Fields in Electromagnetic Stirring of Rectangular Strands With Linear Inductors. II. Computation of Flow Fields in Billets, Blooms, and Slabs of Steel. 595-602B
An Experimental Study on Process Variables in Crystal Growth by Ohno Continuous Casting. 1849-1852A
Initial Development of Thermal and Stress Fields in Continuously Cast Steel Billets. 2589-2602A

Continuous casting, Development

Processing Effects in Spray Casting of Steel Strip. 3077-3086A

Control

See Process control

Controllability

See Stability

Controlled atmospheres

Kinetics of Neck Growth During Loose Stack Sintering. 2153-2161A
Sintering Atmosphere Effects on Tensile Properties of Heavy Alloys. 2467-2476A
Inhibition of Nitrogen Uptake by SiO₂ Surface Films Formed on Stainless Steel During Annealing in H/N Atmospheres. 3045-3055A

Conversion coating (process)

See Chromating

Conversion coatings

See Chromate coatings

Converters

Thermodynamics for Arsenic and Antimony in Copper Matte Converting—Computer Simulation. 547-556B

Cooling

See Supercooling

Cooling rate

Investigation of Panel Crack Formation in Steel Ingots. I. Mathematical Analysis and Mid-Face Panel Cracks. 277-287B

Investigation of Panel Crack Formation in Steel Ingots. II. Off-Corner Panel Cracks. 289-301B

Intermittent Annealing as a Means of Improving Impact Properties of Plate Steel. 1481-1490A

Gravitational Macroseggregation in Unidirectionally Solidified Lead—Tin Alloy. 2687-2694A

Structure and Properties of a Near- α Titanium Alloy After β Solution Treatment and Aging at 625°C. 3025-3033A

Copper, Alloying elements

Diffusion Induced Grain Boundary Migration and Recrystallization During Oxidation of a Ni—48.5% Cu Alloy. 1667-1675A
Erosion of Fiber Reinforced Al—4% Cu Composites. 1785-1793A

Copper, Binary systems

Formation of Amorphous and Metastable Extended Solid Solutions in Cu—Ti Alloys Using the Triode Sputtering Technique. 5-12A
The Cata- or Metatectic Reaction—Occurrence and Microstructural Development. 3097-3100A

Copper, Bonding

A Study of the Transient Liquid Phase Bonding Process Applied to a Ag/Cu/Ag Sandwich Joint. 675-686A

Copper, Coatings

Coating of Graphite Fibers With Tungsten Carbide Using Solid and Liquid Copper as a Transfer Medium. 2109-2113A

Copper, Diffusion

Prediction of Solute Diffusion Coefficients in Liquid Metals. 273-279A
Effect of High Pressure on Interdiffusion in Cu—Zn Alloys at Temperatures Near the Melting Point. 467-471A

Copper, Extraction

Determination of the Diffusion Coefficients of CuSO₄, ZnSO₄, and NiSO₄ in Aqueous Solution. 5-12B
Oxidation of Molten Copper Matte. 47-52B
Leaching of Manganese Nodule in Ammoniacal Medium Using Ferrous Sulfate as the Reductant. 331-334B
The Mathematical Modeling Revolution in Extractive Metallurgy. 525-540B

Copper, Mechanical properties

Modeling of the Plastic Anisotropy of Textured Sheet. 105-120A
Near-Threshold Fatigue Crack Growth in Copper and Alpha-Brass: Grain-Size and Environmental Effects. 2575-2587A
Determination of Parameters for Thermally Activated Glide From Stress—Strain Curves at Different Temperatures and Strain Rates. 2975-2978A

Copper, Melting

Process Mineralogy of Suspended Particles From a Simulated Commercial Flash Smelter. 719-729B
Observations on the Dynamics of Electromagnetically Levitated Liquid Metals and Alloys at Elevated Temperatures. 1939-1943A
Acoustic Levitation Technique for Containerless Processing at High Temperatures in Space. 2619-2623A

Copper, Quaternary systems

Solidus and Solvus Isotherms for Quaternary Al—Li—Cu—Mg Alloys. 1631-1634A

Copper, Reactions (chemical)

Speciation and Reduction Potentials of Metal Ions in Concentrated Chloride and Sulfate Solutions Relevant to Processing Base Metal Sulfides. 37-45B

Copper, Recovering

Studies on the Dry Chlorination of Deep Sea Manganese Nodules. 514-518B

Copper, Reduction (chemical)

An Investigation of Carbonaceous Materials Reducing Ferric Ions in Aqueous Solution. 709-717B

Copper, Refining

Thermodynamics for Arsenic and Antimony in Copper Matte Converting—Computer Simulation. 547-556B
Fluid Dynamics in Channel Reactors Stirred by Submerged Gas Injection. 603-612B
The Interaction Between Oxygen and Bismuth in Dilute Solution in Copper at 1300°C. 623-626B

Copper, Rolling

Changes in the Longitudinal Flow and Apparent Plastic Poisson's Ratio of a Porous Metal Strip During Hot Densification Rolling. 1205-1211A

Copper, Ternary systems

Phase Stability Relationships and Glass Formation in the System Cu—Ag—In. 13-21A
A New Treatment for Determining the Activities From Ternary Miscibility Gap: the O—Cu—Pb System. 373-376A
The Influence of the Ternary Interaction Parameter ϵ_{ij} on the Activity of Bismuth in Molten Copper. 427-432B
Solidification Structures in Rapidly Quenched Cu—Ti—Zr Alloys. 1853-1860A

Copper, Thermal properties

Convective Heat-Transfer Measurements in Liquid Metals Under Different Fluid Flow Conditions. 859-870B
Measurement of Temperature and Emissivity of Specularly Reflecting Glowing Bodies. 1889-1894A

Copper base alloys

See also Brasses
Bronzes

Copper base alloys, Corrosion

Transgranular Stress-Corrosion Cracking of Disordered Cu—25Au in Aqueous Chloride and Sulfate Media. 281-292A

Copper base alloys, Crystal growth

Fractal Analysis of a Nucleation and Growth Process. 1371-1372A

- Copper base alloys, Directional solidification**
The Influence of Interfacial Energies and Gravitational Levels on the Directionally Solidified Structures in Hypermonotectic Alloys 2665-2669A
Directional Solidification of Lead—Copper Immiscible Alloys in a Cyclic Gravity Environment. 2677-2680A
Directional Solidification of Cu—Pb and Bi—Ga Monotectic Alloys Under Normal Gravity and During Parabolic Flight. 2839-2846A
- Copper base alloys, Mechanical properties**
The Effect of Aging on the Fracture Behavior of Cu—Al—Ni β Phase Alloys. 1761-1766A
Preparation and Properties of Fine Grain β -CuAlNi Strain-Memory Alloys. 2921-2929A
- Copper base alloys, Melting**
Influence of Gravity Level and Interfacial Energies on Dispersion-Forming Tendencies in Hypermonotectic Cu—Pb—Al Alloys. 2645-2650A
- Copper base alloys, Microstructure**
Eutectic Structures of Ag—Cu After Melting and Solidification in Microgravity and on Earth. 2659-2664A
- Copper base alloys, Phase transformations**
Orientation Dependence of $\beta_1 \rightarrow \beta_2$ Stress-Induced Martensitic Transformation in a Cu—Al—Ni Alloy. 915-923A
- Copper base alloys, Structural hardening**
Correlation Among Microstructure, Strength, and Electrical Conductivity of Cu—Ni—Be Alloy. 2279-2285A
- Copper base alloys, Surface properties**
Surface Tension of Binary Metal—Surface Active Solute Systems Under Conditions Relevant to Welding Metallurgy. 483-491B
- Copper compounds, Crystal lattices**
The Apparent "Five-Fold" Nature of Large T_2 (Al_6Li_3Cu) Crystals. 2875-2884A
Convergent Beam Electron Diffraction Analysis of the T_1 (Al_2CuLi) Phase in Al—Li—Cu Alloys. 2885-2891B
- Copper mattes, Melting**
Saturation of Copper—Iron Mattes With Solid Magnetite. 935-941B
- Copper mattes, Oxidation**
Oxidation of Molten Copper Matte. 47-52B
- Copper mattes, Refining**
Thermodynamics for Arsenic and Antimony in Copper Matte Converting—Computer Simulation. 547-556B
- Core hardness**
See Hardness
- Corrosion**
See Corrosion fatigue
Hot gas corrosion
Intergranular corrosion
Scale (corrosion)
Sulfurization
- Corrosion cracking**
See Stress corrosion cracking
- Corrosion effects**
See Scale (corrosion)
- Corrosion fatigue**
Corrosion Fatigue Crack Initiation in a Mode II Notch Specimen. 1067-1073A
Fatigue Oxidation Interaction in IN 100 Superalloy. 2259-2268A
High Frequency Stage I Corrosion Fatigue of Austenitic Stainless Steel (316L). 2753-2764A
Stage I Corrosion Fatigue Crack Crystallography in Austenitic Stainless Steel (316L). 2765-2773A
- Corrosion fatigue, Diffusion effects**
The Role of Hydrogen in Corrosion Fatigue of High Purity Al—Zn—Mg Exposed to Water Vapor. 1775-1783A
- Corrosion fatigue, Environmental effects**
Predicting the Kinetics of Hydrogen Generation at the Tips of Corrosion Fatigue Cracks. 1795-1806A
- Corrosion fatigue, Microstructural effects**
The Effect of Microstructure on the Fatigue Crack Growth Behavior of Age-Hardened High Strength Steels in a Corrosive Environment. 1461-1469A
- Corrosion fatigue, Temperature effects**
Effects of Frequency and Temperature on Short Fatigue Crack Growth in Aqueous Environments. 543-548A
- Corrosion prevention**
See also Cathodic protection
Inhibition of Nitrogen Uptake by SiO_2 Surface Films Formed on Stainless Steel During Annealing in H/N Atmospheres. 3045-3055A
Studies on the Determination of Surface Deuterium in AISI 1062, 4037, and 4140 Steels by Secondary Ion Mass Spectrometry. 3071-3075A
- Corrosion products**
See Scale (corrosion)
- Corrosion resistance, Alloying effects**
Effects of Manganese, Phosphorus and Molybdenum on Sulfide Stress Cracking Resistance of High Strength Low Alloy Steels. 2171-2177A
- Cost savings**
See Economics
- Crack growth**
See Crack propagation
- Crack initiation**
Fatigue Oxidation Interaction in IN 100 Superalloy 2259-2268A
- Crack initiation, Impurity effects**
The Nucleation of High Temperature Brittle Intergranular Fracture in 2.25Cr—1Mo Steel. 3005-3011A
- Crack initiation, Microstructural effects**
Crack Initiation and Near-Threshold Surface Fatigue Crack Propagation Behavior of the Iron-Base Superalloy A-286. Effects of Transformed Ferrite Growth on the Tensile Fracture Characteristics of a Dual-Phase Steel. 301-308A
309-317A
- Crack propagation**
Fatigue Crack Propagation in Aluminum—Lithium Alloy 2090. I. Long Crack Behavior. 549-561A
Fatigue Crack Propagation in Aluminum—Lithium Alloy 2090. II. Small Crack Behavior. 563-569A
Effects of Water Vapor on Hydrogen Induced Slow Crack Growth in Stainless Steels. 651-656A
Elevated Temperature Creep—Fatigue Crack Propagation in Nickel-Base Alloys and 1Cr—Mo—V Steel. 855-862A
Application of the dc Potential Drop Technique in Investigating Crack Initiation and Propagation Under Sustained Load in Notched Rupture Tests. 863-871A
Influence of Cyclic to Mean Load Ratio on Creep/Fatigue Crack Growth. 873-880A
Microstructure and Fracture Toughness of the Aged β -Ti Alloy Ti—10V—2Fe—3Al. 1037-1049A
The Effect of Matrix Strength on Void Nucleation and Growth in a Widmanstätten Alpha—Beta Titanium Alloy, Corona-5. 1163-1171A
The Effect of Tin, Aluminum, and Nitrogen on the Hot Ductility of a Carbon—Manganese Steel Between 700-1200°C. 1305-1309A
The Influence of Hydride Size and Matrix Strength on Fracture Initiation at Hydrides in Zirconium Alloys. 1507-1522A
Mechanistic Similarities Between Hydrogen and Temperature Effects on the Ductile-to-Brittle Transition of a Stainless Steel. 1547-1553A
High Frequency Stage I Corrosion Fatigue of Austenitic Stainless Steel (316L). 2753-2764A
Stage I Corrosion Fatigue Crack Crystallography in Austenitic Stainless Steel (316L). 2765-2773A
- Crack propagation, Alloying effects**
Creep Crack Growth Behavior of Two Al—Li Alloys. 847-854A
- Crack propagation, Cryogenic effects**
Cleavage-Like Fracture Along Slip Planes in Fe—18Cr—3Ni—13Mn—0.37N Austenitic Stainless Steel at Liquid Helium Temperature. 1626-1631A
- Crack propagation, Deformation effects**
Dislocation Structures in the Strain Localized Region in Fatigued 85/15 Brass. 1257-1262A
- Crack propagation, Diffusion effects**
Determination of Fracture Initiation in Hydride Blisters Using Acoustic Emission. 2247-2257A
- Crack propagation, Environmental effects**
Chemical and Metallurgical Aspects of Environmentally Assisted Fatigue Crack Growth in 7075-T651 Aluminum Alloy. Predicting the Kinetics of Hydrogen Generation at the Tips of Corrosion Fatigue Cracks. 1739-1750A
1795-1806A
- Crack propagation, Heating effects**
Mode III Fracture of 4340 Steel: Effects of Tempering Temperature and Fracture Surface Interference. 3035-3044A
- Crack propagation, High temperature effects**
Cyclic Deformation and Fracture in Pb—Sn Solid Solution Alloy. 1533-1546A
The Effect of Tempering Temperature on Near-Threshold Fatigue Crack Behavior in Quenched and Tempered 4140 Steel. 2497-2502A
- Crack propagation, Impurity effects**
Influence of Austenitizing Temperature on Stress Corrosion in 4330M Steel—the Role of Impurity Segregation in Stress Corrosion Cracking of High Strength Steel. 2225-2231A
- Crack propagation, Microstructural effects**
Crack Initiation and Near-Threshold Surface Fatigue Crack Propagation Behavior of the Iron-Base Superalloy A-286. Effects of Transformed Ferrite Growth on the Tensile Fracture Characteristics of a Dual-Phase Steel. 301-308A
309-317A
Modeling the Texture Dependence of Environmentally Assisted Growth of Long and Short Cracks. 1009-1020A
The Mechanism of Hydrogen Induced Cleavage in Fe—3% Si Alloy. 1335-1343A
The Effect of Microstructure on the Fatigue Crack Growth Behavior of Age-Hardened High Strength Steels in a Corrosive Environment. 1461-1469A
Microstructure Effects on Tensile Properties of Tungsten—Nickel—Iron Composites. 1523-1532A
Near-Threshold Fatigue Crack Growth in Copper and Alpha-Brass: Grain-Size and Environmental Effects. 2575-2587A
- Crack propagation, Stress effects**
Creep Crack Growth Simulation Under Transient Stress Fields. 829-835A
- Crack propagation, Temperature effects**
Effects of Frequency and Temperature on Short Fatigue Crack Growth in Aqueous Environments. 543-548A
Crack Growth From Internal Hydrogen—Temperature and Microstructural Effects in 4340 Steel. 1319-1334A
The Thermal Activation Energy for Fatigue of Fe—1Cr—0.5Mo. 2979-2987A
- Crack resistance**
See Crack propagation
- Cracking (fracturing)**
See also Crack initiation
Stress corrosion cracking

Cracking (fracturing)

- On the Weldability, Composition, and Hardness of Pulsed and Continuous Nd:YAG Laser Welds in Aluminum Alloys 6061, 5456, and 5086. 319-329B
- Detection of the Initiation and Growth of Hydrogen-Induced Cracks in Armocon Iron Using Continuous Modulus Measurements. 473-478A
- Acoustic Emission Studies of Electron Beam Surface Modification of Aluminum. 493-503B
- The Kinetics of Intergranular Oxygen Penetration in Nickel and Its Relevance to Weldment Cracking. 2305-2313A
- Cracking (fracturing), Cooling effects**
Investigation of Panel Crack Formation in Steel Ingots. I. Mathematical Analysis and Mid-Face Panel Cracks. 277-287B
- Cracking (fracturing), Diffusion effects**
Determination of Fracture Initiation in Hydride Blisters Using Acoustic Emission. 2247-2257A
- Cracking (fracturing), Heating effects**
The Effect of Aging on the Fracture Behavior of Cu—Al—Ni β Phase Alloys. 1761-1766A
- Cracking (fracturing), Microstructural effects**
Effect of Microstructure on Fracture Behavior of Complex Structure in 6Ni—0.3C Steel. 2606-2611A
- Cracking (fracturing), Stress effects**
Investigation of Panel Crack Formation in Steel Ingots. II. Off-Corner Panel Cracks. 289-301B
- Cratering (wear)**
See Wear
- Cratering (welding)**
See Weld defects
- Creep (materials)**
See also Creep life
Creep rate
Creep rupture strength
Creep strength
Creep Cavity Growth From Tritium-Induced Helium Bubbles in Nickel. 821-827A
Measuring Creep Damage Using Microradiography. 837-845A
Elevated Temperature Creep—Fatigue Crack Propagation in Nickel-Base Alloys and 1Cr—Mo—V Steel. 855-862A
Assessment of Service Induced Microstructural Damage and Its Rejuvenation in Turbine Blades. 2049-2066A
Inelastic Deformation and Dislocation Structure of a Nickel Alloy: Effects of Deformation and Thermal Histories. 2477-2486A
- Creep (materials), High temperature effects**
Influence of Solidification Structure on Creep Behavior of Nonalloyed Steel at High Temperatures. 2857-2859A
- Creep (materials), Impurity effects**
Superplastic Deformation Behavior in Commercial and High Purity Zn—22% Al. 2741-2752A
- Creep (materials), Microstructural effects**
A Topological Study of Superplastic Deformation in an Al—Li Alloy With a Bimodal Grain Size Distribution. 1621-1624A
- Creep (materials), Temperature effects**
Determination of Parameters for Thermally Activated Glide From Stress—Strain Curves at Different Temperatures and Strain Rates. 2975-2978A
The Absence of Steady-State Flow During Large Strain Plastic Deformation of Some FCC Metals at Low and Intermediate Temperatures. 3013-3024A
- Creep life**
Creep—Fatigue Life Prediction in Terms of Nucleation and Growth of Fatigue Crack and Creep Cavities. 121-127A
Creep—Fatigue Behavior of Directionally Solidified and Single Crystal Intermetallic Ni₃Al(B,Hf) at an Intermediate Temperature. 479-486A
Creep Deformation of Ni₃Al—Mo In Situ Composites. 987-998A
- Creep limit**
See Creep (materials)
- Creep properties**
See Creep (materials)
- Creep rate**
A15 Compound Deformation and Secondary Slip in V₃Si. 1125-1127A
- Creep resistance**
See Creep strength
- Creep rupture strength**
Creep Crack Growth Behavior of Two Al—Li Alloys. 847-854A
Application of the dc Potential Drop Technique in Investigating Crack Initiation and Propagation Under Sustained Load in Notched Rupture Tests. 863-871A
Creep Deformation of Ni₃Al—Mo In Situ Composites. 987-998A
- Creep strength**
Creep—Fatigue Behavior of Directionally Solidified and Single Crystal Intermetallic Ni₃Al(B,Hf) at an Intermediate Temperature. 479-486A
Fatigue Crack Propagation Behavior of Titanium Alloys 6242S and 5621S at Elevated Temperature. 881-885A
- Creep strength, Alloying effects**
Effect of Antimony on the Creep Fracture of Stainless Steel. 571-577A
- Creep strength, Composition effects**
On the Effect of Carbide Precipitation During Creep of 304 and 316 Type Stainless Steels. 387-389A
- Creep strength, Temperature effects**
Design and Development of an Experimental Wrought Aluminum Alloy for Use at Elevated Temperatures. 1027-1035A
- Creep tests**
Creep Crack Growth Simulation Under Transient Stress Fields. 829-835A
Influence of Cyclic to Mean Load Ratio on Creep/Fatigue Crack Growth. 873-880A
- Creeping**
See Creep (materials)
- Critical temperature**
Premartensitic Anelasticity in Indium—Thallium Alloys. 789-792A
- Cross slip**
A15 Compound Deformation and Secondary Slip in V₃Si. 1125-1127A
Dislocation Network Formation and Coherency Loss Around Gamma-Prime Precipitates in a Nickel-Base Superalloy. 2965-2973A
- Cross slip, Alloying effects**
Effects of Cobalt Concentration on the Relative Resistance to Octahedral and Cube Slip in Nickel-Base Superalloys. 2733-2739A
- Cross tension test**
See Tension tests
- Crushing strength**
See Compressive strength
- Cryogenic temperature**
See Cryogenics
- Cryogenics**
The Effects of Heat Treatment and Cold Working on the Room-Temperature and Cryogenic Mechanical Properties of Fe—30Mn—9Al—0.9C Steel. 1873-1876A
- Cryolite, Solubility**
On the Solubility of Aluminum Carbide in Cryolitic Melts. 441-447B
On the Solubility of Aluminum in Cryolitic Melts. 449-457B
- Crystal defects**
See also Dislocations
Displacements (lattice)
Computer Study of Tweed as a Precursor to a Martensitic Transformation of a BCC Lattice. 783-787A
Diffusion Induced Grain Boundary Migration and Recrystallization During Oxidation of a Ni—48.5% Cu Alloy. 1667-1675A
A Finite Element Model of a Persistent Slip Band Based Upon Electron Microscopic Evidence. 2457-2465A
- Crystal defects, Cooling effects**
Effect of Rapid Solidification and Alloying Addition on Lattice Distortion and Atomic Ordering in L1₀ TiAl Alloys and Their Ternary Alloys. 2445-2455A
- Crystal growth**
See also Epitaxial growth
Structure and Mechanical Properties of Unidirectionally Solidified Fe—Cr—C and Fe—Cr—X—C Alloys. 1235-1241A
Containment of a Silicone Fluid Free Surface in Reduced Gravity. 1883-1888A
Isothermal Dendritic Growth—a Proposed Microgravity Experiment. 1945-1953A
- Crystal growth, Environmental effects**
Ground-Based Microgravity Materials Science Research at NASA's Microgravity Materials Science Laboratory. 1915-1917A
Meteorites as Specimens for Microgravity Research. 1919-1923A
- Crystal lattices**
See also Orthorhombic lattice
Solidification Structures in Rapidly Quenched Cu—Ti—Zr Alloys. 1853-1860A
- Crystal orientation**
See Crystal structure
- Crystal structure**
See also Equiaxed structure
Unit cell
Hematite Single Crystal Reduction Into Magnetite With CO—CO₂. 311-317B
Orientation Mapping. 403-408A
Computer Study of Tweed as a Precursor to a Martensitic Transformation of a BCC Lattice. 783-787A
The Nucleation of Iron on Dense Wustite: a Morphological Study. 787-802B
Microsegregation in Directionally Solidified Pb—8.4 at.% Au Alloy. 1351-1364A
Coupled Growth Zone in Fe—18Cr—C Alloys. 1367-1369A
Intercrystalline Structure Distribution in Polycrystalline Materials. 2611A
The Apparent "Five-Fold" Nature of Large T₂ (Al₃Li₂Cu) Crystals. 2875-2884A
Convergent Beam Electron Diffraction Analysis of the T₁ (Al₂CuLi) Phase in Al—Li—Cu Alloys. 2885-2891B
On the Morphology of the Modulated Precipitation of Extended Multiplets and Fe₃C₄ Epsilon or Eta Carbide Obtained by Aging and Tempering in Fe—C Martensite. 2901-2909A
Structure and Deformation Behavior of T₁ Precipitate Plates in an Al—2Li—1Cu Alloy. 2911-2920A
- Crystal structure, Heating effects**
The Effect of Matrix Strength on Void Nucleation and Growth in a Widmanstätten Alpha—Beta Titanium Alloy, Corona-5. 1163-1171A
- Crystallinity**
See Crystal structure
- Crystallization**
See also Recrystallization
Preparation of Iron-, Cobalt- and Nickel-Based Amorphous Alloy Powders by High-Pressure Gas Atomization and Their Structural Relaxation Behavior. 235-242A
Quasicrystalline Phase in Al—Si—Mn System Prepared by Annealing of Amorphous Phase. 383-385A

- Crystallization, Field effects**
Influence of Microgravity on the Morphology of the Directionally Solidified Front in an AISI Alloy. 2681-2686A
- Crystallization, Heating effects**
Amorphous Cr_2Si_3 Thin Films—Morphology and Kinetics of Crystallization. 1991-2003A
- Crystallization, Radiation effects**
Radiation Induced Crystallization of Amorphous Si:H Alloy. 1345-1349A
- Crystallization, Temperature effects**
Formation of Metal—Metal Type Aluminum-Based Amorphous Alloys. 1369-1371A
- Crystallography**
Orientation Mapping. 403-408A
Effect of Melt Spinning on Grain Size and Texture in Ni—Mo Alloys. 1711-1720A
Stage I Corrosion Fatigue Crack Crystallography in Austenitic Stainless Steel (316L). 2765-2773A
- Crystals**
See Single crystals
Whiskers (metals)
- Curie temperature**
Preparation of Iron-, Cobalt- and Nickel-Based Amorphous Alloy Powders by High-Pressure Gas Atomization and Their Structural Relaxation Behavior. 235-242A
- Current efficiency**
The Behavior of Thiourea and Flotation Reagents in Zinc Electrowinning Circuits. 187-199B
- Curves**
See Stress strain curves
TTT curves
- Cutting tools, Materials selection**
Niobium-Alloyed High Speed Steel by Powder Metallurgy. 1395-1401A
- Cyclic loads**
Influence of Cyclic to Mean Load Ratio on Creep/Fatigue Crack Growth. 873-880A
Dislocation Structures in the Strain Localized Region in Fatigued 85/15 Brass. 1257-1262A
Biaxial Path Dependence of Deformation Substructure of Type 304 Stainless Steel. 1277-1293A
- Czochralski process**
See Crystal growth
- D H process**
See Vacuum degassing
- Damage**
See also Radiation damage
Measuring Creep Damage Using Microradiography. 837-845A
- Damping**
Fluid Oscillation in the Drop Tower. 2625-2630A
- Decarburizing**
The Nucleation of Carbon Monoxide Bubbles in Molten Iron—Carbon Drops Reacting With Oxidizing Gases. 831-837B
- Decomposition**
See Eutectoid decomposition
Phase decomposition
Pyrolysis
Spinodal decomposition
- Decomposition reactions**
See Pyrolysis
- Deep drawability**
See Drawability
- Deep sea nodules**
See Sea nodules
- Defects**
See also Casting defects
Crystal defects
Dislocations
Displacements (lattice)
Surface defects
Weld defects
Effect of Geometrical Defects in Forming Sheet Steel by Biaxial Stretching. 2067-2074A
- Deflagration**
See Combustion
- Deformability**
See Formability
- Deformation**
See also Plastic deformation
Inelastic Deformation and Dislocation Structure of a Nickel Alloy: Effects of Deformation and Thermal Histories. 2477-2486A
- Deforming**
See Deformation
- Degassing**
See Vacuum degassing
- Dendrite**
See Dendritic structure
- Dendritic structure**
Columnar Dendritic Solidification in a Metal-Matrix Composite. 709-721A
Isothermal Dendritic Growth—a Proposed Microgravity Experiment. 1945-1953A
Dendritic Solidification of Alloys in Low Gravity. 2671-2676A
- Dendritic structure, Composition effects**
Study of Solidification Features of Nickel-Base Superalloys in Relation With Composition. 2333-2340A
- Dendritic structure, Cooling effects**
Dendritic Growth of Undercooled Nickel—Tin. III. 1109-1119A
Eutectic Structures of Ag—Cu After Melting and Solidification in Microgravity and on Earth. 2659-2664A
Dendritic Solidification in Binary Alloys. 3087-3096A
- Dendritic structure, Field effects**
Influence of Microgravity on the Morphology of the Directionally Solidified Front in an AISI Alloy. 2681-2686A
Gravitational Macrosegregation in Unidirectionally Solidified Lead—Tin Alloy. 2687-2694A
- Densification**
Kinetics of Neck Growth During Loose Stack Sintering. 2153-2161A
- Densification, Microstructural effects**
Densification of Titanium Powder During Hot Isostatic Pressing. 1767-1773A
- Density, Composition effects**
Densities of Pb—Sn Alloys During Solidification. 2349-2354A
- Density, Deformation effects**
Changes in the Longitudinal Flow and Apparent Plastic Poisson's Ratio of a Porous Metal Strip During Hot Densification Rolling. 1205-1211A
- Density, Microstructural effects**
Intercrystalline Structure Distribution in Alloy 304 Stainless Steel. 1179-1185A
- Density, Pressure effects**
Densification of Oxide Superconductors by Hot Isostatic Pressing. 1841-1847A
- Deoxidation**
See Deoxidizing
- Deoxidizing**
Measurement and Modeling of Alloy—Spinel—Corundum Equilibrium in the Ni—Mn—Al—O System at 1873K. 459-463B
- Dephosphorizing**
Determination of Standard Free Energies of Formation of Ca_3P_2 and Ca_2Sn at High Temperatures. 433-439B
The Calcium—Phosphorus and the Simultaneous Calcium—Oxygen and Calcium—Sulfur Equilibria in Liquid Iron. 617-622B
Thermodynamics of Ca— CaF_2 and Ca— CaCl_2 Systems for the Dephosphorization of Steel. 643-648B
- Deposition**
See Alloy plating
Chromating
Electrodeposition
Platinum plating
- Descaling**
Some Fundamental Aspects of Annealing and Pickling Stainless Steels. 1083-1100A
- Desorption**
Rate of Nitrogen Desorption From Liquid Iron—Carbon and Iron—Chromium Alloys With Argon. 233-242B
- Desorption, Deformation effects**
Wear-Enhanced Hydrogen Evolution From Mild Steel. 1721-1726A
- Desulfurizing**
Reaction Mechanism for the CaO —Al and CaO — CaF_2 Desulfurization of Carbon-Saturated Iron. 261-268B
- Deuterium, Physical properties**
Hydrogen in Iron. 691-707B
Hydrogen in Iron. 2371-2387A
- Development**
See Technology transfer
- Diagrams**
See Phase diagrams
- Diamond pyramid hardness**
Yield Stress as Determined From Hardness Measurements for Mechanically Alloyed Aluminum Base Alloys. 2363-2366A
- Die steel's, Alloy development**
An Approach to Developing an Alternative Hot Work Die Steel. 1751-1760A
- Dielectric constant**
Measurements of Dielectric Properties for Particulate Sphalerite Samples and Zinc Concentrates. 13-24B
- Diffraction**
See Electron diffraction
Neutron diffraction
X ray diffraction
- Diffraction patterns**
See Kikuchi lines
- Diffusion**
See also Thermal diffusion
Literature Survey on Diffusivities of Oxygen, Aluminum, and Vanadium in Alpha Titanium, Beta Titanium, and in Rutile. 1121-1125A
Diffusion Induced Grain Boundary Migration and Recrystallization During Oxidation of a Ni—48.5% Cu Alloy. 1667-1675A
Evaluation of the Effects of Segregation on Austenite Grain Boundary Energy in Fe—C—X Alloys. 1807-1818A
Surface Segregation in MCrAlY Alloys. 2099-2108A
The Kinetics of Intergranular Oxygen Penetration in Nickel and Its Relevance to Weldment Cracking. 2305-2313A
An Experimental Study and a Thermodynamic Evaluation of the Cr—Fe—W System. 2531-2546A

- Diffusion, Coating effects**
Evaluation of High-Temperature Diffusion Barriers for the Pt—Mo System. 2163-2170A
- Diffusion bonding**
See Diffusion welding
- Diffusion coefficient**
See Diffusion
- Diffusion couples**
See Diffusion
- Diffusion rate**
The Reaction Between Solid Iron and Liquid Al—Zn Baths. 1193-1203A
- Diffusion welding**
A Study of the Transient Liquid Phase Bonding Process Applied to a Ag/Cu/Ag Sandwich Joint. 675-686A
- Diffusivity**
Determination of the Diffusion Coefficients of CuSO_4 , ZnSO_4 , and NiSO_4 in Aqueous Solution. 5-12B
Hydrogen in Iron. 691-707B
Hydrogen in Iron. 2371-2387A
- Diffusivity, Alloying effects**
Change in Direction of Carbon Thermotransport in Nb—V System With Alloying. 1429-1435A
- Diffusivity, Coating effects**
Hydrogen Permeation Through Coated and Uncoated Waspaloy. 1187-1192A
- Diffusivity, Composition effects**
Solubility and Diffusion of Hydrogen in Vanadium—Oxygen Alloys. 67-72A
- Diffusivity, Pressure effects**
Effect of High Pressure on Interdiffusion in Cu—Zn Alloys at Temperatures Near the Melting Point. 467-471A
- Dimensional measurements**
See Thickness measurements
- Dimensional stability**
Gravity and Configurational Energy Induced Microstructural Changes in Liquid Phase Sintering. 1905-1913A
- Dimensions**
See Particle size
- Diodes**
Materials for Advanced Studies and Devices. 155-164B
Materials for Advanced Studies and Devices. 749-758A
- Dioxides**
See Carbon dioxide
Silicon dioxide
Titanium dioxide
- Dip coatings**
See Hot dip coatings
- Dipping**
See Hot dipping
- Direct reduction**
See Hydrogen reduction
- Directional solidification**
Structure and Mechanical Properties of Unidirectionally Solidified Fe—Cr—C and Fe—Cr—X—C Alloys. 1235-1241A
Microsegregation in Directionally Solidified Pb—8.4 at.% Au Alloy. 1351-1364A
Coupled Growth Zone in Fe—18Cr—C Alloys. 1367-1369A
Competitive Growth of Stable and Metastable Fe—C—X Eutectics. I. Experiments. 1955-1963A
Competitive Growth of Stable and Metastable Fe—C—X Eutectics. II. Mechanisms. 1965-1971A
- Directional solidification, Environmental effects**
Directional Solidification of Al—Ni/SiC Composites During Parabolic Trajectories. 1899-1904A
- Directionally solidified eutectics**
Creep Deformation of Ni_3Al —Mo In Situ Composites. 987-998A
- Discontinuous precipitates**
See Cellular precipitates
- Dishing**
See Bulging
- Dislocation climb**
See Dislocation mobility
- Dislocation density**
Investigation of Microstructural Changes in a Ferritic Steel Caused by High Temperature Fatigue. 999-1007A
Electron Microscope Study on Martensitic Transformations in Fe—Pt Alloys: General Features of Internal Structure. 2723-2731A
- Dislocation mobility**
A15 Compound Deformation and Secondary Slip in V_3Si . 1125-1127A
- Dislocation mobility, Alloying effects**
The Effect of Alloying Elements and Microstructure on the Strength and Fracture Resistance of Pearlitic Steel. 2819-2829A
- Dislocation mobility, Corrosion effects**
The Role of Dislocations During Transport of Hydrogen in Hydrogen Embrittlement of Iron. 2799-2803A
- Dislocation mobility, Diffusion effects**
Experimental Study of Hydrogen Transport During Plastic Deformation in Iron. 2789-2798A
- Dislocations**
Biaxial Path Dependence of Deformation Substructure of Type 304 Stainless Steel. 1277-1293A
- The Mechanism of Hydrogen Induced Cleavage in Fe—3% Si Alloy. 1335-1343A
- Inelastic Deformation and Dislocation Structure of a Nickel Alloy: Effects of Deformation and Thermal Histories. 2477-2486A
- Dislocation Network Formation and Coherency Loss Around Gamma-Prime Precipitates in a Nickel-Base Superalloy. 2965-2973A
- Dislocations, Microstructure**
Structure of a Small Angle Tilt Grain Boundary in Zinc. 2359-2363A
- Dispersion hardening alloys, Alloy development**
Materials for Advanced Studies and Devices. 155-164B
Materials for Advanced Studies and Devices. 749-758A
Niobium-Alloyed High Speed Steel by Powder Metallurgy. 1395-1401A
- Dispersion hardening alloys, Mechanical properties**
Elevated Temperature Creep—Fatigue Crack Propagation in Nickel-Base Alloys and 1Cr—Mo—V Steel. 855-862A
- Dispersion hardening alloys, Melting**
Melting and Solidification in Microgravity of Sintered Aluminum Powder Alloys. 2695-2703A
- Dispersions**
On the Formation of Dispersoids During Rapid Solidification of an Al—Fe—Ni Alloy. 1101-1107A
- Dispersoids**
See Dispersions
- Displacement spikes**
See Displacements (lattice)
- Displacements (lattice)**
Modulated Lattice Relaxation in β -Based Premartensitic Phase. 777-781A
- Dissimilar metals, Bonding**
A Study of the Transient Liquid Phase Bonding Process Applied to a Ag/Cu/Ag Sandwich Joint. 675-686A
- Dissociation energy**
See Free energy of formation
- Dissolution**
See also Anodic dissolution
Dissolution of Columbite and Tantalite in Acidic Fluoride Media. 355-363B
Dissolution Kinetics of Argentian Plumbojarosite From Old Tailings of Sulfatizing Roasting Pyrites by HCl— CaCl_2 Leaching. 365-373B
Dissolution Kinetics of Particulate Graphite Injected Into Iron/Carbon Melts. 375-382B
Equilibria Between the Rare Earth Elements, Oxygen and Sulfur in Molten Iron. 409-418B
On the Solubility of Aluminum Carbide in Cryolitic Melts. 441-447B
Analysis of Dissolution Rate of Metal Oxide in Acidic Chloride Solution in Terms of Water Activity. 505-507B
- Dissolving**
See Dissolution
- Distortion**
A Wrinkling Index for Press Forming. 2831-2837A
- Domains**
Quasi-One-Dimensional Model of Pretransitional Soft Mode Behavior. 811-818A
Kinetics of Domain Growth in Ordered Ni_4Mo . 941-952A
- Drawability**
The Variation of Plastic Anisotropy During Straining. 2805-2817A
- Drawing (heat treatment)**
See Tempering
- Drying**
A Dynamic Mathematical Model of the Complete Grate/Kiln Iron-Ore Pellet Induration Process. 103-112B
Gas Flow and Pressure Balancing in Modeling Grate/Kiln Induration. 113-121B
Energy Cost Minimization in Grate/Kiln Induration. 123-132B
- Dual phase steels, Heat treatment**
Intercritical Annealing as a Means of Improving Impact Properties of Plate Steel. 1481-1490A
- Dual phase steels, Mechanical properties**
Effects of Transformed Ferrite Growth on the Tensile Fracture Characteristics of a Dual-Phase Steel. 309-317A
Void Formation During Tensile Testing of Dual Phase Steels. 579-589A
The Influence of Mo_2C Morphology and Distribution on the Fatigue Crack Initiation and Propagation Behavior of Fe—C—Mo Dual-Phase Steels. 973-986A
Modeling Tensile Deformation of Dual-Phase Steel. 1263-1268A
The Law of Mixtures Applied to the Plastic Deformation of Two-Phase Alloys of Coarse Microstructures. 2027-2040A
- Dual phase steels, Microstructure**
Statistical Considerations on Uniform Grain Size. 2937-2944A
- Dual phase steels, Structural hardening**
Orowan Strengthening by Mo_2C Fibers and Needle Interphase Precipitates in Fe—C—Mo Dual-Phase Steels. 1617-1620A
- Ductile brittle transition**
Mechanistic Similarities Between Hydrogen and Temperature Effects on the Ductile-to-Brittle Transition of a Stainless Steel. 1547-1553A
- Ductile fracture**
The Effect of Matrix Strength on Void Nucleation and Growth in an Alpha—Beta Titanium Alloy, Corona-5. 591-601A
- Ductile fracture, Deformation effects**
The Mechanism of Hydrogen Induced Cleavage in Fe—3% Si Alloy. 1335-1343A

- Ductile fracture, Microstructural effects**
Correlations of Microstructure With Dynamic and Quasi-Static Fracture in a Plain Carbon Steel. 2179-2206A
- Ductile iron**
See Nodular iron
- Ductility**
Crack Growth From Internal Hydrogen—Temperature and Microstructural Effects in 4340 Steel. 1319-1334A
- Ductility, Alloying effects**
Hydrogen Embrittlement of Pseudobinary $L1_2$ -Type $Ni_3(Al, Mn, a)$ Intermetallic Compound. 353-357A
Effect of Antimony on the Creep Fracture of Stainless Steel. 571-577A
- Ductility, Composition effects**
High Temperature Strength and Ductility of Recrystallized Ni_3Al — Ni_3Mn Alloys. 345-352A
Effects of Oxygen and Heat Treatment on the Mechanical Properties of Alpha and Beta Titanium Alloys. 527-542A
- Ductility, Diffusion effects**
Effect of Cathodic Charging on the Mechanical Properties of Aluminum. 2299-2304A
- Ductility, Heating effects**
The Effects of Austenitization Temperature on the High Temperature Ductility of Fe—P—S Alloys. 887-892A
Effect of Single Aging on Stress Corrosion Cracking Susceptibility of Inconel X-750 Under PWR Conditions. 1295-1304A
- Ductility, Microstructural effects**
Porosity and Tensile Ductility in Al—Zn Alloys. 517-526A
The Effect of Triaxial Stress Field on Intermediate Temperature Embrittlement of Ferritic Spheroidal Graphite Cast Irons. 1213-1219A
Modeling Tensile Deformation of Dual-Phase Steel. 1263-1268A
- Ductility, Stress effects**
Test Temperature and Strain Rate Effects on the Properties of a Tungsten Heavy Alloy. 487-494A
- Ductility, Temperature effects**
The Effect of Tin, Aluminum, and Nitrogen on the Hot Ductility of a Carbon—Manganese Steel Between 700-1200°C. 1305-1309A
- Dump leaching**
Speciation and Reduction Potentials of Metal Ions in Concentrated Chloride and Sulfate Solutions Relevant to Processing Base Metal Sulfides. 37-45B
- Duomelt process**
See Vacuum arc melting
- Duplex stainless steels, Corrosion**
Cracking Kinetics of Two-Phase Stainless Steel Alloys in Hydrogen Gas. 145-152A
- Duplex stainless steels, Mechanical properties**
Effects of Water Vapor on Hydrogen Induced Slow Crack Growth in Stainless Steels. 651-656A
The Law of Mixtures Applied to the Plastic Deformation of Two-Phase Alloys of Coarse Microstructures. 2027-2040A
- Duplex stainless steels, Melting**
The Partitioning of Alloying Elements in Vacuum Arc Remelted, Palladium-Modified PH 13-8 Molybdenum Alloys. 3063-3069A
- Dynamics**
See Fluid dynamics
Hydrodynamics
Kinetics
- Economics**
An Investigation of Carbonaceous Materials Reducing Ferric Ions in Aqueous Solution. 709-717B
- Efficiency**
See Current efficiency
- Elastic anisotropy**
Modeling of the Plastic Anisotropy of Textured Sheet. 105-120A
- Elastic constants**
See also Elastic anisotropy
Modulus of elasticity
- Elastic constants, Heating effects**
Elastic Properties of β -Uranium and the Martensitic α' -Phase in Uranium—Gallium Alloys. 909-913A
- Elastic modulus**
See Modulus of elasticity
- Elastic properties**
See Elastic constants
- Electric arc melting**
See Vacuum arc melting
- Electric arc welding**
See Arc welding
- Electric assemblies**
See Electric devices
- Electric components**
See Electric devices
- Electric conductors (materials)**
See Electrolytes
Superconductors
- Electric connectors, Mechanical properties**
Cyclic Deformation and Fracture in Pb—Sn Solid Solution Alloy. 1533-1546A
- Electric devices, Service life**
Inhibition of Cyclic Grain Boundary Migration Through Cellular Precipitation in Pb—5% Sn Alloy. 2355-2359A
- Electric motors**
Analytical Electron Microscopy of Internally Oxidized Low Si—Al Steel. 953-959A
- Electric potential**
Application of the dc Potential Drop Technique in Investigating Crack Initiation and Propagation Under Sustained Load in Notched Rupture Tests. 863-871A
- Electric power generation**
See Nuclear power generation
- Electric welding**
See Arc welding
Gas tungsten arc welding
Projection welding
Shielded arc welding
Shielded metal arc welding
- Electrical conductivity**
See Resistivity
- Electrical phenomena**
See Electric potential
- Electrical properties**
See Dielectric constant
Resistivity
- Electrical resistivity**
See Resistivity
- Electrical steels, Oxidation**
Analytical Electron Microscopy of Internally Oxidized Low Si—Al Steel. 953-959A
- Electrochemistry**
Predicting the Kinetics of Hydrogen Generation at the Tips of Corrosion Fatigue Cracks. 1795-1806A
- Electrocoatings**
See Electroplating
- Electrodeposition**
Coating of Graphite Fibers With Tungsten Carbide Using Solid and Liquid Copper as a Transfer Medium. 2109-2113A
- Electrolysis**
See Electrowinning
Hall Heroult process
- Electrolytes**
Determination of the Diffusion Coefficients of $CuSO_4$, $ZnSO_4$, and $NiSO_4$ in Aqueous Solution. 5-12B
An Investigation of Carbonaceous Materials Reducing Ferric Ions in Aqueous Solution. 709-717B
- Electrolytes, Electrical properties**
Electrical Conductivity of Acidic Chloride Solutions. 53-58B
- Electrolytic deposition**
See Electrodeposition
- Electrolytic dissolution**
See Anodic dissolution
- Electrolytic pickling**
See Pickling
- Electromagnetic fields**
Observations on the Dynamics of Electromagnetically Levitated Liquid Metals and Alloys at Elevated Temperatures. 1939-1943A
- Electromagnetic induction**
Mathematical Modeling of Meniscus Profile and Melt Flow in Electromagnetic Casters. 397-408B
- Electromagnetic stirring**
On the Flow Criteria for Suspending Solid Particles in Inductively Stirred Melts. I. Newtonian Behavior. 557-562B
Flow Fields in Electromagnetic Stirring of Rectangular Strands With Linear Inductors. I. Theory and Experiments With Cold Models. 581-593B
Flow Fields in Electromagnetic Stirring of Rectangular Strands With Linear Inductors. II. Computation of Flow Fields in Billets, Blooms, and Slabs of Steel. 595-602B
Experimental Measurement and Numerical Computation of Velocity and Turbulence Parameters in a Heated Liquid Metal System. 765-775B
- Electromotive force**
See Electric potential
- Electron beams**
Acoustic Emission Studies of Electron Beam Surface Modification of Aluminum. 493-503B
- Electron diffraction**
Electron Diffraction Study of α - and α' -AlFeSi. 893-898A
- Electron microscopy**
See also Transmission electron microscopy
Low Temperature Electron Microscopy on the Cubic-Tetragonal Transformation of V_3Si . 797-801A
Analytical Electron Microscopy of Internally Oxidized Low Si—Al Steel. 953-959A
- Electron-phonon interactions**
Electron—Phonon Based Local Mode Descriptions of Displacive Transformations. 177-183A
- Electron spectroscopy**
See Auger electron spectroscopy
- Electronic assemblies**
See Electric devices
- Electronic components**
See Electric devices

Electronic devices

Electronic devices

See Electric devices

Electroplates, Mechanical properties

Pulsed Electrodeposition of Layered Brass Structures.

1569-1573A

Electropotential

See Electric potential

Electroreduction

See Electrowinning

Electrorefining

Determination of the Diffusion Coefficients of CuSO_4 , ZnSO_4 , and NiSO_4 in Aqueous Solution.

5-12B

Electrowinning

See also Hall Heroult process

Determination of the Diffusion Coefficients of CuSO_4 , ZnSO_4 , and NiSO_4 in Aqueous Solution.

5-12B

Electrical Conductivity of Acidic Chloride Solutions.

53-58B

Direct Electrowinning of Lead From Suspension Galena Concentrate Anode in Different Electrolytes.

59-65B

Bed Performance in the Direct Electrowinning of Lead From Suspension Galena Anodes.

67-72B

The Behavior of Thiourea and Flotation Reagents in Zinc Electrowinning Circuits.

187-199B

On the Solubility of Aluminum in Cryolitic Melts.

449-457B

An Investigation of Carbonaceous Materials Reducing Ferric Ions in Aqueous Solution.

709-717B

An Electrochemical Study of the Surface Oxidation of Arsenopyrite in Alkaline Media.

943-949B

Electrowinning, Impurity effects

The Effects of Mg^{2+} , Mn^{2+} , Zn^{2+} , and Al^{3+} on the Nickel Deposit During Electrowinning From Sulfate Bath.

823-830B

Elevated temperature

See High temperature

Ellipsometers

See Polarimeters

Elongation

The Effect of Triaxial Stress Field on Intermediate Temperature Embrittlement of Ferritic Spheroidal Graphite Cast Irons.

1213-1219A

Elongation, Alloying effects

Aluminum—Lithium Powder Metallurgy Alloys With Improved Toughness.

603-615A

Elongation, Composition effects

High Temperature Strength and Ductility of Recrystallized Ni_3Al — Ni_3Mn Alloys.

345-352A

Elongation, Deformation effects

Effect of the Thermomechanical Treatments on Size and Distribution of Silicides and Tensile Properties of Alloy Ti—6Al—5Zr—0.5Mo—0.25Si.

389-391A

Elongation, Diffusion effects

Hydrogen Effects in [001] Oriented Nickel-Base Superalloy Single Crystals.

73-82A

Elongation, Heating effects

Development of High Toughness in Austempered Type Ductile Cast Iron and Evaluation of Its Properties.

319-327A

The Effects of Heat Treatment and Cold Working on the Room-Temperature and Cryogenic Mechanical Properties of Fe—30Mn—9Al—0.9C Steel.

1873-1876A

Elongation, Microstructural effects

Structure and Mechanical Properties of Unidirectionally Solidified Fe—Cr—C and Fe—Cr—X—C Alloys.

1235-1241A

Elongation, Stress effects

The Mechanical Properties of the Superplastic Al—33Cu Eutectic Alloy.

2487-2496A

Elongation, Temperature effects

Tensile and Impact Properties Changes of Hastelloy X After Exposure in High-Temperature Helium Environment.

1269-1275A

Embrittlement

See also Hydrogen embrittlement

The Effect of Triaxial Stress Field on Intermediate Temperature Embrittlement of Ferritic Spheroidal Graphite Cast Irons.

1213-1219A

Embrittlement, Composition effects

The Effect of Tin, Aluminum, and Nitrogen on the Hot Ductility of a Carbon—Manganese Steel Between 700-1200°C.

1305-1309A

Embrittlement, Heating effects

The Effect of Aging on the Fracture Behavior of Cu—Al—Ni β Phase Alloys.

1761-1766A

Emission

See Acoustic emission

Emissivity

Measurement of Temperature and Emissivity of Specularly Reflecting Glowing Bodies.

1889-1894A

Endurance (testing)

See Fatigue tests

Energy

See Activation energy

Free energy

Free energy of formation

Free energy of solution

Heat of activation

Heat of formation

Heat of mixing

Heat of reaction

Heat of solution

Stacking fault energy

Surface energy

Energy conservation

Gas Flow and Pressure Balancing in Modeling Grate/Kiln Induration.

113-121B

Energy Cost Minimization in Grate/Kiln Induration.

123-132B

Processing Effects in Spray Casting of Steel Strip.

3077-3086A

Energy consumption

See also Fuel consumption

Bed Performance in the Direct Electrowinning of Lead From Suspension Galena Anodes.

67-72B

Energy of activation

See Activation energy

Energy of dissociation

See Free energy of formation

Energy of formation

See Free energy of formation

Energy of fracture

See Toughness

Energy of solution

See Free energy of solution

Energy storage

See Hydrogen storage

Engineering

See Technology transfer

Enrichment

Evaluation of the Effects of Segregation on Austenite Grain Boundary Energy in Fe—C—X Alloys.

1807-1818A

Enthalpy

Discussion of "Physical Chemistry of Gas Liquid Solder Reactions" and Reply.

513-514B

Thermochemistry of the Intermetallic Compounds RuTi , RuZr , and RuHf .

1061-1066A

Standard Enthalpies of Formation of PtTi , PtZr , and PtHf .

1827-1831A

Enthalpies of Formation of the Ag—Au—Si, Ag—Au—Ge, and Ag—Au—Sn Ternary Liquid Alloys: Experimental Determinations and Application of the Hoch—Arpshofen Model.

2075-2089A

Enthalpy, Cooling effects

Enthalpies of a Binary Alloy During Solidification.

3057-3061A

Entropy

See also Entropy of solution

On the Slopes of Phase Boundaries.

1819-1825A

Entropy of solution

The Solubility of Hydrogen in Liquid Binary Al—Li Alloys.

227-232B

Environment

See Marine environments

Space environment

Epitaxial growth, Field effects

A Proposal for Epitaxial Thin Film Growth in Outer Space.

2639-2643A

Equiaxed structure, Cooling effects

Dendritic Solidification in Binary Alloys.

3087-3096A

Equiaxed structure, Field effects

Directional Solidification of Cu—Pb and Bi—Ga Monotectic Alloys Under Normal Gravity and During Parabolic Flight.

2839-2846A

Equilibrium diagrams

See Phase diagrams

Erosion rate, Composition effects

Erosion of Fiber Reinforced Al—4% Cu Composites.

1785-1793A

Eutectic composition, Alloying effects

Competitive Growth of Stable and Metastable Fe—C—X Eutectics. I. Experiments.

1955-1963A

Competitive Growth of Stable and Metastable Fe—C—X Eutectics. II. Mechanisms.

1965-1971A

Eutectic reactions

Competitive Growth of Stable and Metastable Fe—C—X Eutectics. I. Experiments.

1955-1963A

Eutectics

See also Directionally solidified eutectics

Eutectics, Directional solidification

Eutectic Growth: Selection of Interlamellar Spacings.

2955-2964A

Eutectics, Mechanical properties

The Mechanical Properties of the Superplastic Al—33Cu Eutectic Alloy.

2487-2496A

Eutectics, Microstructure

Eutectic Structures of Ag—Cu After Melting and Solidification in Microgravity and on Earth.

2659-2664A

Eutectoid decomposition

Beta-Eutectoid Decomposition in Rapidly Solidified Titanium—Nickel Alloys.

23-33A

Eutectoid reactions

See also Eutectoid decomposition

The Kinetics of Ferrite Nucleation at Austenite Grain Boundaries in Fe—C Alloys.

427-440A

Eutectoids, Mechanical properties

Preparation and Properties of Fine Grain β -CuAlNi Strain-Memory Alloys.

2921-2929A

Exothermic reactions

See Silicothermic reactions

- Exploding wires**
Reactivity of Al—2.5% Li Alloy With Water as Studied by the Exploding Wire Technique. 255-259B
- Explosions**
Thermal Explosions Resulting From Fuel—Coolant Interactions: Analysis of Single Bubble Hydrodynamics. 563-570B
- Exposure**
Tensile and Impact Properties Changes of Hastelloy X After Exposure in High-Temperature Helium Environment. 1269-1275A
- Extractive metallurgy**
See also Hydrometallurgy
The Mathematical Modeling Revolution in Extractive Metallurgy. 525-540B
- Extrusion**
See Hot extrusion
See Compacting
- Face centered cubic metals**
See FCC metals
- Face centered orthorhombic lattice**
See Orthorhombic lattice
- Failure analysis**
See Fractography
- Fatigue (materials)**
See also Corrosion fatigue
Fatigue life
Fatigue strength
Low cycle fatigue
Growth of Slip Bands During Fatigue of 6061-T6 Aluminum. Effect of Environment and Grain Size on Cyclic Deformation and Surface Hardening of Iron. 83-91A
Microstructural Observations in Cyclically Deformed Pb—Sn Solid Solution Alloy. 337-344A
1437-1443A
- Fatigue (materials), Environmental effects**
Chemical and Metallurgical Aspects of Environmentally Assisted Fatigue Crack Growth in 7075-T651 Aluminum Alloy. 1739-1750A
- Fatigue (materials), High temperature effects**
The Effect of Tempering Temperature on Near-Threshold Fatigue Crack Behavior in Quenched and Tempered 4140 Steel. 2497-2502A
- Fatigue (materials), Microstructural effects**
Near-Threshold Fatigue Crack Growth in Copper and Alpha-Brass: Grain-Size and Environmental Effects. 2575-2587A
- Fatigue cracking**
See Fatigue (materials)
- Fatigue failure**
Fatigue Crack Propagation in Aluminum—Lithium Alloy 2090. I. Long Crack Behavior. 549-561A
Fatigue Crack Propagation in Aluminum—Lithium Alloy 2090. II. Small Crack Behavior. 563-569A
Elevated Temperature Creep—Fatigue Crack Propagation in Nickel-Base Alloys and 1Cr—Mo—V Steel. 855-862A
Isothermal Fatigue of Low Tin Lead Based Solder. 1051-1059A
Fatigue Damage Accumulation in Nickel Modified by Ion Beam Surface Microalloying. 2775-2788A
- Fatigue failure, Environmental effects**
Fatigue Crack Propagation Behavior of Titanium Alloys 6242S and 5621S at Elevated Temperature. 881-885A
- Fatigue failure, High temperature effects**
Cyclic Deformation and Fracture in Pb—Sn Solid Solution Alloy. 1533-1546A
- Fatigue failure, Microstructural effects**
The Influence of Mo₂C Morphology and Distribution on the Fatigue Crack Initiation and Propagation Behavior of Fe—C—Mo Dual-Phase Steels. 973-986A
The Effect of Microstructure on the Fatigue Crack Growth Behavior of Age-Hardened High Strength Steels in a Corrosive Environment. 1461-1469A
- Fatigue failure, Temperature effects**
The Thermal Activation Energy for Fatigue of Fe—1Cr—0.5Mo. 2979-2987A
- Fatigue fracture**
See Fatigue failure
- Fatigue life**
Creep—Fatigue Life Prediction in Terms of Nucleation and Growth of Fatigue Crack and Creep Cavities. 121-127A
Creep—Fatigue Behavior of Directionally Solidified and Single Crystal Intermetallic Ni₃Al(B,Hf) at an Intermediate Temperature. 479-486A
Investigation of Microstructural Changes in a Ferritic Steel Caused by High Temperature Fatigue. 999-1007A
Isothermal Fatigue of Low Tin Lead Based Solder. 1051-1059A
The Role of Hydrogen in Corrosion Fatigue of High Purity Al—Zn—Mg Exposed to Water Vapor. 1775-1783A
Inhibition of Cyclic Grain Boundary Migration Through Cellular Precipitation in Pb—5% Sn Alloy. 2355-2359A
- Fatigue life, Microstructural effects**
Preparation and Properties of Fine Grain β -CuAlNi Strain-Memory Alloys. 2921-2929A
- Fatigue life, Temperature effects**
Influence of Time and Temperature Dependent Processes on Strain Controlled Low Cycle Fatigue Behavior of Alloy 617. 359-371A
- Fatigue properties**
See Fatigue (materials)
- Fatigue strength**
Creep—Fatigue Behavior of Directionally Solidified and Single Crystal Intermetallic Ni₃Al(B,Hf) at an Intermediate Temperature. 479-486A
Fatigue Crack Propagation Behavior of Titanium Alloys 6242S and 5621S at Elevated Temperature. 881-885A
- Fatigue strength, Heating effects**
Fatigue Strength Improvement of Age-Hardened 18Ni Maraging Steel by Stress-Laser Surface Treatment of Subsequent Aging. 2603-2606A
- Fatigue strength, Microstructural effects**
Crack Initiation and Near-Threshold Surface Fatigue Crack Propagation Behavior of the Iron-Base Superalloy A-286. The Effect of Microstructure on the Fatigue Crack Growth Behavior of Age-Hardened High Strength Steels in a Corrosive Environment. 301-308A
1461-1469A
- Fatigue tests**
Biaxial Path Dependence of Deformation Substructure of Type 304 Stainless Steel. 1277-1293A
- FCC metals, Mechanical properties**
The Absence of Steady-State Flow During Large Strain Plastic Deformation of Some FCC Metals at Low and Intermediate Temperatures. 3013-3024A
- Ferric compounds**
See Iron compounds
- Ferrite, Crystal growth**
Effect of Deformation on the Austenite-to-Ferrite Transformation in a Plain Carbon and Two Microalloyed Steels. The Kinetics of Ferrite Nucleation at Austenite Grain Boundaries in Fe—C Alloys. 417-426A
427-440A
- Ferrites**
The Mechanism of Ferrite Formation From Iron Sulfides During Zinc Roasting. 777-785B
The Evidence for a Miscibility Gap in the Fe₃O₄—ZnFe₂O₄ System—a Review. 919-925B
- Ferrites, Reactions (chemical)**
On the Interfacial Rate of Reaction of CO₂ With a Calcium Ferrite Melt. 959-965B
- Ferritic stainless steels, Mechanical properties**
Effects of Water Vapor on Hydrogen Induced Slow Crack Growth in Stainless Steels. 651-656A
Investigation of Microstructural Changes in a Ferritic Steel Caused by High Temperature Fatigue. 999-1007A
- Ferromagnetic materials**
See Magnetite
- Ferrous alloys**
See also Alloy steels
Cast iron
Steels
- Ferrous alloys, Casting**
Structure and Mechanical Properties of Unidirectionally Solidified Fe—Cr—C and Fe—Cr—X—C Alloys. 1235-1241A
- Ferrous alloys, Directional solidification**
Dendritic Solidification of Alloys in Low Gravity. 2671-2676A
- Ferrous alloys, Mechanical properties**
Crack Initiation and Near-Threshold Surface Fatigue Crack Propagation Behavior of the Iron-Base Superalloy A-286. Elevated Temperature Creep—Fatigue Crack Propagation in Nickel-Base Alloys and 1Cr—Mo—V Steel. 301-308A
855-862A
The Mechanism of Hydrogen Induced Cleavage in Fe—3% Si Alloy. 1335-1343A
The Effects of Heat Treatment and Cold Working on the Room-Temperature and Cryogenic Mechanical Properties of Fe—30Mn—9Al—0.9C Steel. 1873-1878A
Characterization of Residual Stresses in Bent Incoloy-800 Tubing by Neutron Diffraction. 2207-2214A
- Ferrous alloys, Microstructure**
Discussion of "Microdistribution of Cerium in Steel" and Author's Reply. 723A
Measuring Creep Damage Using Microradiography. 837-845A
Evaluation of the Effects of Segregation on Austenite Grain Boundary Energy in Fe—C—X Alloys. 1807-1818A
Meteorites as Specimens for Microgravity Research. 1919-1923A
Grain Boundary Segregation of Sulfur and Antimony in Iron Alloys. 2005-2011A
- Ferrous alloys, Oxidation**
Rutherford Backscattering Study of High Temperature Oxidation of Melt-Spun Glassy Fe—22.5Al—10Zr. 2567-2573A
- Ferrous alloys, Phase transformations**
Electron Diffuse Scattering Studies of Premartensitic Alloys: β Cu—Zn, β Ni—Al, In—Ti, and Fe—Ni. 199-205A
Tweed Structures Associated With FCC—FCT Transformations in Fe—Pd Alloys. 803-810A
Coupled Growth Zone in Fe—18Cr—C Alloys. 1367-1369A
- Ferrous alloys, Physical properties**
Hydrogen in Iron. 691-707B
Hydrogen in Iron. 2371-2387A
- Ferrous alloys, Powder technology**
Melting Metal Powder Particles in an Inductively Coupled R.F. Plasma Torch. 213-226B
Preparation of Iron-, Cobalt- and Nickel-Based Amorphous Alloy Powders by High-Pressure Gas Atomization and Their Structural Relaxation Behavior. 235-242A
Formation of Ultra-Fine Amorphous Powders in Fe—M—B (M = Transition Metal) Systems by Chemical Reduction Method and Their Thermal and Magnetic Properties. 2315-2318A

Ferrous alloys

- Mechanical Alloying of Brittle Materials.**
Texture Induced Magnetic Anisotropy in Fe—Nd—B Magnet Prepared via Rapid Solidification and Hot Extrusion Techniques. 2867-2874A
- Ferrous alloys, Solubility**
Thermodynamics of Nitrogen in CaO—SiO₂—Al₂O₃ Slags and Its Reaction With Fe—C_{sat} Melts. 419-425B
- Ferrous alloys, Sorption**
Rate of Nitrogen Desorption From Liquid Iron—Carbon and Iron—Chromium Alloys With Argon. 233-242B
- Ferrous alloys, Structural hardening**
Coarsening and Morphology of β' Particles in Fe—Ni—Al—Mo Ferritic Alloys.
On the Morphology of the Modulated Precipitation of Extended Multiplets and Fe₃C₂ Epsilon or Eta Carbide Obtained by Aging and Tempering in Fe—C Martensite. 1135-1146A
2901-2909A
- Ferrous alloys, Surface properties**
Surface Tension of Binary Metal—Surface Active Solute Systems Under Conditions Relevant to Welding Metallurgy.
Surface Segregation in MCRAI Alloys. 483-491B
2099-2108A
- Ferrous alloys, Welding**
An Analytical Electron Microscope Investigation of the Phase Transformations in a Simulated Heat-Affected Zone in Alloy 800.
Consolidation of Metallic Glass Ribbons Using Electric Discharge Welding. 35-50A
1634-1638A
- Ferrous compounds**
See Iron compounds
- Ferrous metals**
See Ferrous alloys
- Fiber composites**
Directional Solidification of Cu—Pb and Bi—Ga Monotectic Alloys Under Normal Gravity and During Parabolic Flight. 2839-2846A
- Fiber composites, Crystal growth**
Columnar Dendritic Solidification in a Metal-Matrix Composite. 709-721A
- Fiber composites, Mechanical properties**
Transverse Elastic Moduli of Unidirectional Fiber Composites With Interfacial Debonding.
A Computer Simulation on Tensile Strength of Metal Matrix Composites Reinforced With Surface-Damaged Fibers.
A Computer Simulation on Tensile Strength of Surface-Damaged Fibers.
Erosion of Fiber Reinforced Al—4% Cu Composites. 129-135A
1491-1497A
1499-1506A
1785-1793A
- Fiber metallurgy**
See Mechanical alloying
- Fibers**
See also Carbon fibers
Whiskers (metals)
- Fibers, Mechanical properties**
A Computer Simulation on Tensile Strength of Surface-Damaged Fibers. 1499-1506A
- Fields (physics)**
See Electromagnetic fields
- Films**
See Thin films
- Finish rolling**
Evaluation of the Fracture Toughness of Hot-Rolled Low-Alloy Ti—V Plate Steel. 505-516A
- Finishing**
See Descaling
- Finite element method**
Creep Crack Growth Simulation Under Transient Stress Fields.
Effect of Temperature and Strain Distribution on Martensitic Transformation During Uniaxial Testing of AISI-304 Stainless Steel.
Elastic Interaction Stresses. I. The Influence of Bicrystal Size on Stresses in [213] Iso-Axial 70-30 Alpha-Brass Bicrystals.
A Finite Element Model of a Persistent Slip Band Based Upon Electron Microscopic Evidence.
The Nucleation of High Temperature Brittle Intergranular Fracture in 2.25Cr—1Mo Steel. 829-835A
1021-1026A
1727-1737A
2457-2465A
3005-3011A
- Flakes, Phase transformations**
Beta-Eutectoid Decomposition in Rapidly Solidified Titanium—Nickel Alloys. 23-33A
- Flame descaling**
See Descaling
- Flash smelting**
Oxidation of Molten Copper Matte.
Process Mineralogy of Suspended Particles From a Simulated Commercial Flash Smelter.
The Trajectories and Distribution of Particles in a Turbulent Axisymmetric Gas Jet Injected Into a Flash Furnace Shaft. 47-52B
719-729B
871-884B
- Flaw detection**
See Ultrasonic testing
- Flaws**
See Defects
- Flexural vibration**
See Fatigue (materials)
- Flotation**
Mineralogical Characterization of Silver Flotation Concentrates Made From Zinc Neutral Leach Residues. 803-817B
- Flow**
See Fluid flow
Gas flow
Liquid flow
- Flow measurement**
Changes in the Longitudinal Flow and Apparent Plastic Poisson's Ratio of a Porous Metal Strip During Hot Densification Rolling. 1205-1211A
- Flow stress**
See Yield strength
- Fluid bed roasting**
See Fluidized bed roasting
- Fluid dynamics**
See also Hydrodynamics
Fluid Dynamics in Bubble Stirred Ladies. I. Experiments.
Fluid Dynamics in Bubble Stirred Ladies. II. Mathematical Modeling.
Experimental Study of Thermocapillary Flows in a Thin Liquid Layer With Heat Fluxes Imposed on the Free Surface.
The Bubble, Drop, and Particle Unit (BDPU). 745-754B
755-764B
1895-1898A
1925-1929A
- Fluid flow**
See also Gas flow
Liquid flow
Convective Heat-Transfer Measurements in Liquid Metals Under Different Fluid Flow Conditions. 859-870B
- Fluid mechanics**
See also Fluid dynamics
Hydrodynamics
Fluid Dynamics in Channel Reactors Stirred by Submerged Gas Injection. 603-612B
- Fluidity**
See Viscosity
- Fluidized bed roasting**
The Mechanism of Ferrite Formation From Iron Sulfides During Zinc Roasting. 777-785B
- Fluorine**
Dissolution of Columbite and Tantalite in Acidic Fluoride Media. 355-363B
- Fluosolids roasting**
See Fluidized bed roasting
- Focussons**
See Displacements (lattice)
- Force**
See Cyclic loads
- Forehearth**
See Holding furnaces
- Formability**
Effect of Geometrical Defects in Forming Sheet Steel by Biaxial Stretching. 2067-2074A
- Formability, Anisotropy**
The Variation of Plastic Anisotropy During Straining. 2805-2817A
- Formability, Microstructural effects**
The Effect of Grain Size on the Bulk Formability and Tensile Properties of Austenitic Stainless Steel Types 304 and 316. 2287-2298A
- Forming**
See Bending
Bulging
Finish rolling
Hot extrusion
Hot isostatic pressing
Hot pressing
Hot rolling
Press forming
Stamping
Stretch forming
Thermomechanical treatment
- Forms (molds)**
See Molds
- Fractography**
Quantitative Fractography: a Modern Perspective.
Stage I Corrosion Fatigue Crack Crystallography in Austenitic Stainless Steel (316L). 961-971A
2765-2773A
- Fracture mechanics**
Creep—Fatigue Life Prediction in Terms of Nucleation and Growth of Fatigue Crack and Creep Cavities.
Investigation of Panel Crack Formation in Steel Ingots. II. Off-Corner Panel Cracks.
Fatigue Crack Propagation in Aluminum—Lithium Alloy 2090. I. Long Crack Behavior.
Fatigue Crack Propagation in Aluminum—Lithium Alloy 2090. II. Small Crack Behavior.
Influence of Cyclic to Mean Load Ratio on Creep/Fatigue Crack Growth.
Quantitative Fractography: a Modern Perspective.
Modeling the Texture Dependence of Environmentally Assisted Growth of Long and Short Cracks.
Isothermal Fatigue of Low Tin Lead Based Solder.
Corrosion Fatigue Crack Initiation in a Mode II Notch Specimen.
Chemical and Metallurgical Aspects of Environmentally Assisted Fatigue Crack Growth in 7075-T651 Aluminum Alloy. 121-127A
289-301B
549-561A
563-569A
873-880A
961-971A
1009-1020A
1051-1059A
1067-1073A
1739-1750A
- Fracture mechanics, Microstructural effects**
The Effect of Alloying Elements and Microstructure on the Strength and Fracture Resistance of Pearlitic Steel. 2819-2829A

- Fracture strength, Alloying effects**
A Preliminary Study of the Influence of Separate and Combined Aluminum and Nickel Additions on the Properties of a Secondary Hardening Steel. 3103-3107A
- Fracture strength, Microstructural effects**
The Effect of Alloying Elements and Microstructure on the Strength and Fracture Resistance of Pearlitic Steel. 2819-2829A
Preparation and Properties of Fine Grain β -CuAlNi Strain-Memory Alloys. 2921-2929A
- Fracture strength, Stress effects**
Test Temperature and Strain Rate Effects on the Properties of a Tungsten Heavy Alloy. 487-494A
- Fracture toughness**
Fatigue Crack Propagation in Aluminum—Lithium Alloy 2090. I. Long Crack Behavior. 549-561A
Correlation of Mechanical and Ultrasonic Properties of Al—SiC Metal-Matrix Composite. 2233-2246A
- Fracture toughness, Alloying effects**
Aluminum—Lithium Powder Metallurgy Alloys With Improved Toughness. 603-615A
An Approach to Developing an Alternative Hot Work Die Steel. 1751-1760A
- Fracture toughness, Cryogenic effects**
Cleavage-Like Fracture Along Slip Planes in Fe—18Cr—3Ni—13Mn—0.37N Austenitic Stainless Steel at Liquid Helium Temperature. 1626-1631A
- Fracture toughness, Deformation effects**
Evaluation of the Fracture Toughness of Hot-Rolled Low-Alloy Ti—V Plate Steel. 505-516A
Effect of Hot-Rolling Reduction on Shape of Sulfide Inclusions and Fracture Toughness of AISI 4340 Ultrahigh Strength Steel. 1555-1561A
- Fracture toughness, Heating effects**
The Effect of Austenitizing Temperature on the Fracture Initiation Toughness of As-Quenched HP9-4-20 Steel. 2989-3003A
Mode III Fracture of 4340 Steel: Effects of Tempering Temperature and Fracture Surface Interference. 3035-3044A
- Fracture toughness, Impurity effects**
Clean Steels for Steam Turbine Rotors—Their Stress Corrosion Cracking Resistance. 1583-1596A
- Fracture toughness, Microstructural effects**
Microstructure and Fracture Toughness of the Aged β -Ti Alloy Ti—10V—2Fe—3Al. 1037-1049A
The Effect of Aging on the Fracture Behavior of Cu—Al—Ni β Phase Alloys. 1761-1766A
Correlations of Microstructure With Dynamic and Quasi-Static Fracture in a Plain Carbon Steel. 2179-2206A
The Effect of Matrix Strength on the Fracture Resistance of an Alpha—Beta Titanium Alloy, Corona-5. 2503-2512A
Effect of Microstructure on Plane-Strain Fracture Toughness of AISI 4340 Steel. 2513-2521A
- Fracturing**
See also Brittle fracture
Ductile fracture
Intergranular fracture
Transgranular fracture
- Fracturing, Microstructural effects**
Effects of Transformed Ferrite Growth on the Tensile Fracture Characteristics of a Dual-Phase Steel. 309-317A
- Free energy**
See also Activation energy
Free energy of formation
Free energy of solution
Stacking fault energy
An Experimental Study and a Thermodynamic Evaluation of the Cr—Fe—W System. 2531-2546A
A Thermodynamic Evaluation of the C—Cr—Fe—W System. 2547-2554A
- Free energy of activation**
See Activation energy
- Free energy of dissociation**
See Free energy of formation
- Free energy of formation**
Equilibria Between the Rare Earth Elements, Oxygen and Sulfur, in Molten Iron. 409-418B
Determination of Standard Free Energies of Formation of Ca_3P_2 and Ca_3Sn at High Temperatures. 433-439B
High Temperature Thermodynamics of the Cr—Cr₂N—N₂ System. 471-476B
Standard Gibbs Energies of Formation of the Carbides of Manganese by EMF Measurements. 951-957B
Enthalpies of Formation of the Ag—Au—Si, Ag—Au—Ge, and Ag—Au—Sn Ternary Liquid Alloys; Experimental Determinations and Application of the Hoch—Arpshofen Model. 2075-2089A
Gibbs Free Energy of Formation of Cementite, Fe₃C. 2115-2117A
- Free energy of solution**
Volume Effects and Associations in Liquid Alloys. 465-470B
- Freezing points**
See Melting points
- Friction**
Wear-Enhanced Hydrogen Evolution From Mild Steel. 1721-1726A
- Fuel consumption**
Gas Flow and Pressure Balancing in Modeling Grate/Kiln Induration. 113-121B
- Fuel elements**
See Nuclear fuel elements
- Fuming (slag)**
See Slag fuming
- Furnaces**
See Converters
Holding furnaces
Kilns
Smelting furnaces
- Fused baths (metals)**
See Metal baths
- Fused salt electrolysis**
See Hall Heroult process
- Fusion welding**
See Arc welding
Gas tungsten arc welding
Laser beam welding
Shielded arc welding
Shielded metal arc welding
- Galena, Recovering**
Kinetics of Nonoxidative Leaching of Galena in Perchloric, Hydrobromic, and Hydrochloric Acid Solutions. 541-546B
- Galena, Reduction (electrolytic)**
Direct Electrowinning of Lead From Suspension Galena Concentrate Anodes in Different Electrolytes. 59-65B
Bed Performance in the Direct Electrowinning of Lead From Suspension Galena Anodes. 67-72B
- Gallium, Alloying elements**
Elastic Properties of β -Uranium and the Martensitic α' -Phase in Uranium—Gallium Alloys. 909-913A
- Gallium, Diffusion**
Prediction of Solute Diffusion Coefficients in Liquid Metals. 273-279A
- Gallium base alloys, Directional solidification**
Directional Solidification of Cu—Pb and Bi—Ga Monotectic Alloys Under Normal Gravity and During Parabolic Flight. 2839-2846A
- Galvanized steels, Coating**
Scanning Auger Microprobe Study of Hot-Dipped Regular-Spangle Galvanized Steel. II. Surface Composition of Chromated Sheet. 1609-1616A
- Galvanizing**
See Hot dip galvanizing
- Galvannealing**
See Annealing
- Gas flow**
Characterization of Two-Phase Axisymmetric Plume in a Gas Stirred Liquid Bath—a Water Model Study. 885-892B
- Gas permeability**
See Permeability
- Gas tungsten arc welding**
A Study of the Weldability and Weld Related Microstructure of Cabot Alloy 214. 657-667A
Welding Parameters and the Grain Structure of Weld Metal—a Thermodynamic Consideration. 1075-1082A
- Gas turbines, Microstructure**
Dislocation Network Formation and Coherency Loss Around Gamma-Prime Precipitates in a Nickel-Base Superalloy. 2965-2973A
- Germanium, Alloying additive**
Creep Crack Growth Behavior of Two Al—Li Alloys. 847-854A
- Germanium, Binary systems**
Mass Spectrometric Study of the Activities of the Fe—Ge System at 1550°C. 511-513B
- Germanium, Ternary systems**
Experimental and Calculated Ag + Au + Ge Phase Diagram. 409-416A
Enthalpies of Formation of the Ag—Au—Si, Ag—Au—Ge, and Ag—Au—Sn Ternary Liquid Alloys; Experimental Determinations and Application of the Hoch—Arpshofen Model. 2075-2089A
- Gibbs free energy**
See Free energy
- Glass**
See Metallic glasses
- Glass transition temperature**
Preparation of Iron-, Cobalt- and Nickel-Based Amorphous Alloy Powders by High-Pressure Gas Atomization and Their Structural Relaxation Behavior. 235-242A
- Gold, Alloying elements**
Microsegregation in Directionally Solidified Pb—8.4 at.% Au Alloy. 1351-1364A
- Gold, Extraction**
An Electrochemical Study of the Surface Oxidation of Arsenopyrite in Alkaline Media. 943-949B
- Gold, Ternary systems**
Experimental and Calculated Ag + Au + Ge Phase Diagram. 409-416A
Enthalpies of Formation of the Ag—Au—Si, Ag—Au—Ge, and Ag—Au—Sn Ternary Liquid Alloys; Experimental Determinations and Application of the Hoch—Arpshofen Model. 2075-2089A
- Gold, Thermal properties**
Measurement of Temperature and Emissivity of Specularly Reflecting Glowing Bodies. 1889-1894A
- Gold base alloys, Phase transformations**
X-Ray Study of the Premartensitic Phenomena in AuCd. 265-271A

Gold silver alloy plating

Gold silver alloy plating

See Alloy plating

GP zone

See Guinier Preston zone

Grain boundaries

Grain Boundary Segregation in the Nickel-Base Alloy 182. 137-143A

Grain Boundary Segregation in Austenitic Stainless Steels and Its Effect on Intergranular Corrosion and Stress Corrosion Cracking. 495-504A

The Precipitation Behavior of a Zr—2.5 wt.% Nb Alloy. 1153-1162A

The Effect of Matrix Strength on Void Nucleation and Growth in a Widmanstätten Alpha—Beta Titanium Alloy, Corona-5. 1163-1171A

Intercrystalline Structure Distribution in Alloy 304 Stainless Steel. 1179-1185A

Effect of Single Aging on Stress Corrosion Cracking Susceptibility of Inconel X-750 Under PWR Conditions. 1295-1304A

Evaluation of the Effects of Segregation on Austenite Grain Boundary Energy in Fe—C—X Alloys. 1807-1818A

Grain Boundary Segregation of Sulfur and Antimony in Iron Alloys. 2005-2011A

Calculation of the Product Phase Grain Boundary Area During Solid State Transformations. 2123-2131A

Grain boundaries, Impurity effects

The Influence of Boron on the Grain Boundary Chemistry and Microstructure of Ni—16Cr—9Fe—0.03C. 2555-2566A

Grain boundaries, Microstructure

Structure of a Small Angle Tilt Grain Boundary in Zinc. 2359-2363A

Grain boundary migration

A Topological Study of Superplastic Deformation in an Al—Li Alloy With a Bimodal Grain Size Distribution. 1621-1624A

Inhibition of Cyclic Grain Boundary Migration Through Cellular Precipitation in Pb—5% Sn Alloy. 2355-2359A

The Absence of Steady-State Flow During Large Strain Plastic Deformation of Some FCC Metals at Low and Intermediate Temperatures. 3013-3024A

Grain boundary migration, Deformation effects

Microstructural Observations in Cyclically Deformed Pb—Sn Solid Solution Alloy. 1437-1443A

Grain boundary migration, Heating effects

Diffusion Induced Grain Boundary Migration and Recrystallization During Oxidation of a Ni—48.5% Cu Alloy. 1667-1675A

Grain boundary migration, High temperature effects

Cyclic Deformation and Fracture in Pb—Sn Solid Solution Alloy. 1533-1546A

Grain growth

Kinetics of Domain Growth in Ordered Ni₃Mo. 941-952A

The Effect of Matrix Strength on Void Nucleation and Growth in a Widmanstätten Alpha—Beta Titanium Alloy, Corona-5. 1163-1171A

Ostwald Ripening in a System With a High Volume Fraction of Coarsening Phase. 2713-2721A

Nucleation and Growth in Martensitic Transformations of Ordered Fe₃Pt Alloys. 2931-2936A

Grain growth, Size effects

Calculation of the Product Phase Grain Boundary Area During Solid State Transformations. 2123-2131A

Grain orientation

Intercrystalline Structure Distribution in Alloy 304 Stainless Steel. 1179-1185A

Elastic Interaction Stresses. I. The Influence of Bicrystal Size on Stresses in [213] Iso-Axial 70-30 Alpha-Brass Bicrystals. 1727-1737A

Intercrystalline Structure Distribution in Polycrystalline Materials. 2611A

Grain refinement

Discussion of "The Role of Boron in the Grain Refinement of Aluminum With Titanium" and Authors' Reply. 385-387A

Modeling of Thermomechanical Processing of Heat-Treatable Aluminum Alloys. 617-625A

Grain refinement, Alloying effects

Microstructural Refinement of W—Ni—Fe Heavy Alloys by Alloying Additions. 3100-3103A

Grain size

An Analysis for the Effect of a Grain Size Gradient on Torsional and Tensile Properties. 329-335A

The Strength of Ni₃Al Containing Titanium and Boron. 732-733A

The Effects of Austenitization Temperature on the High Temperature Ductility of Fe—P—S Alloys. 887-892A

Grain Shape and Its Influence on the Experimental Measurement of Grain Size. 933-940A

The Effect of Triaxial Stress Field on Intermediate Temperature Embrittlement of Ferritic Spheroidal Graphite Cast Irons. 1213-1219A

Effects of Thermomechanical Processing on the Microstructure and Mechanical Properties of a Ti—V—N Steel. 1221-1234A

Observations on Void Nucleation and Growth in α/β Ti—Mn Alloys. 1311-1317A

Radiation Induced Crystallization of Amorphous Si:H Alloy. 1345-1349A

Effect of Melt Spinning on Grain Size and Texture in Ni—Mo Alloys. 1711-1720A

Calculation of the Product Phase Grain Boundary Area During Solid State Transformations. 2123-2131A

Tensile Fracture of Coarse-Grained Cast Austenitic Manganese Steels. 2269-2277A

The Effect of Grain Size on the Bulk Formability and Tensile Properties of Austenitic Stainless Steel Types 304 and 316. 2287-2298A

Near-Threshold Fatigue Crack Growth in Copper and Alpha-Brass: Grain-Size and Environmental Effects. 2575-2587A

Thermodynamics and Kinetics of $\delta \rightarrow \alpha$ Martensitic Transformation in Plutonium Alloys. 2705-2711A

Ostwald Ripening in a System With a High Volume Fraction of Coarsening Phase. 2713-2721A

Preparation and Properties of Fine Grain β -CuAlNi Strain-Memory Alloys. 2921-2929A

Statistical Considerations on Uniform Grain Size. 2937-2944A

Grain size, Deformation effects

Modeling of Thermomechanical Processing of Heat-Treatable Aluminum Alloys. 617-625A

Grain size, Heating effects

Correlations of Microstructure With Dynamic and Quasi-Static Fracture in a Plain Carbon Steel. 2179-2206A

Grain structure

The Evolution of Microcrystalline Structures in Supercooled Metal Powders. 699-708A

Grain Shape and Its Influence on the Experimental Measurement of Grain Size. 933-940A

Grain structure, Welding effects

Welding Parameters and the Grain Structure of Weld Metal—a Thermodynamic Consideration. 1075-1082A

Graphite, Coating

Coating of Graphite Fibers With Tungsten Carbide Using Solid and Liquid Copper as a Transfer Medium. 2109-2113A

Graphite, Composite materials

Some Observations on the Matrix Microstructure of Aluminum—Silicon Alloy—Graphite Particle Composites. 1365-1367A

Graphite, Reactions (chemical)

Dissolution Kinetics of Particulate Graphite Injected Into Iron/Carbon Melts. 375-382B

Gravitation

Containment of a Silicone Fluid Free Surface in Reduced Gravity. 1883-1888A

Experimental Study of Thermocapillary Flows in a Thin Liquid Layer With Heat Fluxes Imposed on the Free Surface. 1895-1898A

Directional Solidification of Al—Ni/SiC Composites During Parabolic Trajectories. 1899-1904A

Gravity and Configurational Energy Induced Microstructural Changes in Liquid Phase Sintering. 1905-1913A

Ground-Based Microgravity Materials Science Research at NASA's Microgravity Materials Science Laboratory. 1915-1917A

The Bubble, Drop, and Particle Unit (BDPU). 1925-1929A

Mixing Fuel Particles for Space Combustion Research Using Acoustics. 1931-1937A

Isothermal Dendritic Growth—a Proposed Microgravity Experiment. 1945-1953A

Making Acceleration Data More Accessible and Useful to Microgravity Investigators. 2631-2637A

Gravity

See Gravitation

Gray cast iron

See Gray iron

Gray iron

See also Nodular iron

Gray iron, Phase transformations

Competitive Growth of Stable and Metastable Fe—C—X Eutectics. I. Experiments. 1955-1963A

Competitive Growth of Stable and Metastable Fe—C—X Eutectics. II. Mechanisms. 1965-1971A

Grey iron

See Gray iron

Growth

See Crystal growth

Epitaxial growth

Grain growth

Growth rate

Growth rate

The Effect of Matrix Strength on Void Nucleation and Growth in an Alpha—Beta Titanium Alloy, Corona-5. 591-601A

Creep Deformation of Ni₃Al—Mo In Situ Composites. 987-998A

Microsegregation in Directionally Solidified Pb—8.4 at.% Au Alloy. 1351-1364A

Coupled Growth Zone in Fe—18Cr—C Alloys. 1367-1369A

Fractal Analysis of a Nucleation and Growth Process. 1371-1372A

Guinier Preston zone

Growth and Coarsening of G.P. Zones in Al—Zn Alloys. 1973-1980A

Precipitation of Guinier—Preston Zones in Aluminum—Magnesium; a Calorimetric Analysis of Liquid-Quenched and Solid-Quenched Alloys. 2433-2443A

Guinier Preston zone, Heating effects

Effects of SiC Whiskers and Particles on Precipitation in Aluminum Matrix Composites. 2945-2953A

Hafnium, Alloying elements

Microstructure of Laser Clad Ni—Cr—Al—Hf Alloy on a γ' Strengthened Nickel-Base Superalloy. 1981-1990A

Hafnium base alloys, Phase transformations

Simple Models for the Omega Phase Transformation. 169-175A

Hafnium compounds, Thermal properties

Thermochemistry of the Intermetallic Compounds RuTi, RuZr, and RuHf. 1061-1066A

Standard Enthalpies of Formation of PtTi, PtZr, and PtHf. 1827-1831A

Halides

See Chlorides

Hall Heroult process

The Moreau—Evans Hydrodynamic Model Applied to Actual Hall—Heroult Cells. 737-744B

- Halogenation**
See Chlorination
- Halogens**
See Fluorine
Iodine
- Hardenability, Alloying effects**
An Approach to Developing an Alternative Hot Work Die Steel. 1751-1760A
- Hardening**
See Aging (artificial)
Laser beam hardening
Precipitation hardening
Quench hardening
Strain hardening
Structural hardening
Surface hardening
- Hardness**
See also Diamond pyramid hardness
Microhardness
On the Weldability, Composition, and Hardness of Pulsed and Continuous Nd:YAG Laser Welds in Aluminum Alloys 6061, 5456, and 5086. 319-329B
Hardness, Composition effects
Ductile Al—Cu—V Amorphous Alloys Without Metalloid. 391-393A
Effects of Oxygen and Heat Treatment on the Mechanical Properties of Alpha and Beta Titanium Alloys. 527-542A
Hardness, Diffusion effects
Hydrogen Effects in [001] Oriented Nickel-Base Superalloy Single Crystals. 73-82A
Hardness, Heating effects
Development of High Toughness in Austempered Type Ductile Cast Iron and Evaluation of Its Properties. 319-327A
The Tempering of Iron—Carbon Martensite; Dilatometric and Calorimetric Analysis. 2415-2426A
Hardness, Microstructural effects
Effect of Microstructure on Fracture Behavior of Complex Structure in 6Ni—0.3C Steel. 2606-2611A
Microstructural Refinement of W—Ni—Fe Heavy Alloys by Alloying Additions. 3100-3103A
Hardness tests
Characterization of the Aging Response of a Melt-Spun Al—Be—Li Alloy Ribbon. 1173-1178A
Hazelett process
See Continuous casting
- Heat affected zone, Corrosion**
Environmental Cracking of Type 316 Austenitic Stainless Steel Weldments in High Temperature CO₂ Gas. 1445-1460A
Heat affected zone, Mechanical properties
The Kinetics of Intergranular Oxygen Penetration in Nickel and Its Relevance to Weldment Cracking. 2305-2313A
Heat affected zone, Microstructure
An Analytical Electron Microscope Investigation of the Phase Transformations in a Simulated Heat-Affected Zone in Alloy 800. 35-50A
- Heat flow**
See Heat transmission
- Heat flux**
See Heat transmission
- Heat of activation**
Nonlinear and Nonlocal Continuum Model of Transformation Precursors in Martensites. 761-775A
- Heat of combination**
See Heat of reaction
- Heat of decomposition**
See Heat of formation
- Heat of dissociation**
See Heat of formation
- Heat of dissolution**
See Heat of solution
- Heat of formation**
Thermochemistry of the Intermetallic Compounds RuTi, RuZr, and RuHf. 1061-1066A
- Heat of hydrogenation**
See Heat of reaction
- Heat of isomerization**
See Heat of reaction
- Heat of mixing**
Thermodynamics of Molten Li—Sn Alloys. 637-644A
- Heat of neutralization**
See Heat of reaction
- Heat of reaction**
Discussion of "Physical Chemistry of Gas Liquid Solder Reactions" and Reply. 513-514B
- Heat of solution**
The Effect of Temperature on Nickel Solubility in Silica Saturated Fayalite Slags From 1523-1623K. 243-247B
Thermodynamics of Molten Li—Sn Alloys. 637-644A
- Heat resistant alloys**
See Superalloys
- Heat transfer**
Influence of Mold Length and Mold Heat Transfer on Horizontal Continuous Casting of Nonferrous Alloy Rods. 201-212B
- Convective Heat-Transfer Measurements in Liquid Metals Under Different Fluid Flow Conditions. 859-870B
- Heat transmission**
Performance Analysis of the Aluminum Casting Furnace. 171-180B
- Heat treatment**
See also Aging (artificial)
Annealing
Austempering
Austenitizing
Bright annealing
Grain refinement
Precipitation hardening
Precipitation heat treatment
Quench aging
Quench hardening
Solution heat treatment
Tempering
Assessment of Service Induced Microstructural Damage and Its Rejuvenation in Turbine Blades. 2049-2066A
- Heating**
See Laser beam heating
- Heats (energies)**
See Heat of activation
Heat of formation
Heat of mixing
Heat of reaction
Heat of solution
- Heavy metals**
See Antimony
Bismuth
Lead (metal)
Mercury (metal)
Thallium
Tin
- Heliarc welding**
See Gas tungsten arc welding
- Helium, Environment**
Tensile and Impact Properties Changes of Hastelloy X After Exposure in High-Temperature Helium Environment. 1269-1275A
- Helium, Impurities**
Creep Cavity Growth From Tritium-Induced Helium Bubbles in Nickel. 821-827A
- Helmholtz free energy**
See Free energy
- Hematite, Reduction (chemical)**
Hematite Single Crystal Reduction Into Magnetite With CO—CO₂. 311-317B
- High alloy steels**
See Austenitic stainless steels
Duplex stainless steels
Ferritic stainless steels
Maraging steels
Stainless steels
- High energy milling**
See Mechanical alloying
- High speed tool steels, Alloy development**
Niobium-Alloyed High Speed Steel by Powder Metallurgy. 1395-1401A
- High speed tool steels, Casting**
Processing Effects in Spray Casting of Steel Strip. 3077-3086A
- High speed tool steels, Heat treatment**
Laser Melting of Ti-High Speed Tool Steel. 377-382A
- High speed tool steels, Physical properties**
Hydrogen in Iron. 691-707B
Hydrogen in Iron. 2371-2387A
- High strength low alloy steels, Corrosion**
Effects of Manganese, Phosphorus and Molybdenum on Sulfide Stress Cracking Resistance of High Strength Low Alloy Steels. 2171-2177A
- High strength low alloy steels, Forming**
Effect of Geometrical Defects in Forming Sheet Steel by Biaxial Stretching. 2067-2074A
- High strength low alloy steels, Heat treatment**
Intercritical Annealing as a Means of Improving Impact Properties of Plate Steel. 1481-1490A
- High strength low alloy steels, Magnetic properties**
Analytical Electron Microscopy of Internally Oxidized Mn—P Steel. 1876-1878A
- High strength low alloy steels, Mechanical properties**
Evaluation of the Fracture Toughness of Hot-Rolled Low-Alloy Ti—V Plate Steel. 505-516A
Predicting the Kinetics of Hydrogen Generation at the Tips of Corrosion Fatigue Cracks. 1795-1806A
- High strength low alloy steels, Phase transformations**
Effect of Deformation on the Austenite-to-Ferrite Transformation in a Plain Carbon and Two Microalloyed Steels. 417-426A
- High strength low alloy steels, Structural hardening**
The Prediction of Precipitation Strengthening in Microalloyed Steels. 1471-1480A
- High strength steels, Corrosion**
Discussion of "Sulfide Stress Cracking Susceptibility of Nickel Containing Steels" and Authors' Reply. 153A
- High strength steels, Mechanical properties**
The Effect of Microstructure on the Fatigue Crack Growth Behavior of Age-Hardened High Strength Steels in a Corrosive Environment. 1461-1469A

High strength steels

- The Effect of Austenitizing Temperature on the Fracture Initiation Toughness of As-Quenched HP9-4-20 Steel. 2989-3003A
- High temperature**
Thermodynamic Activity of Na_2O in $\text{Na}_2\text{O}-\text{CaO}-\text{SiO}_2$, $\text{Na}_2\text{O}-\text{MgO}-\text{SiO}_2$, and $\text{Na}_2\text{O}-\text{CaO}-\text{SiO}_2-\text{Al}_2\text{O}_3$ Melts at 1400°C. 655-661B
- HIP**
See Hot isostatic pressing
- Holding furnaces**
Performance Analysis of the Aluminum Casting Furnace. 171-180B
- Horizontal continuous casting**
Influence of Mold Length and Mold Heat Transfer on Horizontal Continuous Casting of Nonferrous Alloy Rods. 201-212B
- Hot brittleness**
See Brittleness
- Hot compacting**
See Compacting
- Hot compression**
See Hot pressing
- Hot cracking**
See Cracking (fracturing)
- Hot cracking (welds)**
See Weld defects
- Hot deformation**
See Deformation
- Hot dip coating**
See Hot dip galvanizing
- Hot dip coatings, Microstructure**
Scanning Auger Microprobe Study of Hot-Dipped Regular-Spangle Galvanized Steel. I. Surface Composition of As-Produced Sheet. 1603-1608A
- Hot dip galvanizing**
Scanning Auger Microprobe Study of Hot-Dipped Regular-Spangle Galvanized Steel. I. Surface Composition of As-Produced Sheet. 1603-1608A
- Hot dipping**
The Reaction Between Solid Iron and Liquid Al—Zn Baths. 1193-1203A
- Hot ductility**
See Ductility
- Hot extrusion**
Dislocation Structures in the Strain Localized Region in Fatigued 85/15 Brass. 1257-1262A
Texture Induced Magnetic Anisotropy in Fe—Nd—B Magnet Prepared via Rapid Solidification and Hot Extrusion Techniques. 3109-3112A
- Hot gas corrosion, Welding effects**
Environmental Cracking of Type 316 Austenitic Stainless Steel Weldments in High Temperature CO_2 Gas. 1445-1460A
- Hot hardness**
See Hardness
- Hot isostatic pressing**
Densification of Titanium Powder During Hot Isostatic Pressing. 1767-1773A
Densification of Oxide Superconductors by Hot Isostatic Pressing. 1841-1847A
- Hot pressing**
See also Hot isostatic pressing
Effects of Thermomechanical Processing on the Microstructure and Mechanical Properties of a Ti—V—N Steel. 1221-1234A
- Hot rolling**
Changes in the Longitudinal Flow and Apparent Plastic Poisson's Ratio of a Porous Metal Strip During Hot Densification Rolling. 1205-1211A
The Effect of Triaxial Stress Field on Intermediate Temperature Embrittlement of Ferritic Spheroidal Graphite Cast Irons. 1213-1219A
Effect of Hot-Rolling Reduction on Shape of Sulfide Inclusions and Fracture Toughness of AISI 4340 Ultrahigh Strength Steel. 1555-1561A
Microscopic Shear Localization in Nickel. 2041-2048A
- Hot roughing**
See Hot rolling
- Hot shortness**
See Brittleness
- Hot strength**
See Tensile strength
- Hot stretch forming**
See Stretch forming
- Hot tensile strength**
See Tensile strength
- Hot work tool steels, Alloy development**
An Approach to Developing an Alternative Hot Work Die Steel. 1751-1760A
- Hot working**
See Hot extrusion
Hot rolling
- Hydrides**
The Influence of Hydride Size and Matrix Strength on Fracture Initiation at Hydrides in Zirconium Alloys. 1507-1522A
- Hydrodynamics**
Thermal Explosions Resulting From Fuel—Coolant Interactions: Analysis of Single Bubble Hydrodynamics. 563-570B
The Moreau—Evans Hydrodynamic Model Applied to Actual Hall—Héroult Cells. 737-744B
- Hydrogen**
See also Deuterium
Wear-Enhanced Hydrogen Evolution From Mild Steel. 1721-1726A
Predicting the Kinetics of Hydrogen Generation at the Tips of Corrosion Fatigue Cracks. 1795-1806A
- Hydrogen, Diffusion**
Hydrogen Effects in [001] Oriented Nickel-Base Superalloy Single Crystals. 73-82A
Nature of the γ and γ^* Phases in Austenitic Stainless Steels Cathodically Charged With Hydrogen. 723-730A
Determination of Fracture Initiation in Hydride Blisters Using Acoustic Emission. 2247-2257A
Experimental Study of Hydrogen Transport During Plastic Deformation in Iron. 2789-2798A
- Hydrogen, Environment**
The Mechanism of Hydrogen Induced Cleavage in Fe—3% Si Alloy. 1335-1343A
- Hydrogen, Physical properties**
Hydrogen in Iron. 691-707B
Hydrogen Permeation Through Coated and Uncoated Waspaloy. 1187-1192A
Hydrogen in Iron. 2371-2387A
- Hydrogen, Solubility**
Solubility and Diffusion of Hydrogen in Vanadium—Oxygen Alloys. 67-72A
The Solubility of Hydrogen in Liquid Binary Al—Li Alloys. 227-232B
- Hydrogen, Sorption**
Kinetics of Hydrogen Absorption in Alpha Titanium. 1425-1427A
- Hydrogen compounds**
See Inorganic acids
- Hydrogen embrittlement**
Hydrogen Effects in [001] Oriented Nickel-Base Superalloy Single Crystals. 73-82A
Cracking Kinetics of Two-Phase Stainless Steel Alloys in Hydrogen Gas. 145-152A
Hydrogen Embrittlement of Pseudobinary L_{12} -Type $\text{Ni}_3(\text{Al}, \text{Mn})$ Intermetallic Compound. 353-357A
Detection of the Initiation and Growth of Hydrogen-Induced Cracks in Armco Iron Using Continuous Modulus Measurements. 473-478A
Effects of Water Vapor on Hydrogen Induced Slow Crack Growth in Stainless Steels. 651-656A
The Influence of Hydride Size and Matrix Strength on Fracture Initiation at Hydrides in Zirconium Alloys. 1507-1522A
Mechanistic Similarities Between Hydrogen and Temperature Effects on the Ductile-to-Brittle Transition of a Stainless Steel. 1547-1553A
The Role of Hydrogen in Corrosion Fatigue of High Purity Al—Zn—Mg Exposed to Water Vapor. 1775-1783A
Determination of Fracture Initiation in Hydride Blisters Using Acoustic Emission. 2247-2257A
Effect of Cathodic Charging on the Mechanical Properties of Aluminum. 2299-2304A
The Role of Dislocations During Transport of Hydrogen in Hydrogen Embrittlement of Iron. 2799-2803A
- Hydrogen embrittlement, Microstructural effects**
The Effect of Microstructure on the Fatigue Crack Growth Behavior of Age-Hardened High Strength Steels in a Corrosive Environment. 1461-1469A
- Hydrogen reduction**
Reducibility of Laterite Ores. 181-186B
- Hydrogen storage**
Kinetics of Hydrogen Absorption in Alpha Titanium. 1425-1427A
- Hydrogenation**
Corrosion Fatigue Crack Initiation in a Mode II Notch Specimen. 1067-1073A
Crack Growth From Internal Hydrogen—Temperature and Microstructural Effects in 4340 Steel. 1319-1334A
- Hydromechanics**
See Hydrodynamics
- Hydrometallurgy**
Speciation and Reduction Potentials of Metal Ions in Concentrated Chloride and Sulfate Solutions Relevant to Processing Base Metal Sulfides. 37-45B
- I R drop**
See Electric potential
- Immersion coating**
See Hot dip galvanizing
- Immersion testing (ultrasonic)**
See Ultrasonic testing
- Impact strength**
Tensile and Impact Properties Changes of Hastelloy X After Exposure in High-Temperature Helium Environment. 1269-1275A
Mechanistic Similarities Between Hydrogen and Temperature Effects on the Ductile-to-Brittle Transition of a Stainless Steel. 1547-1553A
- Impact strength, Alloying effects**
A Preliminary Study of the Influence of Separate and Combined Aluminum and Nickel Additions on the Properties of a Secondary Hardening Steel. 3103-3107A

- Impact strength, Deformation effects**
Effect of Hot-Rolling Reduction on Shape of Sulfide Inclusions and Fracture Toughness of AISI 4340 Ultrahigh Strength Steel. 1555-1561A
- Impact strength, Heating effects**
Development of High Toughness in Austempered Type Ductile Cast Iron and Evaluation of Its Properties. 319-327A
Intercritical Annealing as a Means of Improving Impact Properties of Plate Steel. 1481-1490A
The Effect of Austenitizing Temperature on the Fracture Initiation Toughness of As-Quenched HP9-4-20 Steel. 2989-3003A
- Impact strength, Microstructural effects**
Effects of Thermomechanical Processing on the Microstructure and Mechanical Properties of a Ti—V—N Steel. 1221-1234A
Effect of Microstructure on Fracture Behavior of Complex Structure in 6Ni—0.3C Steel. 2606-2611A
The Effect of Alloying Elements and Microstructure on the Strength and Fracture Resistance of Pearlitic Steel. 2819-2829A
- Impact toughness**
See Impact strength
- Imperfections**
See Defects
- Impermeability**
See Permeability
- In situ leaching**
Study by SEM-EDS of the In Situ Dynamic Leaching of Mercury Ores. 165-170B
- Incineration**
See Combustion
- Inclusions**
See Nonmetallic inclusions
- Indium, Ternary systems**
Phase Stability Relationships and Glass Formation in the System Cu—Ag—In. 13-21A
- Indium base alloys, Phase transformations**
Symmetry Aspects of Pretransformation Behavior in Metallic Alloys. 159-167A
Pretransformation Phenomena as Revealed by Elastic Waves. 185-191A
Neutron Scattering Studies of Premartensitic Indium—Thallium Alloys. 193-198A
Electron Diffuse Scattering Studies of Premartensitic Alloys: β' Cu—Zn, β' Ni—Al, In—Ti, and Fe—Ni. 199-205A
Nonlinear and Nonlocal Continuum Model of Transformation Precursors in Martensites. 761-775A
Premartensitic Anelasticity in Indium—Thallium Alloys. 789-792A
- Induction (electromagnetic)**
See Electromagnetic induction
- Inert gas welding**
See Gas tungsten arc welding
- Infiltration**
Modeling of Infiltration Kinetics for Liquid Metal Processing of Composites. 95-101B
- Ingots, Directional solidification**
Channel Formation in Pb—Sn, Pb—Sb, and Pb—Sn—Sb Alloy Ingots and Comparison With the System $\text{NH}_4\text{Cl—H}_2\text{O}$. 1861-1871A
- Ingots, Mechanical properties**
Investigation of Panel Crack Formation in Steel Ingots. I. Mathematical Analysis and Mid-Face Panel Cracks. 277-287B
Investigation of Panel Crack Formation in Steel Ingots. II. Off-Corner Panel Cracks. 289-301B
- Initiation**
See Crack initiation
- Inorganic acids, Reactions (chemical)**
Dissolution of Columbite and Tantalite in Acidic Fluoride Media. 355-363B
- Instability**
See Stability
- Intensity**
See Stress intensity
- Intercrystalline structure**
See Intergranular structure
- Interface reactions**
On the Interfacial Rate of Reaction of CO_2 With a Calcium Ferrite Melt. 959-965B
Microstructure of Laser Clad Ni—Cr—Al—Hf Alloy on a γ' Strengthened Nickel-Base Superalloy. 1981-1990A
- Interface reactions, Coating effects**
Evaluation of High-Temperature Diffusion Barriers for the Pt—Mo System. 2163-2170A
- Interfaces**
Transverse Elastic Moduli of Unidirectional Fiber Composites With Interfacial Debonding. 129-135A
Fluid Oscillation in the Drop Tower. 2625-2630A
Behavior of Ceramic Particles at the Solid/Liquid Metal Interface in Metal Matrix Composites. 2847-2855A
Effects of SiC Whiskers and Particles on Precipitation in Aluminum Matrix Composites. 2945-2953A
Dislocation Network Formation and Coherency Loss Around Gamma-Prime Precipitates in a Nickel-Base Superalloy. 2965-2973A
- Interfaces, Mechanical properties**
A Computer Simulation on Tensile Strength of Metal Matrix Composites Reinforced With Surface-Damaged Fibers. 1491-1497A
- Interfacial energy**
See Surface energy
- Interfacial surface tension**
See Surface tension
- Intergranular corrosion, Alloying effects**
Effects of Manganese, Phosphorus and Molybdenum on Sulfide Stress Cracking Resistance of High Strength Low Alloy Steels. 2171-2177A
- Intergranular corrosion, Diffusion effects**
Grain Boundary Segregation in Austenitic Stainless Steels and Its Effect on Intergranular Corrosion and Stress Corrosion Cracking. 495-504A
- Intergranular corrosion, Heating effects**
Inhibition of Nitrogen Uptake by SiO_2 Surface Films Formed on Stainless Steel During Annealing in H/N Atmospheres. 3045-3055A
- Intergranular corrosion, Impurity effects**
Influence of Austenitizing Temperature on Stress Corrosion in 430M Steel—the Role of Impurity Segregation in Stress Corrosion Cracking of High Strength Steel. 2225-2231A
- Intergranular fracture**
Creep Cavity Growth From Tritium-Induced Helium Bubbles in Nickel. 821-827A
Crack Growth From Internal Hydrogen—Temperature and Microstructural Effects in 4340 Steel. 1319-1334A
- Intergranular fracture, Alloying effects**
Effect of Antimony on the Creep Fracture of Stainless Steel. 571-577A
- Intergranular precipitation**
The Influence of Boron on the Grain Boundary Chemistry and Microstructure of Ni—16Cr—9Fe—0.03C. 2555-2566A
- Intergranular structure**
Intercrystalline Structure Distribution in Alloy 304 Stainless Steel. 1179-1185A
- Intergranular structure, Impurity effects**
The Effects of Austenitization Temperature on the High Temperature Ductility of Fe—P—S Alloys. 887-892A
- Intermetallic compounds**
See Intermetallics
- Intermetallic phases**
Simple Models for the Omega Phase Transformation. 169-175A
Theoretical Investigation of the Precipitation of δ' in Al—Li. 249-258A
- Intermetallic phases, Cooling effects**
Effect of Melt Spinning on the Microstructure and Mechanical Properties of Three Nickel-Base Superalloys. 93-103A
- Intermetallic phases, Crystal growth**
Precipitation of the δ -Ni₃Nb Phase in Two Nickel Base Superalloys. 453-465A
- Intermetallic phases, Phase transformations**
Investigation of Phase Transformation in an Al—0.58 wt.% Fe Alloy by Mossbauer Spectroscopy. 259-264A
- Intermetallics**
See also A15 compounds
Precipitation of Guinier—Preston Zones in Aluminum—Magnesium; a Calorimetric Analysis of Liquid-Quenched and Solid-Quenched Alloys. 2433-2443A
- Intermetallics, Crystal lattices**
Microstructural Characterization of the Dispersed Phases in Al—Ce—Fe System. 1645-1656A
Effect of Rapid Solidification and Alloying Addition on Lattice Distortion and Atomic Ordering in L1₀ TiAl Alloys and Their Ternary Alloys. 2445-2455A
The Apparent "Five-Fold" Nature of Large T₂ (Al₆Li₃Cu) Crystals. 2875-2884A
Convergent Beam Electron Diffraction Analysis of the T₁ (Al₂CuLi) Phase in Al—Li—Cu Alloys. 2885-2891B
- Intermetallics, Phase transformations**
Quasi-One-Dimensional Model of Pretransitional Soft Mode Behavior. 811-818A
Electron Microscope Study on Martensitic Transformations in Fe—Pt Alloys: General Features of Internal Structure. 2723-2731A
Nucleation and Growth in Martensitic Transformations of Ordered Fe₃Pt Alloys. 2931-2936A
- Intermetallics, Phases (state of matter)**
An Experimental Study and a Thermodynamic Evaluation of the Cr—Fe—W System. 2531-2546A
- Intermetallics, Powder technology**
Mechanical Alloying of Brittle Materials. 2867-2874A
- Intermetallics, Thermal properties**
Standard Enthalpies of Formation of PtTi, PtZr, and PtHf. 1827-1831A
- Internal friction**
Premartensitic Anelasticity in Indium—Thallium Alloys. 789-792A
Fluid Oscillation in the Drop Tower. 2625-2630A
- Internal oxidation**
Analytical Electron Microscopy of Internally Oxidized Low Si—Al Steel. 953-959A
Analytical Electron Microscopy of Internally Oxidized Mn—P Steel. 1876-1878A
- Internal stress**
See Residual stress
- Iodine, Environment**
Modeling the Texture Dependence of Environmentally Assisted Growth of Long and Short Cracks. 1009-1020A

Ion beam mixing

Ion beam mixing

Fatigue Damage Accumulation in Nickel Modified by Ion Beam Surface Microalloying.

2775-2788A

Ions

An Ionic Diffusion Mechanism of Chromite Reduction.

677-684B

Iron

See also Alloy steels

Cast iron
Gray iron
Nodular iron
White iron

Effect of Temperature on Magnetizing Reduction of Agbaja Iron Ore.

731-735B

The Mechanism of Ferrite Formation From Iron Sulfides During Zinc Roasting.

777-785B

Iron, Binary systems

Mass Spectrometric Study of the Activities of the Fe—Ge System at 1550°C.

511-513B

The Cata- or Metatectic Reaction—Occurrence and Microstructural Development.

3097-3100A

Iron, Corrosion

The Role of Dislocations During Transport of Hydrogen in Hydrogen Embrittlement of Iron.

2799-2803A

Iron, Crystal growth

Influence of Rare Earth Metals on the Nucleation and Solidification Behavior of Iron and 1045 Steel.

383-395B

The Nucleation of Iron on Dense Wustite: a Morphological Study.

787-802B

Iron, Diffusion

Experimental Study of Hydrogen Transport During Plastic Deformation in Iron.

2789-2798A

Iron, Extraction

Correlations of Electrical Conductivity to Slag Composition and Temperature.

133-140B

Reducibility of Laterite Ores.

181-186B

Iron, Mechanical properties

Effect of Environment and Grain Size on Cyclic Deformation and Surface Hardening of Iron.

337-344A

Detection of the Initiation and Growth of Hydrogen-Induced Cracks in Armco Iron Using Continuous Modulus Measurements.

473-478A

The Effects of Austenitization Temperature on the High Temperature Ductility of Fe—P—S Alloys.

887-892A

Iron, Phase transformations

Quasi-One-Dimensional Model of Pretransitional Soft Mode Behavior.

811-818A

Analysis of Nonisothermal Transformation Kinetics; Tempering of Iron—Carbon and Iron—Nitrogen Martensites.

925-932A

Iron, Physical properties

Hydrogen in Iron.

631-707B

Hydrogen in Iron.

2371-2387A

Iron, Powder technology

Kinetics of Neck Growth During Loose Stack Sintering.

2153-2161A

Iron, Quaternary systems

A Thermodynamic Evaluation of the C—Cr—Fe—W System.

2547-2554A

Iron, Reactions (chemical)

Speciation and Reduction Potentials of Metal Ions in Concentrated Chloride and Sulfate Solutions Relevant to Processing Base Metal Sulfides.

37-45B

Dissolution Kinetics of Particulate Graphite Injected Into Iron/Carbon Melts.

375-382B

Equilibria Between the Rare Earth Elements, Oxygen and Sulfur, in Molten Iron.

409-418B

The Reaction Between Solid Iron and Liquid Al—Zn Baths.

1193-1203A

Iron, Refining

Reaction Mechanism for the CaO—Al and CaO—CaF₂ Desulfurization of Carbon-Saturated Iron.

261-268B

The Calcium—Phosphorus and the Simultaneous Calcium—Oxygen and Calcium—Sulfur Equilibria in Liquid Iron.

617-622B

Iron, Sorption

Rate of Nitrogen Desorption From Liquid Iron—Carbon and Iron—Chromium Alloys With Argon.

233-242B

Iron, Ternary systems

The Influence of the Ternary Interaction Parameter ϵ_{Fe}^{Fe} on the Activity of Bismuth in Molten Copper.

427-432B

A Thermodynamic Evaluation of the Fe—Cr—C System. Phase Relationships in the Fe—Cr—Ni System at Solidification Temperatures.

627-636A

An Experimental Study and a Thermodynamic Evaluation of the Fe—Cr—Mo System.

899-908A

An Experimental Study and a Thermodynamic Evaluation of the Cr—Fe—W System.

1385-1394A

Iron, Welding

Free Surface Flow and Heat Transfer in Conduction Mode Laser Welding.

851-858B

Effects of Oxygen and Sulfur on Alloying Element Vaporization Rates During Laser Welding.

967-972B

Iron and steel making

See Oxygen steel making

Steel making

Iron base alloys

See Ferrous alloys

Iron compounds

See also Hematite

Iron oxides
Magnetite
Wustite

Iron compounds, Phase transformations

Electron Microscope Study on Martensitic Transformations in Fe—Pt Alloys; General Features of Internal Structure.

2723-2731A

Nucleation and Growth in Martensitic Transformations of Ordered FePt Alloys.

2931-2936A

Iron compounds, Reactions (chemical)

Leaching of Manganese Nodule in Ammoniacal Medium Using Ferrous Sulfate as the Reductant.

331-334B

Iron ores

See also Hematite

Magnetite

A Dynamic Mathematical Model of the Complete Grate/Kiln Iron-Ore Pellet Induration Process.

103-112B

Gas Flow and Pressure Balancing in Modeling Grate/Kiln Induration.

113-121B

Energy Cost Minimization in Grate/Kiln Induration.

123-132B

Iron ores, Beneficiation

Effect of Temperature on Magnetizing Reduction of Agbaja Iron Ore.

731-735B

Iron oxides

See also Hematite

Magnetite

Wustite

Iron oxides, Thermal properties

Thermal Explosions Resulting From Fuel—Coolant Interactions: Analysis of Single Bubble Hydrodynamics.

563-570B

Iron powder

See Iron

Irradiation damage

See Radiation damage

Isostatic pressing

See Hot isostatic pressing

Isothermal treatment

See Austempering

Jacks (electrical)

See Electric connectors

Joints

See Welded joints

Junghans Rossi casting

See Continuous casting

Kaldo process

See Oxygen steel making

Kikuchi lines

Electron Diffraction Study of α - and α_1 -AlFeSi.

893-898A

Killed steels

See also Aluminum killed steels

Killed steels, Mechanical properties

Investigation of Panel Crack Formation in Steel Ingots. I. Mathematical Analysis and Mid-Face Panel Cracks.

277-287B

Kilns

Gas Flow and Pressure Balancing in Modeling Grate/Kiln Induration.

113-121B

Kinetics

See also Reaction kinetics

Rate of Nitrogen Desorption From Liquid Iron—Carbon and Iron—Chromium Alloys With Argon.

233-242B

The Kinetics of Ferrite Nucleation at Austenite Grain Boundaries in Fe—C Alloys.

427-440A

Analysis of Nonisothermal Transformation Kinetics; Tempering of Iron—Carbon and Iron—Nitrogen Martensites.

925-932A

Chemical and Metallurgical Aspects of Environmentally Assisted Fatigue Crack Growth in 7075-T651 Aluminum Alloy.

1739-1750A

Predicting the Kinetics of Hydrogen Generation at the Tips of Corrosion Fatigue Cracks.

1795-1806A

Ladle metallurgy

Possible Roles of Upper Slag Phases on the Fluid Dynamics of Gas Stirred Ladles.

507-511B

On the Flow Criteria for Suspending Solid Particles in Inductively Stirred Melts. I. Newtonian Behavior.

557-562B

Experimental Investigation of Mixing Phenomena in a Gas Stirred Liquid Bath.

839-850B

Ladles

Fluid Dynamics in Bubble Stirred Ladles. I. Experiments.

745-754B

Fluid Dynamics in Bubble Stirred Ladles. II. Mathematical Modeling.

755-764B

Lamellar structure, Cooling effects

Eutectic Structures of Ag—Cu After Melting and Solidification in Microgravity and on Earth.

2659-2664A

Laminates

See Bimetals

Lanthanide metal alloys

See Thulium base alloys

Lanthanide metals

See Cerium

Laser beam hardening

Laser Melting of Ti-High Speed Tool Steel.

377-382A

Laser Transformation Hardening of Iron—Carbon and Iron—Carbon—Chromium Steels.

2013-2025A

Laser beam heating

Microstructure of Laser Clad Ni—Cr—Al—Hf Alloy on a γ' Strengthened Nickel-Base Superalloy.

1981-1990A

- Fatigue Strength Improvement of Age-Hardened 18Ni Maraging Steel by Stress-Laser Surface Treatment of Subsequent Aging. 2603-2606A
- Laser beam welding**
On the Weldability, Composition, and Hardness of Pulsed and Continuous Nd:YAG Laser Welds in Aluminum Alloys 6061, 5456, and 5086. 319-329B
Free Surface Flow and Heat Transfer in Conduction Mode Laser Welding. 851-858B
Effects of Oxygen and Sulfur on Alloying Element Vaporization Rates During Laser Welding. 967-972B
- Laser processing**
See Laser beam hardening
Laser beam heating
Laser beam welding
- Laser welding**
See Laser beam welding
- Lasers**
Materials for Advanced Studies and Devices. 155-164B
Materials for Advanced Studies and Devices. 749-758A
- Laterites, Reduction (chemical)**
Reducibility of Laterite Ores. 181-186B
- Lattice constant**
See Lattice parameters
- Lattice defects**
See Crystal defects
- Lattice displacements**
See Displacements (lattice)
- Lattice parameters**
The Mechanism of Hydrogen Induced Cleavage in Fe—3% Si Alloy. 1335-1343A
The Competition Between Martensite and Omega in Quenched Ti—Ni Alloys. 1677-1686A
The Apparent "Five-Fold" Nature of Large T_2 (Al_6Li_3Cu) Crystals. 2875-2884A
Convergent Beam Electron Diffraction Analysis of the T_1 (Al_2CuLi) Phase in Al—Li—Cu Alloys. 2885-2891B
- Lattices**
See Crystal lattices
Orthorhombic lattice
- Laves phase**
An Experimental Study and a Thermodynamic Evaluation of the Cr—Fe—W System. 2531-2546A
- Leaching**
See also Acid leaching
Dump leaching
In situ leaching
Measurements of Dielectric Properties for Particulate Sphalerite Samples and Zinc Concentrates. 13-24B
Correlation Between Dielectric Properties and Aqueous Oxidation Rate for Pulverized Sphalerites and Zinc Concentrates. 25-36B
Leaching of Manganese Nodule in Ammoniacal Medium Using Ferrous Sulfate as the Reductant. 331-334B
Dissolution of Columbite and Tantalite in Acidic Fluoride Media. 355-363B
Dissolution Kinetics of Argentinian Plumbojarosite From Old Tailings of Sulfatizing Roasting Pyrites by HCl—CaCl₂ Leaching. 365-373B
Mineralogical Characterization of Silver Flotation Concentrates Made From Zinc Neutral Leach Residues. 803-817B
- Lead (metal), Binary systems**
Densities of Pb—Sn Alloys During Solidification. 2349-2354A
Enthalpies of a Binary Alloy During Solidification. 3057-3061A
- Lead (metal), Casting**
Influence of Mold Length and Mold Heat Transfer on Horizontal Continuous Casting of Nonferrous Alloy Rods. 201-212B
- Lead (metal), Extraction**
Direct Electrowinning of Lead From Suspension Galena Concentrate Anode in Different Electrolytes. 59-65B
Bed Performance in the Direct Electrowinning of Lead From Suspension Galena Anodes. 67-72B
An Intrinsic-Transport Model for Solid—Solid Reactions Involving a Gaseous Intermediate. 73-81B
Correction to "An Intrinsic-Transport Model for Solid—Solid Reactions Involving a Gaseous Intermediate". 519B
- Lead (metal), Reactions (chemical)**
Speciation and Reduction Potentials of Metal Ions in Concentrated Chloride and Sulfate Solutions Relevant to Processing Base Metal Sulfides. 37-45B
- Lead (metal), Ternary systems**
A New Treatment for Determining the Activities From Ternary Miscibility Gap: the O—Cu—Pb System. 373-376A
- Lead base alloys, Crystal growth**
Bulk Undercooling, Nucleation, and Macrosegregation of Pb—Sn Alloys. 2651-2658A
Ostwald Ripening in a System With a High Volume Fraction of Coarsening Phase. 2713-2721A
- Lead base alloys, Directional solidification**
Channel Formation in Pb—Sn, Pb—Sb, and Pb—Sn—Sb Alloy Ingots and Comparison With the System NH_4Cl — H_2O . 1861-1871A
Dendritic Solidification of Alloys in Low Gravity. 2671-2676A
Directional Solidification of Lead—Copper Immiscible Alloys in a Cyclic Gravity Environment. 2677-2680A
Gravitational Macrosegregation in Unidirectionally Solidified Lead—Tin Alloy. 2687-2694A
- Directional Solidification of Cu—Pb and Bi—Ga Monotectic Alloys Under Normal Gravity and During Parabolic Flight. 2839-2846A
- Lead base alloys, Mechanical properties**
Isothermal Fatigue of Low Tin Lead Based Solder. 1051-1059A
Microstructural Observations in Cyclically Deformed Pb—Sn Solid Solution Alloy. 1437-1443A
Cyclic Deformation and Fracture in Pb—Sn Solid Solution Alloy. 1533-1546A
- Lead base alloys, Phase transformations**
Microsegregation in Directionally Solidified Pb—8.4 at.% Au Alloy. 1351-1364A
- Lead base alloys, Structural hardening**
Inhibition of Cyclic Grain Boundary Migration Through Cellular Precipitation in Pb—5% Sn Alloy. 2355-2359A
- Lead ores**
See Galena
- Lead lines**
See Lead lines
- Levitation melting**
Observations on the Dynamics of Electromagnetically Levitated Liquid Metals and Alloys at Elevated Temperatures. 1939-1943A
- Levitation melting, High temperature effects**
Acoustic Levitation Technique for Containerless Processing at High Temperatures in Space. 2619-2623A
- Life**
See Fatigue life
- Light metals**
See Aluminum
Aluminum base alloys
Beryllium
Magnesium
Titanium
Titanium base alloys
- Lime, Reactions (chemical)**
Reaction Mechanism for the CaO—Al and CaO—CaF₂ Desulfurization of Carbon-Saturated Iron. 261-268B
- Line defects**
See Dislocations
- Liquid flow**
Mathematical Modeling of Meniscus Profile and Melt Flow in Electromagnetic Casters. 397-408B
- Liquid metals**
Enthalpies of Formation of the Ag—Au—Si, Ag—Au—Ge, and Ag—Au—Sn Ternary Liquid Alloys; Experimental Determinations and Application of the Hoch—Arpschoven Model. 2075-2089A
- Liquid metals, Diffusion**
Prediction of Solute Diffusion Coefficients in Liquid Metals. 273-279A
- Liquid metals, Physical properties**
Experimental Measurement and Numerical Computation of Velocity and Turbulence Parameters in a Heated Liquid Metal System. 765-775B
The Wetting Characteristics and Surface Tension of Some Nickel-Based Alloys on Yttria, Hafnia, Alumina, and Zirconia Substrates. 1833-1839A
- Liquid metals, Reactions (chemical)**
The Reaction Between Solid Iron and Liquid Al—Zn Baths. 1193-1203A
- Liquid metals, Refining**
The Calcium—Phosphorus and the Simultaneous Calcium—Oxygen and Calcium—Sulfur Equilibria in Liquid Iron. 617-622B
- Liquid metals, Thermal properties**
Thermodynamics of Molten Li—Sn Alloys. 637-644A
Convective Heat-Transfer Measurements in Liquid Metals Under Different Fluid Flow Conditions. 859-870B
- Liquid phase diffusion**
See Diffusion
- Liquid phase sintering**
Microstructure Effects on Tensile Properties of Tungsten—Nickel—Iron Composites. 1523-1532A
Gravity and Configurational Energy Induced Microstructural Changes in Liquid Phase Sintering. 1905-1913A
Microstructural Refinement of W—Ni—Fe Heavy Alloys by Alloying Additions. 3100-3103A
- Liquid phases**
A Study of the Transient Liquid Phase Bonding Process Applied to a Ag/Cu/Ag Sandwich Joint. 675-686A
- Liquidus**
Thermodynamics of Molten Li—Sn Alloys. 637-644A
- Lithium, Alloying elements**
The Aging Characteristics of an Al—2% Li—3% Cu—0.12% Zn Alloy at 190°C. 51-66A
The Solubility of Hydrogen in Liquid Binary Al—Li Alloys. 227-232B
Theoretical Investigation of the Precipitation of δ' in Al—Li. 249-258A
Reactivity of Al—2.5% Li Alloy With Water as Studied by the Exploding Wire Technique. 255-259B
Fatigue Crack Propagation in Aluminum—Lithium Alloy 2090. I. Long Crack Behavior. 549-561A
Fatigue Crack Propagation in Aluminum—Lithium Alloy 2090. II. Small Crack Behavior. 563-569A
- Lithium, Binary systems**
The Cata- or Metatectic Reaction—Occurrence and Microstructural Development. 3097-3100A

Lithium

- Lithium, Quaternary systems**
Solidus and Solvus Isotherms for Quaternary Al—Li—Cu—Mg Alloys. 1631-1634A
- Lithium, Recovering**
The Reaction Between Spodumene and Tachyhydrite. 663-668B
- Lithium, Thermal properties**
Thermodynamics of Molten Li—Sn Alloys. 637-644A
- Lithium compounds, Crystal lattices**
The Apparent "Five-Fold" Nature of Large T_2 (Al_2Li_3Cu) Crystals. 2875-2884A
Convergent Beam Electron Diffraction Analysis of the T_1 (Al_2CuLi) Phase in Al—Li—Cu Alloys. 2885-2891B
- Live loads**
See Cyclic loads
- Lixivation**
See Leaching
- Loads (forces)**
See Cyclic loads
- Loose powder sintering**
Kinetics of Neck Growth During Loose Stack Sintering. 2153-2161A
- Low alloy steels**
See also Carbon manganese steels
Electrical steels
- Low alloy steels, Welding**
The Nonuniform Distribution of Inclusions in Low-Alloy Steel Weld Deposits. 669-674A
- Low cycle fatigue**
Creep—Fatigue Life Prediction in Terms of Nucleation and Growth of Fatigue Crack and Creep Cavities. 121-127A
The Influence of Mo_2C Morphology and Distribution on the Fatigue Crack Initiation and Propagation Behavior of Fe—C—Mo Dual-Phase Steels. 973-986A
Investigation of Microstructural Changes in a Ferritic Steel Caused by High Temperature Fatigue. 999-1007A
Fatigue Oxidation Interaction in IN 100 Superalloy. 2259-2268A
Fatigue Damage Accumulation in Nickel Modified by Ion Beam Surface Microalloying. 2775-2788A
- Low cycle fatigue, Stress effects**
Influence of Time and Temperature Dependent Processes on Strain Controlled Low Cycle Fatigue Behavior of Alloy 617. 359-371A
- Luders bands**
See Luders lines
- Luders lines**
Microscopic Shear Localization in Nickel. 2041-2048A
- Macrofractography**
See Fractography
- Magnesium, Alloying elements**
Precipitation of Guinier—Preston Zones in Aluminum—Magnesium; a Calorimetric Analysis of Liquid-Quenched and Solid-Quenched Alloys. 2433-2443A
Microstructure—Property Relationship in a 2XXX Aluminum Alloy With Magnesium Addition. 2523-2530A
- Magnesium, Binary systems**
The Cata- or Metatectic Reaction—Occurrence and Microstructural Development. 3097-3100A
- Magnesium, Extraction**
An Intrinsic-Transport Model for Solid—Solid Reactions Involving a Gaseous Intermediate. 73-81B
Correction to "An Intrinsic-Transport Model for Solid—Solid Reactions Involving a Gaseous Intermediate". 519B
- Magnesium, Impurities**
The Effects of Mg^{2+} , Mn^{2+} , Zn^{2+} , and Al^{3+} on the Nickel Deposit During Electrowinning From Sulfate Bath. 823-830B
- Magnesium, Quaternary systems**
Solidus and Solvus Isotherms for Quaternary Al—Li—Cu—Mg Alloys. 1631-1634A
- Magnetic anisotropy**
Texture Induced Magnetic Anisotropy in Fe—Nd—B Magnet Prepared via Rapid Solidification and Hot Extrusion Techniques. 3109-3112A
- Magnetic induction**
See Electromagnetic induction
- Magnetic materials**
See also Magnetite
- Magnetic materials, Crystal growth**
A Proposal for Epitaxial Thin Film Growth in Outer Space. 2639-2643A
- Magnetic materials, Powder technology**
Texture Induced Magnetic Anisotropy in Fe—Nd—B Magnet Prepared via Rapid Solidification and Hot Extrusion Techniques. 3109-3112A
- Magnetic permeability**
Magnetic Properties of Rare Earth—Barium—Copper Oxides in the Normal and Superconducting States. 734-738A
- Magnetic permeability, Corrosion effects**
Analytical Electron Microscopy of Internally Oxidized Mn—P Steel. 1876-1878A
- Magnetic properties**
See Curie temperature
Magnetic anisotropy
Magnetic permeability
- Magnetic susceptibility**
See Magnetic permeability

- Magnetic transitions**
Magnetic-Induced Tricritical Points in Alloys. 441-446A
- Magnetite**
Effect of Temperature on Magnetizing Reduction of Agbaja Iron Ore. 731-735B
The Evidence for a Miscibility Gap in the Fe_3O_4 — $ZnFe_2O_4$ System—a Review. 919-925B
- Magnetite, Crystal growth**
Hematite Single Crystal Reduction Into Magnetite With CO_2 . 311-317B
- Magnetization, Temperature effects**
Effect of Temperature on Magnetizing Reduction of Agbaja Iron Ore. 731-735B
- Manganese, Alloying elements**
Hydrogen Embrittlement of Pseudobinary $L1_2$ -Type $Ni_3(Al_{0.4}Mn_{0.6})$ Intermetallic Compound. 353-357A
Measurement and Modeling of Alloy—Spinel—Corundum Equilibrium in the Ni—Mn—Al—O System at 1873K. 459-463B
Observations on Void Nucleation and Growth in α/β Ti—Mn Alloys. 1311-1317A
Effects of Manganese, Phosphorus and Molybdenum on Sulfide Stress Cracking Resistance of High Strength Low Alloy Steels. 2171-2177A
The Effect of Alloying Elements and Microstructure on the Strength and Fracture Resistance of Pearlitic Steel. 2819-2829A
- Manganese, Binary systems**
Thermodynamics of the Cr—Mn System Using an Isopiestic Technique. 649-654B
- Manganese, Extraction**
Leaching of Manganese Nodule in Ammoniacal Medium Using Ferrous Sulfate as the Reductant. 331-334B
- Manganese, Impurities**
The Effects of Mg^{2+} , Mn^{2+} , Zn^{2+} , and Al^{3+} on the Nickel Deposit During Electrowinning From Sulfate Bath. 823-830B
- Manganese, Recovering**
Studies on the Dry Chlorination of Deep Sea Manganese Nodules. 514-518B
- Manganese base alloys, Phase transformations**
Pretransformation Phenomena as Revealed by Elastic Waves. 185-191A
- Manganese base alloys, Thermal properties**
Standard Gibbs Energies of Formation of the Carbides of Manganese by EMF Measurements. 951-957B
- Manganese compounds, Mechanical properties**
High Temperature Strength and Ductility of Recrystallized Ni_3Al — Ni_3Mn Alloys. 345-352A
Hydrogen Embrittlement of Pseudobinary $L1_2$ -Type $Ni_3(Al_{0.4}Mn_{0.6})$ Intermetallic Compound. 353-357A
- Manganese compounds, Powder technology**
Mechanical Alloying of Brittle Materials. 2867-2874A
- Manganese compounds, Reactions (chemical)**
Kinetics of Manganous Oxide Sulfidization in Carbonyl Sulfide (CO_2) Contaminated Atmospheres. 303-310B
- Manganese steels, Mechanical properties**
The Effect of Tin, Aluminum, and Nitrogen on the Hot Ductility of a Carbon—Manganese Steel Between 700-1200°C. 1305-1309A
Tensile Deformation Behavior of Mechanically Stabilized Fe—Mn Austenite. 1563-1568A
Tensile Fracture of Coarse-Grained Cast Austenitic Manganese Steels. 2269-2277A
- Manganese steels, Metal working**
Effects of Thermomechanical Processing on the Microstructure and Mechanical Properties of a Ti—V—N Steel. 1221-1234A
- Manual metal arc welding**
See Shielded metal arc welding
- Maraging steels, Heat treatment**
Fatigue Strength Improvement of Age-Hardened 18Ni Maraging Steel by Stress-Laser Surface Treatment of Subsequent Aging. 2603-2606A
- Marine atmospheres**
See Marine environments
- Marine environments**
Predicting the Kinetics of Hydrogen Generation at the Tips of Corrosion Fatigue Cracks. 1795-1806A
- Martensite**
The Competition Between Martensite and Omega in Quenched Ti—Nb Alloys. 1677-1686A
Effect of Microstructure on Plane-Strain Fracture Toughness of AISI 4340 Steel. 2513-2521A
Effect of Microstructure on Fracture Behavior of Complex Structure in 6Ni—0.3C Steel. 2606-2611A
- Martensite, Crystal lattices**
X-Ray and Neutron Diffraction Anomalies Preceding Martensitic Phase Transformation in $AuCuZn_2$ Alloys. 793-796A
- Martensite, Phase transformations**
Analysis of Nonisothermal Transformation Kinetics; Tempering of Iron—Carbon and Iron—Nitrogen Martensites. 925-932A
- Martensitic transformations**
Symmetry Aspects of Pretransformation Behavior in Metallic Alloys. 159-167A
Electron—Phonon Based Local Mode Descriptions of Displacive Transformations. 177-183A
Pretransformation Phenomena as Revealed by Elastic Waves. 185-191A

- Neutron Scattering Studies of Premartensitic Indium—Thallium Alloys. 193-198A
- Electron Diffuse Scattering Studies of Premartensitic Alloys: β' Cu—Zn, β' Ni—Al, In—Ti, and Fe—Ni. 199-205A
- Beta-Phase Stability and Martensitic Nucleation in Hume-Rothery Alloys. 207-216A
- Premartensitic Strain Tensor Analysis of $\text{Ni}_{35}\text{Al}_{65}$ by the X-Ray Divergent Beam Method. 217-223A
- X-Ray Study of the Premartensitic Phenomena in AuCd. 265-271A
- Swing Back in Kinetics Near M_s in Hyperitectoid Steels. 447-452A
- Nonlinear and Nonlocal Continuum Model of Transformation Precursors in Martensites. 761-775A
- Modulated Lattice Relaxation in β -Based Premartensitic Phase. 777-781A
- Computer Study of Tweed as a Precursor to a Martensitic Transformation of a BCC Lattice. 783-787A
- Premartensitic Anelasticity in Indium—Thallium Alloys. 789-792A
- X-Ray and Neutron Diffraction Anomalies Preceding Martensitic Phase Transformation in AuCuZn_{75} Alloys. 793-796A
- Tweed Structures Associated With FCC—FCT Transformations in Fe—Pd Alloys. 803-810A
- Quasi-One-Dimensional Model of Pretransitional Soft Mode Behavior. 811-818A
- Elastic Properties of β -Uranium and the Martensitic α' -Phase in Uranium—Gallium Alloys. 909-913A
- Some Stress—Strain—Temperature Relationships for Shape Memory Alloys. 2407-2413A
- A Theoretical Analysis of the Spinodal Decomposition in Fe—C Martensite During Aging Stage of Tempering. 2427-2432A
- Electron Microscope Study on Martensitic Transformations in Fe—Pt Alloys: General Features of Internal Structure, Nucleation and Growth in Martensitic Transformations of Ordered Fe₃Pt Alloys. 2723-2731A
- 2931-2936A
- Martensitic transformations, Alloying effects**
- Tensile Deformation Behavior of Mechanically Stabilized Fe—Mn Austenite. 1563-1568A
- Martensitic transformations, Diffusion effects**
- Nature of the γ and γ' Phases in Austenitic Stainless Steels Cathodically Charged With Hydrogen. 723-730A
- Martensitic transformations, Low temperature effects**
- Low Temperature Electron Microscopy on the Cubic-Tetragonal Transformation of V_3Si . 797-801A
- Martensitic transformations, Microstructural effects**
- Thermodynamics and Kinetics of $\delta \rightarrow \alpha$ Martensitic Transformation in Plutonium Alloys. 2705-2711A
- Martensitic transformations, Stress effects**
- Orientation Dependence of $\beta_1 \rightarrow \beta'$ Stress-Induced Martensitic Transformation in a Cu—Al—Ni Alloy. 915-923A
- Effect of Temperature and Strain Distribution on Martensitic Transformation During Uniaxial Testing of AISI-304 Stainless Steel. 1021-1026A
- Mass transfer**
- Kinetics of Manganese Oxide Sulfidization in Carbonyl Sulfide (COS) Contaminated Atmospheres. 303-310B
- Master alloys, Development**
- Discussion of "The Role of Boron in the Grain Refinement of Aluminum With Titanium" and Authors' Reply. 385-387A
- Materials testing**
- See Surface analysis (chemical)
- Ultrasonic testing
- Volumetric analysis
- Mathematical analysis**
- Thermodynamic Consistency of the Interaction Parameter Formalism. 269-275B
- Flow Fields in Electromagnetic Stirring of Rectangular Strands With Linear Inductors. II. Computation of Flow Fields in Billets, Blooms, and Slabs of Steel. 595-602B
- Thermochemistry of the Intermetallic Compounds RuTi, RuZr, and RuHf. 1061-1066A
- Determination of Dihedral Angle Distributions in Polycrystals: Application to $\alpha + \beta$ Brass. 1147-1151A
- Intercrystalline Structure Distribution in Alloy 304 Stainless Steel. 1179-1185A
- Hydrogen Permeation Through Coated and Uncoated Waspaloy. 1187-1192A
- The Effect of Triaxial Stress Field on Intermediate Temperature Embrittlement of Ferritic Spheroidal Graphite Cast Irons. 1213-1219A
- Modeling Tensile Deformation of Dual-Phase Steel. 1263-1268A
- The Mechanism of Hydrogen Induced Cleavage in Fe—3% Si Alloy. 1335-1343A
- Microsegregation in Directionally Solidified Pb—8.4 at.% Au Alloy. 1351-1364A
- Some Stress—Strain—Temperature Relationships for Shape Memory Alloys. 2407-2413A
- Mathematical models**
- Creep—Fatigue Life Prediction in Terms of Nucleation and Growth of Fatigue Crack and Creep Cavities. 121-127A
- Energy Cost Minimization in Grate/Kiln Induration. 123-132B
- Transverse Elastic Moduli of Unidirectional Fiber Composites With Interfacial Debonding. 129-135A
- Performance Analysis of the Aluminum Casting Furnace. 171-180B
- Influence of Mold Length and Mold Heat Transfer on Horizontal Continuous Casting of Nonferrous Alloy Rods. 201-212B
- Melting Metal Powder Particles in an Inductively Coupled R.F. Plasma Torch. 213-226B
- Prediction of Solute Diffusion Coefficients in Liquid Metals. 273-279A
- Investigation of Panel Crack Formation in Steel Ingots. I. Mathematical Analysis and Mid-Face Panel Cracks. 277-287B
- Investigation of Panel Crack Formation in Steel Ingots. II. Off-Corner Panel Cracks. 289-301B
- Mathematical Modeling of Meniscus Profile and Melt Flow in Electromagnetic Casters. 397-408B
- Measurement and Modeling of Alloy—Spinel—Corundum Equilibrium in the Ni—Mn—Al—O System at 1873K. 459-463B
- Volume Effects and Associations in Liquid Alloys. 465-470B
- The Mathematical Modeling Revolution in Extractive Metallurgy. 525-540B
- Thermodynamics for Arsenic and Antimony in Copper Matte Converting—Computer Simulation. 547-556B
- On the Flow Criteria for Suspending Solid Particles in Inductively Stirred Melts. I. Newtonian Behavior. 557-562B
- Thermal Explosions Resulting From Fuel—Coolant Interactions: Analysis of Single Bubble Hydrodynamics. 563-570B
- A Simple Fluid Mechanical Model for Planar Flow Casting Melt-Spinning. 571-579B
- Flow Fields in Electromagnetic Stirring of Rectangular Strands With Linear Inductors. I. Theory and Experiments With Cold Models. 581-593B
- The Calcium—Phosphorus and the Simultaneous Calcium—Oxygen and Calcium—Sulfur Equilibria in Liquid Iron. 617-622B
- Modeling of Thermomechanical Processing of Heat-Treatable Aluminum Alloys. 617-625A
- Fluid Dynamics in Bubble Stirred Ladles. II. Mathematical Modeling. 755-764B
- Experimental Measurement and Numerical Computation of Velocity and Turbulence Parameters in a Heated Liquid Metal System. 765-775B
- Quasi-One-Dimensional Model of Pretransitional Soft Mode Behavior. 811-818A
- The Trajectories and Distribution of Particles in a Turbulent Axisymmetric Gas Jet Injected Into a Flash Furnace Shaft. 871-884B
- Characterization of Two-Phase Axisymmetric Plume in a Gas Stirred Liquid Bath—a Water Model Study. 885-892B
- Phase Relationships in the Fe—Cr—Ni System at Solidification Temperatures. 899-908A
- Modeling the Texture Dependence of Environmentally Assisted Growth of Long and Short Cracks. 1009-1020A
- Microstructure and Fracture Toughness of the Aged β -Ti Alloy Ti—10V—2Fe—3Al. 1037-1049A
- Changes in the Longitudinal Flow and Apparent Plastic Poisson's Ratio of a Porous Metal Strip During Hot Densification Rolling. 1205-1211A
- Effect of Annealing Temperature on Yield Anisotropy of Zircaloy-4 TREX. 1243-1255A
- Crack Growth From Internal Hydrogen—Temperature and Microstructural Effects in 4340 Steel. 1319-1334A
- Fractal Analysis of a Nucleation and Growth Process. 1371-1372A
- Wear-Enhanced Hydrogen Evolution From Mild Steel. 1721-1726A
- Predicting the Kinetics of Hydrogen Generation at the Tips of Corrosion Fatigue Cracks. 1795-1806A
- On the Slopes of Phase Boundaries. 1819-1825A
- Thermodynamics of Segregation in Alloys. 2091-2098A
- A New Model for Precipitation at Moving Interphase Boundaries. 2133-2138A
- Initial Development of Thermal and Stress Fields in Continuously Cast Steel Billets. 2589-2602A
- Enthalpies of a Binary Alloy During Solidification. 3057-3061A
- Mathematics**
- See Finite element method
- Mathematical analysis
- Mathematical models
- Mattes**
- See Copper mattes
- Measurement**
- See also Flow measurement
- Thickness measurements
- Measurement, Shape effects**
- Grain Shape and Its Influence on the Experimental Measurement of Grain Size. 933-940A
- Measuring**
- See Measurement
- Measuring instruments**
- See Accelerometers
- Polarimeters
- Temperature measuring instruments
- Mechanical alloying**
- Aluminum—Lithium Powder Metallurgy Alloys With Improved Toughness. 603-615A
- Yield Stress as Determined From Hardness Measurements for Mechanically Alloyed Aluminum Base Alloys. 2363-2366A
- Mechanical alloying, Temperature effects**
- Mechanical Alloying of Brittle Materials. 2867-2874A
- Mechanical properties**
- See Bend strength
- Bonding strength
- Brittleness
- Compressive strength
- Creep (materials)
- Creep life
- Creep rate
- Creep rupture strength
- Creep strength
- Diamond pyramid hardness
- Ductile brittle transition
- Ductility
- Elastic anisotropy
- Elastic constants
- Elongation
- Fatigue (materials)
- Fatigue life
- Fatigue strength

Mechanical properties

- Fracture strength
 - Fracture toughness
 - Hardness
 - Hydrogen embrittlement
 - Impact strength
 - Internal friction
 - Microhardness
 - Modulus of elasticity
 - Notch sensitivity
 - Plasticity
 - Residual stress
 - Shear strength
 - Shear stress
 - Stress relaxation
 - Superplasticity
 - Temper brittleness
 - Tensile properties
 - Tensile strength
 - Thermoelastic properties
 - Toughness
 - True strain
 - Yield point
 - Yield strength
- Mechanical tests**
See Creep tests
Fatigue tests
Hardness tests
Tension tests
- Mechanics**
See Fluid dynamics
Fluid mechanics
Fracture mechanics
Hydrodynamics
Kinetics
- Melt spinning**
Effect of Melt Spinning on the Microstructure and Mechanical Properties of Three Nickel-Base Superalloys. 93-103A
A Simple Fluid Mechanical Model for Planar Flow Casting Melt-Spinning. 571-579B
Characterization of the Aging Response of a Melt-Spun Al—Be—Li Alloy Ribbon. 1173-1178A
Formation of Metal—Metal Type Aluminum-Based Amorphous Alloys. 1369-1371A
Effect of Melt Spinning on Grain Size and Texture in Ni—Mo Alloys. 1711-1720A
Solidification Structures in Rapidly Quenched Cu—Ti—Zr Alloys. 1853-1860A
Rutherford Backscattering Study of High Temperature Oxidation of Melt-Spun Glassy Fe—22.5Al—10Zr. 2567-2573A
Texture Induced Magnetic Anisotropy in Fe—Nd—B Magnet Prepared via Rapid Solidification and Hot Extrusion Techniques. 3109-3112A
- Melting**
See Levitation melting
Plasma arc melting
Vacuum arc melting
- Melting furnaces**
See Converters
- Melting points**
The Influence of the Ternary Interaction Parameter ϵ_{ij}^E on the Activity of Bismuth in Molten Copper. 427-432B
- Melting points, Composition effects**
A Melting and Solidification Study of Alloy 625. 2319-2331A
- Melts**
On the Flow Criteria for Suspending Solid Particles in Inductively Stirred Melts. I. Newtonian Behavior. 557-562B
- Melts, Reactions (chemical)**
On the Interfacial Rate of Reaction of CO₂ With a Calcium Ferrite Melt. 959-965B
- Memory (shape)**
See Shape memory
- Mercury (metal), Extraction**
Study by SEM-EDS of the In Situ Dynamic Leaching of Mercury Ores. 165-170B
- Mercury compounds, Beneficiation**
Study by SEM-EDS of the In Situ Dynamic Leaching of Mercury Ores. 165-170B
- Metal baths**
The Reaction Between Solid Iron and Liquid Al—Zn Baths. 1193-1203A
- Metal carbides**
See Tungsten carbide
- Metal powders**
See also Alloy powders
- Metal powders, Melting**
Melting Metal Powder Particles in an Inductively Coupled R.F. Plasma Torch. 213-226B
- Metal powders, Microstructure**
The Evolution of Microcrystalline Structures in Supercooled Metal Powders. 699-708A
The Microstructure and Phase Relationships in Rapidly Solidified Type 304 Stainless Steel Powders. 2399-2405A
- Metal working**
See Finish rolling
Hot rolling
Stretch forming
Thermomechanical treatment
- Metallic glasses**
Formation of Amorphous and Metastable Extended Solid Solutions in Cu—Ti Alloys Using the Triode Sputtering Technique. 5-12A
- Metallic glasses, Alloy development**
Ductile Al—Cu—V Amorphous Alloys Without Metalloid. 391-393A
- Metallic glasses, Casting**
Formation of Metal—Metal Type Aluminum-Based Amorphous Alloys. 1369-1371A
- Metallic glasses, Microstructure**
Amorphous Cr₅Si₃ Thin Films—Morphology and Kinetics of Crystallization. 1991-2003A
- Metallic glasses, Oxidation**
Rutherford Backscattering Study of High Temperature Oxidation of Melt-Spun Glassy Fe—22.5Al—10Zr. 2567-2573A
- Metallic glasses, Phase transformations**
Quasicrystalline Phase in Al—Si—Mn System Prepared by Annealing of Amorphous Phase. 383-385A
Phase Transformation During Annealing of Rapidly Solidified Aluminum-Rich Al—Fe—Si Alloys. 2893-2900A
- Metallic glasses, Phases (state of matter)**
Solidification Structures in Rapidly Quenched Cu—Ti—Zr Alloys. 1853-1860A
- Metallic glasses, Physical properties**
Hydrogen in Iron. 691-707B
Hydrogen in Iron. 2371-2387A
- Metallic glasses, Powder technology**
Preparation of Iron-, Cobalt- and Nickel-Based Amorphous Alloy Powders by High-Pressure Gas Atomization and Their Structural Relaxation Behavior. 235-242A
Mechanical Alloying of Brittle Materials. 2867-2874A
- Metallic glasses, Synthesis**
Formation of Ultra-Fine Amorphous Powders in Fe—M—B (M = Transition Metal) Systems by Chemical Reduction Method and Their Thermal and Magnetic Properties. 2315-2318A
- Metallic glasses, Welding**
Consolidation of Metallic Glass Ribbons Using Electric Discharge Welding. 1634-1638A
- Metallographic structures**
See Microstructure
- Metallography**
See Quantitative metallography
- Metalloid alloys**
See Silicon base alloys
- Metalloid compounds**
See Silicon carbide
Silicon compounds
Silicon dioxide
- Metalloids**
See Arsenic
Boron
Silicon
- Metallurgical constituents**
See Laves phase
- Metastable phases**
Formation of Amorphous and Metastable Extended Solid Solutions in Cu—Ti Alloys Using the Triode Sputtering Technique. 5-12A
Theoretical Investigation of the Precipitation of δ' in Al—Li. 249-258A
Investigation of Phase Transformation in an Al—0.58 wt.% Fe Alloy by Mossbauer Spectroscopy. 259-264A
Quasicrystalline Phase in Al—Si—Mn System Prepared by Annealing of Amorphous Phase. 383-385A
The Competition Between Martensite and Omega in Quenched Ti—Nb Alloys. 1677-1686A
The Competition Between the Alpha and Omega Phases in Aged Ti—Nb Alloys. 1687-1694A
Competitive Growth of Stable and Metastable Fe—C—X Eutectics. I. Experiments. 1955-1963A
Competitive Growth of Stable and Metastable Fe—C—X Eutectics. II. Mechanisms. 1965-1971A
The Stable and Metastable Ti—Nb Phase Diagrams. 2389-2397A
The Microstructure and Phase Relationships in Rapidly Solidified Type 304 Stainless Steel Powders. 2399-2405A
- Metastable phases, Crystal lattices**
Microstructural Characterization of the Dispersed Phases in Al—Ce—Fe System. 1645-1656A
- Metastable phases, Heating effects**
Phase Transformation During Annealing of Rapidly Solidified Aluminum-Rich Al—Fe—Si Alloys. 2893-2900A
- Meteorites, Microstructure**
Meteorites as Specimens for Microgravity Research. 1919-1923A
- Metering (measurement)**
See Measurement
- Microalloyed steels**
See High strength low alloy steels
- Microcracking**
See Crack initiation
- Microfractography**
See Fractography
- Microhardness, Alloying effects**
Formation of Metal—Metal Type Aluminum-Based Amorphous Alloys. 1369-1371A

- Microhardness, Diffusion effects**
Effect of Cathodic Charging on the Mechanical Properties of Aluminum. 2299-2304A
- Microporosity, Composition effects**
Study of Microporosity Formation in Nickel-Base Superalloys. 2341-2348A
- Microradiography**
Measuring Creep Damage Using Microradiography. 837-845A
- Microscopy**
See Electron microscopy
Microradiography
Transmission electron microscopy
- Microstructure**
See also Lamellar structure
Investigation of Panel Crack Formation in Steel Ingots. II. Off-Corner Panel Cracks. 289-301B
Fatigue Crack Propagation Behavior of Titanium Alloys 6242S and 5621S at Elevated Temperature. 881-885A
Investigation of Microstructural Changes in a Ferritic Steel Caused by High Temperature Fatigue. 999-1007A
The Competition Between the Alpha and Omega Phases in Aged Ti-Nb Alloys. 1687-1694A
Gravity and Configurational Energy Induced Microstructural Changes in Liquid Phase Sintering. 1905-1913A
- Microstructure, Alloying effects**
The Effect of Varying Aluminum, Titanium, and Niobium Content on the Phase Stability of Inconel 718. 1657-1666A
Correction to "The Effects of Varying Aluminum, Titanium, and Niobium Content on the Phase Stability of Inconel 718". 1657-1666A
Competitive Growth of Stable and Metastable Fe-C-X Eutectics. II. Mechanisms. 1965-1971A
Microstructure of Laser Clad Ni-Cr-Al-Hf Alloy on a γ' Strengthened Nickel-Base Superalloy. 1981-1990A
Laser Transformation Hardening of Iron-Carbon and Iron-Carbon-Chromium Steels. 2013-2025A
Microstructure-Property Relationship in a 2XXX Aluminum Alloy With Magnesium Addition. 2523-2530A
- Microstructure, Composition effects**
The Influence of Interfacial Energies and Gravitational Levels on the Directionally Solidified Structures in Hypermonotectic Alloys. 2665-2669A
The Partitioning of Alloying Elements in Vacuum Arc Remelted, Palladium-Modified PH 13-8 Molybdenum Alloys. 3063-3069A
- Microstructure, Deformation effects**
Microscopic Shear Localization in Nickel. 2041-2048A
Assessment of Service Induced Microstructural Damage and Its Rejuvenation in Turbine Blades. 2049-2066A
- Microstructure, Impurity effects**
The Influence of Boron on the Grain Boundary Chemistry and Microstructure of Ni-16Cr-9Fe-0.03C. 2555-2566A
- Mill scale**
See Scale (corrosion)
- Mineral acids**
See Inorganic acids
- Miscibility**
A New Treatment for Determining the Activities From Ternary Miscibility Gap: the O-Cu-Pb System. 373-376A
- Mixing**
See also Ion beam mixing
Mechanical alloying
Fluid Dynamics in Channel Reactors Stirred by Submerged Gas Injection. 603-612B
- Mobility**
See Dislocation mobility
- Modulus of elasticity**
Transverse Elastic Moduli of Unidirectional Fiber Composites With Interfacial Debonding. 129-135A
Structure and Mechanical Properties of Unidirectionally Solidified Fe-Cr-C and Fe-Cr-X-C Alloys. 1235-1241A
- Modulus of elasticity, High temperature effects**
The Elastic Modulus and Flow Stress of Nb₃Sn at Elevated Temperatures. 1127-1128A
- Modulus of elasticity, Microstructural effects**
Orientation Dependence of $\beta_1 \rightarrow \beta'$ Stress-Induced Martensitic Transformation in a Cu-Al-Ni Alloy. 915-923A
- Moistening**
See Wetting
- Moisture**
See Water
- Molds, Design**
Influence of Mold Length and Mold Heat Transfer on Horizontal Continuous Casting of Nonferrous Alloy Rods. 201-212B
- Molten metal baths**
See Metal baths
- Molten metals**
See Liquid metals
- Molybdenum, Alloying elements**
Activity of Carbon in Nickel-Rich Ni-Mo and Ni-W Alloys. Effect of Melt Spinning on Grain Size and Texture in Ni-Mo Alloys. 645-650A
Effects of Manganese, Phosphorus and Molybdenum on Sulfide Stress Cracking Resistance of High Strength Low Alloy Steels. 1711-1720A
Microstructural Refinement of W-Ni-Fe Heavy Alloys by Alloying Additions. 2171-2177A
3100-3103A
- Molybdenum, Recovering**
Studies on Oxychlorination of MoS₂ in a Fluid Bed Reactor. 669-675B
- Molybdenum, Ternary systems**
An Experimental Study and a Thermodynamic Evaluation of the Fe-Cr-Mo System. 1385-1394A
- Molybdenum, Thermal properties**
Measurement of Temperature and Emissivity of Specularly Reflecting Glowing Bodies. 1889-1894A
- Molybdenum base alloys, Coating**
Evaluation of High-Temperature Diffusion Barriers for the Pt-Mo System. 2163-2170A
- Molybdenum chromium nickel steels**
See Nickel chromium molybdenum steels
- Molybdenum chromium steels**
See Chromium molybdenum steels
- Molybdenum compounds, Crystal lattices**
Kinetics of Domain Growth in Ordered Ni₃Mo. 941-952A
- Molybdenum nickel chromium steels**
See Nickel chromium molybdenum steels
- Molybdenum steels**
See also Chromium molybdenum steels
Chromium molybdenum vanadium steels
Nickel chromium molybdenum steels
- Molybdenum steels, Cleaning**
Studies on the Determination of Surface Deuterium in AISI 1062, 4037, and 4140 Steels by Secondary Ion Mass Spectrometry. 3071-3075A
- Molybdenum steels, Mechanical properties**
The Influence of Mo₂C Morphology and Distribution on the Fatigue Crack Initiation and Propagation Behavior of Fe-C-Mo Dual-Phase Steels. 973-986A
- Molybdenum steels, Phase transformations**
Effect of Deformation on the Austenite-to-Ferrite Transformation in a Plain Carbon and Two Microalloyed Steels. 417-426A
- Molybdenum steels, Structural hardening**
Orowan Strengthening by Mo₂C Fibers and Needle Interphase Precipitates in Fe-C-Mo Dual-Phase Steels. 1617-1620A
- Monocrystals**
See Single crystals
- Natural strain**
See True strain
- Necking**
Void Formation During Tensile Testing of Dual Phase Steels. 579-589A
- Necking, Temperature effects**
The Flow Equation and its Necking Criterion in Austenitic Cryogenic Fe-Mn-Al-X Steels. 1625-1626A
- Neutron diffraction**
X-Ray and Neutron Diffraction Anomalies Preceding Martensitic Phase Transformation in AuCuZn₂ Alloys. 793-796A
Characterization of Residual Stresses in Bent Incoloy-800 Tubing by Neutron Diffraction. 2207-2214A
- Nickel, Alloying elements**
Discussion of "Sulfide Stress Cracking Susceptibility of Nickel Containing Steels" and Authors' Reply. 153A
Directional Solidification of Al-Ni/SiC Composites During Parabolic Trajectories. 1899-1904A
The Effect of Alloying Elements and Microstructure on the Strength and Fracture Resistance of Pearlitic Steel. 2819-2829A
A Preliminary Study of the Influence of Separate and Combined Aluminum and Nickel Additions on the Properties of a Secondary Hardening Steel. 3103-3107A
- Nickel, Diffusion**
Thermodynamics of Segregation in Alloys. 2091-2098A
- Nickel, Extraction**
Determination of the Diffusion Coefficients of CuSO₄, ZnSO₄, and NiSO₄ in Aqueous Solution. 5-12B
Reducibility of Laterite Ores. 181-186B
Leaching of Manganese Nodule in Ammoniacal Medium Using Ferrous Sulfate as the Reductant. 331-334B
The Effects of Mg²⁺, Mn²⁺, Zn²⁺, and Al³⁺ on the Nickel Deposit During Electrowinning From Sulfate Bath. 823-830B
- Nickel, Irradiation**
Creep Cavity Growth From Tritium-Induced Helium Bubbles in Nickel. 821-827A
- Nickel, Melting**
Observations on the Dynamics of Electromagnetically Levitated Liquid Metals and Alloys at Elevated Temperatures. 1939-1943A
- Nickel, Microstructure**
Microscopic Shear Localization in Nickel. 2041-2048A
- Nickel, Powder technology**
The Evolution of Microcrystalline Structures in Supercooled Metal Powders. 699-708A
- Nickel, Reactions (chemical)**
Speciation and Reduction Potentials of Metal Ions in Concentrated Chloride and Sulfate Solutions Relevant to Processing Base Metal Sulfides. 37-45B
- Nickel, Recovering**
Studies on the Dry Chlorination of Deep Sea Manganese Nodules. 514-518B
- Nickel, Solubility**
The Effect of Temperature on Nickel Solubility in Silica Saturated Fayalite Slags From 1523-1623K. 243-247B

Nickel

Nickel, Ternary systems

Phase Relationships in the Fe—Cr—Ni System at Solidification Temperatures.

899-908A

Nickel base alloys, Casting

Effect of Melt Spinning on the Microstructure and Mechanical Properties of Three Nickel-Base Superalloys.

93-103A

Nickel base alloys, Cladding

Microstructure of Laser Clad Ni—Cr—Al—Hf Alloy on a γ' Strengthened Nickel-Base Superalloy.

1981-1990A

Nickel base alloys, Composite materials

Creep Deformation of Ni₃Al—Mo In Situ Composites.

987-998A

Nickel base alloys, Corrosion

Fatigue Oxidation Interaction in IN 100 Superalloy.

2259-2268A

Nickel base alloys, Crystal growth

Dendritic Growth of Undercooled Nickel—Tin. III.

1109-1119A

Nickel base alloys, Crystal lattices

Diffusion Induced Grain Boundary Migration and Recrystallization During Oxidation of a Ni—48.5% Cu Alloy.

1667-1675A

Nickel base alloys, Diffusion

Grain Boundary Segregation in the Nickel-Base Alloy 182. Thermodynamics of Segregation in Alloys.

137-143A

2091-2098A

Nickel base alloys, Directional solidification

Study of Solidification Features of Nickel-Base Superalloys in Relation With Composition.

2333-2340A

Study of Microporosity Formation in Nickel-Base Superalloys.

2341-2348A

Dendritic Solidification of Alloys in Low Gravity.

2671-2675A

Nickel base alloys, Heat treatment

Effect of Single Aging on Stress Corrosion Cracking Susceptibility of Inconel X-750 Under PWR Conditions.

1295-1304A

Nickel base alloys, Mechanical properties

Hydrogen Effects in [001] Oriented Nickel-Base Superalloy Single Crystals.

73-82A

Influence of Time and Temperature Dependent Processes on Strain Controlled Low Cycle Fatigue Behavior of Alloy 617. Creep—Fatigue Behavior of Directionally Solidified and Single Crystal Intermetallic Ni₃Al(B,H) at an Intermediate Temperature.

479-486A

Elevated Temperature Creep—Fatigue Crack Propagation in Nickel-Base Alloys and 1Cr—Mo—V Steel.

855-862A

Application of the dc Potential Drop Technique in Investigating Crack Initiation and Propagation Under Sustained Load in Notched Rupture Tests.

863-871A

Influence of Cyclic to Mean Load Ratio on Creep/Fatigue Crack Growth.

873-880A

Tensile and Impact Properties Changes of Hastelloy X After Exposure in High-Temperature Helium Environment.

1269-1275A

Effects of Cobalt Concentration on the Relative Resistance to Octahedral and Cube Slip in Nickel-Diase Superalloys.

2733-2739A

The Absence of Steady-State Flow During Large Strain Plastic Deformation of Some FCC Metals at Low and Intermediate Temperatures.

3013-3024A

Nickel base alloys, Melting

Observations on the Dynamics of Electromagnetically Levitated Liquid Metals and Alloys at Elevated Temperatures.

1939-1943A

Nickel base alloys, Microstructure

Effect of Melt Spinning on Grain Size and Texture in Ni—Mo Alloys.

1711-1720A

Assessment of Service Induced Microstructural Damage and Its Rejuvenation in Turbine Blades.

2049-2066A

Inelastic Deformation and Dislocation Structure of a Nickel Alloy: Effects of Deformation and Thermal Histories.

2477-2486A

The Influence of Boron on the Grain Boundary Chemistry and Microstructure of Ni—16Cr—9Fe—0.03C.

2555-2566A

Dislocation Network Formation and Coherency Loss Around Gamma-Prime Precipitates in a Nickel-Base Superalloy.

2965-2973A

Nickel base alloys, Phase transformations

Electron Diffuse Scattering Studies of Premartensitic Alloys: β' Cu—Zn, β' Ni—Al, In—Ti, and Fe—Ni.

199-205A

Premartensitic Strain Tensor Analysis of Ni₅₈Al₄₂ by the X-Ray Divergent Beam Method.

217-223A

Modulated Lattice Relaxation in β -Based Premartensitic Phase.

777-781A

A Melting and Solidification Study of Alloy 625.

2319-2331A

Nickel base alloys, Phases (state of matter)

The Effect of Varying Aluminum, Titanium, and Niobium Content on the Phase Stability of Inconel 718.

1657-1666A

Correction to "The Effects of Varying Aluminum, Titanium, and Niobium Content on the Phase Stability of Inconel 718".

1657-1666A

Nickel base alloys, Physical properties

Hydrogen Permeation Through Coated and Uncoated Waspaloy.

1187-1192A

The Wetting Characteristics and Surface Tension of Some Nickel-Based Alloys on Yttria, Hafnia, Alumina, and Zirconia Substrates.

1833-1839A

Nickel base alloys, Powder technology

Preparation of Iron-, Cobalt- and Nickel-Based Amorphous Alloy Powders by High-Pressure Gas Atomization and Their Structural Relaxation Behavior.

235-242A

Mechanical Alloying of Brittle Materials.

2867-2874A

Nickel base alloys, Reactions (chemical)

Activity of Carbon in Nickel-Rich Ni—Mo and Ni—W Alloys.

645-650A

Nickel base alloys, Solubility

Thermodynamic Consistency of the Interaction Parameter Formalism.

269-275B

Measurement and Modeling of Alloy—Spinel—Corundum Equilibrium in the Ni—Mn—Al—O System at 1873K.

459-463B

Nickel base alloys, Structural hardening

Precipitation of the δ -Ni₃Nb Phase in Two Nickel Base Superalloys.

453-465A

Nickel base alloys, Surface properties

Surface Tension of Binary Metal—Surface Active Solute Systems Under Conditions Relevant to Welding Metallurgy.

483-491B

Surface Segregation in MCRAIY Alloys.

2099-2108A

Fatigue Damage Accumulation in Nickel Modified by Ion Beam Surface Microalloying.

2775-2788A

Nickel base alloys, Welding

A Study of the Weldability and Weld Related Microstructure of Cabot Alloy 214.

657-667A

The Kinetics of Intergranular Oxygen Penetration in Nickel and Its Relevance to Weldment Cracking.

2305-2313A

Nickel chromium molybdenum steels, Corrosion

Effects of Frequency and Temperature on Short Fatigue Crack Growth in Aqueous Environments.

543-548A

Corrosion Fatigue Crack Initiation in a Mode II Notch Specimen.

1067-1073A

Clean Steels for Steam Turbine Rotors—Their Stress Corrosion Cracking Resistance.

1583-1596A

Influence of Austenitizing Temperature on Stress Corrosion in 4330M Steel—the Role of Impurity Segregation in Stress Corrosion Cracking of High Strength Steel.

2225-2231A

Nickel chromium molybdenum steels, Heat treatment

Crack Growth From Internal Hydrogen—Temperature and Microstructural Effects in 4340 Steel.

1319-1334A

Nickel chromium molybdenum steels, Mechanical properties

Effect of Hot-Rolling Reduction on Shape of Sulfide Inclusions and Fracture Toughness of AISI 4340 Ultrahigh Strength Steel.

1555-1561A

Effect of Microstructure on Plane-Strain Fracture Toughness of AISI 4340 Steel.

2513-2521A

Mode III Fracture of 4340 Steel: Effects of Tempering Temperature and Fracture Surface Interference.

3035-3044A

Nickel chromium steels

See also Nickel chromium molybdenum steels

Nickel chromium steels, Corrosion

Clean Steels for Steam Turbine Rotors—Their Stress Corrosion Cracking Resistance.

1583-1596A

Nickel chromium steels, Phases (state of matter)

Bainite Formation in Low Carbon Cr—Ni Steels.

1695-1701A

Nickel compounds, Crystal lattices

Kinetics of Domain Growth in Ordered Ni₄Mo.

941-952A

Nickel compounds, Mechanical properties

High Temperature Strength and Ductility of Recrystallized Ni₃Al—Ni₃Mn Alloys.

345-352A

Hydrogen Embrittlement of Pseudobinary L₁₂-Type Ni₃(Al_{0.5}Mn_{0.5}) Intermetallic Compound.

353-357A

Creep—Fatigue Behavior of Directionally Solidified and Single Crystal Intermetallic Ni₃Al(B,H) at an Intermediate Temperature.

479-486A

The Strength of Ni₃Al Containing Titanium and Boron.

732-733A

Nickel compounds, Reduction (chemical)

The Effect of Alkali Salt Catalyst on the Carbothermic Reduction of Nickel Oxide.

685-686B

Nickel molybdenum chromium steels

See Nickel chromium molybdenum steels

Nickel molybdenum steels

See Nickel chromium molybdenum steels

Nickel steels

See also Nickel chromium molybdenum steels

Nickel chromium steels

Nickel steels, Mechanical properties

Effect of Microstructure on Fracture Behavior of Complex Structure in 6Ni—0.3C Steel.

2606-2611A

Niobium, Alloying elements

The Effect of Varying Aluminum, Titanium, and Niobium Content on the Phase Stability of Inconel 718.

1657-1666A

Correction to "The Effects of Varying Aluminum, Titanium, and Niobium Content on the Phase Stability of Inconel 718".

1657-1666A

The Competition Between the Alpha and Omega Phases in Aged Ti—Nb Alloys.

1687-1694A

Niobium, Binary systems

The Stable and Metastable Ti—Nb Phase Diagrams.

2389-2397A

Niobium, Solubility

Nitrogen Solubility in Solid Niobium.

613-616B

Niobium base alloys, Diffusion

Change in Direction of Carbon Thermotransport in Nb—V System With Alloying.

1429-1435A

Niobium base alloys, Phases (state of matter)

The Competition Between Martensite and Omega in Quenched Ti—Nb Alloys.

1677-1686A

Niobium base alloys, Thermal properties

The Generalized Lewis Acid-Base Titration of Palladium and Niobium.

893-917B

Niobium compounds, Mechanical properties

The Elastic Modulus and Flow Stress of Nb₃Sn at Elevated Temperatures.

1127-1128A

Niobium compounds, Reactions (chemical)

Dissolution of Columbite and Tantalite in Acidic Fluoride Media.

355-363B

- Nitrogen, Alloying elements**
The Prediction of Precipitation Strengthening in Microalloyed Steels. 1471-1480A
- Nitrogen, Binary systems**
High Temperature Thermodynamics of the Cr—Cr₂N—N₂ System. 471-476B
- Nitrogen, Solubility**
Thermodynamics of Nitrogen in CaO—SiO₂—Al₂O₃ Slags and Its Reaction With Fe—C_{sat} Melts. 419-425B
Nitrogen Solubility in Solid Niobium. 613-616B
- Nitrogen, Sorption**
Rate of Nitrogen Desorption From Liquid Iron—Carbon and Iron—Chromium Alloys With Argon. 233-242B
- Nitrogen, Trace elements**
Analysis of Nonisothermal Transformation Kinetics; Tempering of Iron—Carbon and Iron—Nitrogen Martensites. 925-932A
- Nodular iron, Heat treatment**
Development of High Toughness in Austempered Type Ductile Cast Iron and Evaluation of Its Properties. 319-327A
- Nodules**
See Sea nodules
- Nondestructive testing**
See Microradiography
Ultrasonic testing
- Nonferrous metals**
Correlations of Electrical Conductivity to Slag Composition and Temperature. 133-140B
- Nonferrous metals, Mechanical properties**
Effects of Work-Hardening and Rate Sensitivity on the Sheet Tensile Test. 293-300A
- Nonferrous metals, Recovering**
Bubbling at High Flow Rates in Inviscid and Viscous Liquids (Slags). 83-94B
- Nonferrous smelting**
See Smelting
- Nonmetallic inclusions**
The Nonuniform Distribution of Inclusions in Low-Alloy Steel Weld Deposits. 669-674A
- Nonmetallic inclusions, Deformation effects**
Effect of Hot-Rolling Reduction on Shape of Sulfide Inclusions and Fracture Toughness of AISI 4340 Ultrahigh Strength Steel. 1555-1561A
- Notch brittleness**
See Brittleness
- Notch ductility**
See Ductility
- Notch effect**
See Notch sensitivity
- Notch impact strength**
See Impact strength
- Notch sensitivity**
Application of the dc Potential Drop Technique in Investigating Crack Initiation and Propagation Under Sustained Load in Notched Rupture Tests. 863-871A
Correlations of Microstructure With Dynamic and Quasi-Static Fracture in a Plain Carbon Steel. 2179-2206A
High Frequency Stage I Corrosion Fatigue of Austenitic Stainless Steel (316L). 2753-2764A
The Nucleation of High Temperature Brittle Intergranular Fracture in 2.25Cr—1Mo Steel. 3005-3011A
- Notched bar tensile test**
See Tension tests
- Nuclear energy**
See Nuclear power generation
- Nuclear fuel claddings**
See Nuclear fuel elements
- Nuclear fuel elements, Corrosion**
The Influence of Hydride Size and Matrix Strength on Fracture Initiation at Hydrides in Zirconium Alloys. 1507-1522A
- Nuclear power generation**
Characterization of Residual Stresses in Bent Incoloy-800 Tubing by Neutron Diffraction. 2207-2214A
Determination of Fracture Initiation in Hydride Blisters Using Acoustic Emission. 2247-2257A
- Nuclear power plants**
See Nuclear power generation
- Nucleation**
The Kinetics of Ferrite Nucleation at Austenite Grain Boundaries in Fe—C Alloys. 427-440A
The Effect of Matrix Strength on Void Nucleation and Growth in an Alpha—Beta Titanium Alloy, Corona-5. 591-601A
The Evolution of Microcrystalline Structures in Supercooled Metal Powders. 699-708A
The Nucleation of Iron on Dense Wustite: a Morphological Study. 787-802B
The Effect of Matrix Strength on Void Nucleation and Growth in a Widmanstätten Alpha—Beta Titanium Alloy, Corona-5. 1163-1171A
Observations on Void Nucleation and Growth in α/β Ti—Mn Alloys. 1311-1317A
Radiation Induced Crystallization of Amorphous Si—H Alloy. 1345-1349A
Fractal Analysis of a Nucleation and Growth Process. 1371-1372A
A New Model for Precipitation at Moving Interphase Boundaries. 2133-2138A
- Nucleation and Growth in Martensitic Transformations of Ordered Fe₃Pt Alloys.** 2931-2936A
- Nucleation, Alloying effects**
Influence of Rare Earth Metals on the Nucleation and Solidification Behavior of Iron and 1045 Steel. 383-395B
- Nucleation, Cooling effects**
Bulk Undercooling, Nucleation, and Macroseggregation of Pb—Sn Alloys. 2651-2658A
- Nucleation, Size effects**
Calculation of the Product Phase Grain Boundary Area During Solid State Transformations. 2123-2131A
- Nuclei (transformation)**
See Nucleation
- O ring seals, Nondestructive testing**
Correlation of Mechanical Properties With Nondestructive Evaluation of Babbitt Metal/Bronze Composite Interface. 2215-2224A
- Optical instruments**
See Polarimeters
- Optical masers**
See Lasers
- Order disorder**
See also Short range order
Magnetic-Induced Tricritical Points in Alloys. 441-446A
Quasi-One Dimensional Model of Pretransitional Soft Mode Behavior. 811-818A
Kinetics of Domain Growth in Ordered Ni₃Mo. 941-952A
Effect of Rapid Solidification and Alloying Addition on Lattice Distortion and Atomic Ordering in L₁₀ TiAl Alloys and Their Ternary Alloys. 2445-2455A
- Ordering**
See Order disorder
- Ores**
See Chromium ores
Galena
Hematite
Iron ores
Laterites
Magnetite
Rutile
Sphalerite
- Organic compounds**
The Behavior of Thiourea and Flotation Reagents in Zinc Electrowinning Circuits. 187-199B
- Orientation**
See also Grain orientation
Orientation relationships
Orientation Dependence of $\beta_1 \rightarrow \beta'$; Stress-Induced Martensitic Transformation in a Cu—Al—Ni Alloy. 915-923A
- Orientation relationships**
Intercrystalline Structure Distribution in Polycrystalline Materials. 2611A
- Orthorhombic lattice**
Microstructural Characterization of the Dispersed Phases in Al—Ce—Fe System. 1645-1658A
- OSM process**
See Oxygen steel making
- Oxidation**
See also Internal oxidation
Diffusion Induced Grain Boundary Migration and Recrystallization During Oxidation of a Ni—48.5% Cu Alloy. 1667-1675A
Fatigue Oxidation Interaction in IN 100 Superalloy. 2259-2268A
- Oxidation rate**
Correlation Between Dielectric Properties and Aqueous Oxidation Rate for Pulverized Sphalerites and Zinc Concentrates. 25-36B
Oxidation of Molten Copper Matte. 47-52B
- Oxide coatings**
Rutherford Backscattering Study of High Temperature Oxidation of Melt-Spun Glassy Fe—22.5Al—10Zr. 2567-2573A
- Oxide films**
See Oxide coatings
- Oxides**
See also Aluminum oxide
Carbon dioxide
Iron oxides
Lime
Silicon dioxide
Titanium dioxide
Wustite
- Oxides, Reactions (chemical)**
Kinetics of Manganese Oxide Sulfidization in Carbonyl Sulfide (COS) Contaminated Atmospheres. 303-310B
Analysis of Dissolution Rate of Metal Oxide in Acidic Chloride Solution in Terms of Water Activity. 505-507B
- Oxides, Reduction (chemical)**
The Effect of Alkali Salt Catalyst on the Carbothermic Reduction of Nickel Oxide. 685-686B
- Oxides, Superconductivity**
Magnetic Properties of Rare Earth—Barium—Copper Oxides in the Normal and Superconducting States. 734-738A
Electrical Properties of High T_c EuBa₂Cu₃O_{7-x}. 738-743A
- Oxidizing**
See Oxidation

Oxygen

Oxygen, Alloying elements

- Surface Tension of Binary Metal—Surface Active Solute Systems Under Conditions Relevant to Welding Metallurgy. 483-491B
Effects of Oxygen and Heat Treatment on the Mechanical Properties of Alpha and Beta Titanium Alloys. 527-542A
Electrical Properties of High T_c $\text{EuBa}_2\text{Cu}_3\text{O}_{7-x}$. 738-743A

Oxygen, Diffusion

- Literature Survey on Diffusivities of Oxygen, Aluminum, and Vanadium in Alpha Titanium, Beta Titanium, and in Rutile. 1121-1125A

Oxygen, Dopants

- Effects of Oxygen and Sulfur on Alloying Element Vaporization Rates During Laser Welding. 967-972B

Oxygen, Impurities

- Solubility and Diffusion of Hydrogen in Vanadium—Oxygen Alloys. 67-72A
The Interaction Between Oxygen and Bismuth in Dilute Solution in Copper at 1300°C. 623-626B

Oxygen, Solubility

- Measurement and Modeling of Alloy—Spinel—Corundum Equilibrium in the Ni—Mn—Al—O System at 1873K. 459-463B

Oxygen, Ternary systems

- A New Treatment for Determining the Activities From Ternary Miscibility Gap: the O—Cu—Pb System. 373-376A

Oxygen conversion processes

- See Oxygen steel making

Oxygen steel making

- The Nucleation of Carbon Monoxide Bubbles in Molten Iron—Carbon Drops Reacting With Oxidizing Gases. 831-837B
Experimental Investigation of Mixing Phenomena in a Gas Stirred Liquid Bath. 839-850B

Packing (crystal density)

- See Crystal structure

Palladium, Alloying elements

- Tweed Structures Associated With FCC—FCT Transformations in Fe—Pd Alloys. 803-810A

Parameters

- See Lattice parameters
Welding parameters

Particle interactions, Heating effects

- The Precipitation Behavior of a Zr—2.5 wt.% Nb Alloy. 1153-1162A

Particle shape

- On the Formation of Dispersoids During Rapid Solidification of an Al—Fe—Ni Alloy. 1101-1107A

Particle size

- Melting Metal Powder Particles in an Inductively Coupled R.F. Plasma Torch. 213-226B
Dissolution Kinetics of Particulate Graphite Injected Into Iron/Carbon Melts. 375-382B
Analytical Electron Microscopy of Internally Oxidized Low Si—Al Steel. 953-959A
Some Observations on the Matrix Microstructure of Aluminum—Silicon Alloy—Graphite Particle Composites. 1365-1367A

Particles (of physics)

- Characterization of the Aging Response of a Melt-Spun Al—Be—Li Alloy Ribbon. 1173-1178A

Particulate composites, Directional solidification

- Behavior of Ceramic Particles at the Solid/Liquid Metal Interface in Metal Matrix Composites. 2847-2955A

Particulate composites, Fabrication

- A Method of Assessing the Reactivity Between SiC and Molten Aluminum. 3107-3109A

Particulate composites, Structural hardening

- Effects of SiC Whiskers and Particles on Precipitation in Aluminum Matrix Composites. 2945-2953A

Pearlite, Alloying effects

- The Effect of Alloying Elements and Microstructure on the Strength and Fracture Resistance of Pearlitic Steel. 2819-2829A

Pellets

- A Dynamic Mathematical Model of the Complete Grate/Kiln Iron-Ore Pellet Induration Process. 103-112B
Gas Flow and Pressure Balancing in Modeling Grate/Kiln Induration. 113-121B
Energy Cost Minimization in Grate/Kiln Induration. 123-132B

Permeability

- Hydrogen in Iron. 691-707B
Hydrogen in Iron. 2371-2387A

Permeability, Temperature effects

- Hydrogen Permeation Through Coated and Uncoated Waspaloy. 1187-1192A

Permeability (magnetic)

- See Magnetic permeability

Permittivity

- See Dielectric constant

Phase boundary

- On the Slopes of Phase Boundaries. 1819-1825A
A New Model for Precipitation at Moving Interphase Boundaries. 2133-2138A
Application of a New Model to the Interphase Precipitation Reaction in Vanadium Steels. 2139-2151A

Phase decomposition

- See also Eutectoid decomposition
Spinodal decomposition

- Phase Transformations and Modulated Microstructures in Ti—Al—Nb Alloys. 225-234A
Swing Back in Kinetics Near M_s in Hypereutectoid Steels. 447-452A

Phase decomposition, Deformation effects

- Effect of Deformation on the Austenite-to-Ferrite Transformation in a Plain Carbon and Two Microalloyed Steels. 417-426A

Phase diagram reactions

- See also Austenitizing
Eutectic reactions
Eutectoid decomposition
Eutectoid reactions
Martensitic transformations
Phase decomposition
Spinodal decomposition
The Cata- or Metatectic Reaction—Occurrence and Microstructural Development. 3097-3100A

Phase diagram reactions, Alloying effects

- The Prediction of Precipitation Strengthening in Microalloyed Steels. 1471-1480A

Phase diagram reactions, Composition effects

- A Melting and Solidification Study of Alloy 625. 2319-2331A
Study of Solidification Features of Nickel-Base Superalloys in Relation With Composition. 2333-2340A
Densities of Pb—Sn Alloys During Solidification. 2349-2354A

Phase diagrams

- Phase Stability Relationships and Glass Formation in the System Cu—Ag—In. 13-21A
Calculation of the Titanium—Aluminum Phase Diagram. 243-247A
Experimental and Calculated Ag + Au + Ge Phase Diagram. 409-416A
The Influence of the Ternary Interaction Parameter ϵ_{ij}^E on the Activity of Bismuth in Molten Copper. 427-432B
Magnetic-Induced Tricritical Points in Alloys. 441-446A
A Thermodynamic Evaluation of the Fe—Cr—C System. 627-636A
Thermodynamics of the Cr—Mn System Using an Isopiestic Technique. 649-654B
The Generalized Lewis Acid-Base Titration of Palladium and Niobium. 893-917B
Phase Relationships in the Fe—Cr—Ni System at Solidification Temperatures. 899-908A
Standard Gibbs Energies of Formation of the Carbides of Manganese by EMF Measurements. 951-957B
An Experimental Study and a Thermodynamic Evaluation of the Fe—Cr—Mo System. 1385-1394A
Solidus and Solvus Isotherms for Quaternary Al—Li—Cu—Mg Alloys. 1631-1634A
Microstructural Characterization of the Dispersed Phases in Al—Ce—Fe System. 1645-1656A
On the Slopes of Phase Boundaries. 1819-1825A
Solidification Structures in Rapidly Quenched Cu—Ti—Zr Alloys. 1853-1860A
The Stable and Metastable Ti—Nb Phase Diagrams. 2389-2397A
An Experimental Study and a Thermodynamic Evaluation of the Cr—Fe—W System. 2531-2546A
A Thermodynamic Evaluation of the C—Cr—Fe—W System. 2547-2554A
Influence of Gravity Level and Interfacial Energies on Dispersion-Forming Tendencies in Hypermonotectic Cu—Pb—Al Alloys. 2645-2650A
Bulk Undercooling, Nucleation, and Macrosegregation of Pb—Sn Alloys. 2651-2658A
Eutectic Structures of Ag—Cu After Melting and Solidification in Microgravity and on Earth. 2659-2664A
The Influence of Interfacial Energies and Gravitational Levels on the Directionally Solidified Structures in Hypermonotectic Alloys. 2665-2669A
Directional Solidification of Lead—Copper Immiscible Alloys in a Cyclic Gravity Environment. 2677-2680A
Enthalpies of a Binary Alloy During Solidification. 3057-3061A

Phase stability

- Beta-Phase Stability and Martensitic Nucleation in Hume-Rothery Alloys. 207-216A
Carbothermic Reduction of Silicon Dioxide—a Thermodynamic Investigation. 249-253B
The Competition Between the Alpha and Omega Phases in Aged Ti—Nb Alloys. 1687-1694A

Phase stability, Alloying effects

- The Effect of Varying Aluminum, Titanium, and Niobium Content on the Phase Stability of Inconel 718. 1657-1666A
Correction to "The Effects of Varying Aluminum, Titanium, and Niobium Content on the Phase Stability of Inconel 718". 1657-1666A
Competitive Growth of Stable and Metastable Fe—C—X Eutectics. II. Mechanisms. 1965-1971A

Phase stability, High temperature effects

- Thermodynamics of the Cr—Mn System Using an Isopiestic Technique. 649-654B

Phase structure

- See Solid phases

Phase transformations

- See also Austenitizing
Martensitic transformations
Analysis of Nonisothermal Transformation Kinetics: Tempering of Iron—Carbon and Iron—Nitrogen Martensites. 925-932A
Bainite Formation in Low Carbon Cr—Ni Steels. 1695-1701A
Spinodal Decomposition of a Co—Ti—Nb Alloy. 1703-1709A
On the Slopes of Phase Boundaries. 1819-1825A
Calculation of the Product Phase Grain Boundary Area During Solid State Transformations. 2123-2131A
The Stable and Metastable Ti—Nb Phase Diagrams. 2389-2397A

Phase transformations, Alloying effects

- The Competition Between Martensite and Omega in Quenched Ti—Nb Alloys. 1677-1686A

- Phase transformations, Heating effects**
Laser Transformation Hardening of Iron—Carbon and Iron—Carbon—Chromium Steels. 2013-2025A
- Phases (state of matter)**
See also Intermetallic phases
Laves phase
Liquid phases
Metastable phases
Solid phases
- Phases (state of matter), Crystal lattices**
Modulated Lattice Relaxation in β -Based Premartensitic Phase. 777-781A
- Phosphides, Crystal growth**
Determination of Standard Free Energies of Formation of Ca_3P_2 and Ca_2Sn at High Temperatures. 433-439B
- Phosphorus, Alloying elements**
Effects of Manganese, Phosphorus and Molybdenum on Sulfide Stress Cracking Resistance of High Strength Low Alloy Steels. 2171-2177A
- Phosphorus, Impurities**
Influence of Austenitizing Temperature on Stress Corrosion in 4330M Steel—the Role of Impurity Segregation in Stress Corrosion Cracking of High Strength Steel. 2225-2231A
- Phosphorus, Trace elements**
The Effects of Austenitization Temperature on the High Temperature Ductility of Fe—P—S Alloys. 887-892A
- Photo oxidation**
See Oxidation
- Photography**
See Microradiography
- Physical properties**
See Capillarity
Curie temperature
Density
Dielectric constant
Diffusivity
Emissivity
Heat of activation
Heat of formation
Heat of mixing
Heat of reaction
Heat of solution
Magnetic anisotropy
Magnetic permeability
Melting points
Microporosity
Miscibility
Permeability
Porosity
Resistivity
Solubility
Surface tension
Thermal stability
Vapor pressure
Viscosity
- Pickling**
Some Fundamental Aspects of Annealing and Pickling Stainless Steels. 1083-1100A
Studies on the Determination of Surface Deuterium in AISI 1082, 4037, and 4140 Steels by Secondary Ion Mass Spectrometry. 3071-3075A
- Plasma arc melting**
Melting Metal Powder Particles in an Inductively Coupled R.F. Plasma Torch. 213-226B
- Plasma arc torches**
Melting Metal Powder Particles in an Inductively Coupled R.F. Plasma Torch. 213-226B
- Plasma processing**
See Plasma arc melting
- Plaster of Paris**
See Calcium compounds
- Plastic deformation**
The Law of Mixtures Applied to the Plastic Deformation of Two-Phase Alloys of Coarse Microstructures. 2027-2040A
The Absence of Steady-State Flow During Large Strain Plastic Deformation of Some FCC Metals at Low and Intermediate Temperatures. 3013-3024A
- Plastic deformation, Diffusion effects**
Experimental Study of Hydrogen Transport During Plastic Deformation in Iron. 2789-2798A
- Plastic deformation, Microstructural effects**
Tensile Fracture of Coarse-Grained Cast Austenitic Manganese Steels. 2269-2277A
- Plastic strain**
See Plastic deformation
- Plasticity**
See also Superplasticity
Modeling of the Plastic Anisotropy of Textured Sheet. 105-120A
- Plasticity, Microstructural effects**
Correlations of Microstructure With Dynamic and Quasi-Static Fracture in a Plain Carbon Steel. 2179-2206A
- Plastics**
See Silicone resins
- Plate metal, Mechanical properties**
Creep Crack Growth Behavior of Two Al—Li Alloys. 847-854A
- Plating**
See Alloy plating
Brass plating
Platinum plating
Pulse plating
- Platinizing**
See Platinum plating
- Platinum, Melting**
Acoustic Levitation Technique for Containerless Processing at High Temperatures in Space. 2619-2623A
- Platinum, Thermal properties**
Measurement of Temperature and Emissivity of Specularly Reflecting Glowing Bodies. 1889-1894A
- Platinum compounds, Phase transformations**
Nucleation and Growth in Martensitic Transformations of Ordered Fe_3Pt Alloys. 2931-2936A
- Platinum compounds, Thermal properties**
Standard Enthalpies of Formation of PtTi , PtZr , and PtHf . 1827-1831A
- Platinum metal alloys, Thermal properties**
The Generalized Lewis Acid-Base Titration of Palladium and Niobium. 893-917B
- Platinum metal compounds**
See Platinum compounds
Ruthenium compounds
- Platinum metals**
See Palladium
Platinum
- Platinum plating**
Evaluation of High-Temperature Diffusion Barriers for the Pt—Mo System. 2163-2170A
- Plutonium, Binary systems**
The Cata- or Metatectic Reaction—Occurrence and Microstructural Development. 3097-3100A
- Plutonium base alloys, Phase transformations**
Thermodynamics and Kinetics of $\delta \rightarrow \alpha$ Martensitic Transformation in Plutonium Alloys. 2705-2711A
- Plutonium compounds, Phase transformations**
Electron Microscope Study on Martensitic Transformations in Fe—Pt Alloys: General Features of Internal Structure. 2723-2731A
- Polarimeters**
Measurement of Temperature and Emissivity of Specularly Reflecting Glowing Bodies. 1889-1894A
- Polariscopes**
See Polarimeters
- Polarographs**
See Polarimeters
- Polarography**
See Polarimeters
- Pole figures**
Orientation Mapping. 403-408A
- Poling**
See Deoxidizing
- Pollution abatement**
Kinetics of Manganese Oxide Sulfidization in Carbonyl Sulfide (COS) Contaminated Atmospheres. 303-310B
- Polymers**
See Silicone resins
- Pores**
See Porosity
- Porosity**
See also Microporosity
Porosity and Tensile Ductility in Al—Zn Alloys. 517-526A
- Porosity, Environmental effects**
Sintering Atmosphere Effects on Tensile Properties of Heavy Alloys. 2467-2476A
- Porosity, Microstructural effects**
Changes in the Longitudinal Flow and Apparent Plastic Poisson's Ratio of a Porous Metal Strip During Hot Densification Rolling. 1205-1211A
- Porous materials**
See Porous metals
- Porous metals, Rolling**
Changes in the Longitudinal Flow and Apparent Plastic Poisson's Ratio of a Porous Metal Strip During Hot Densification Rolling. 1205-1211A
- Potassium, Binary systems**
On the Slopes of Phase Boundaries. 1819-1825A
- Potential (electric)**
See Electric potential
- Powder compacts**
See also Sintered compacts
- Powder compacts, Mechanical properties**
Aluminum—Lithium Powder Metallurgy Alloys With Improved Toughness. 603-615A
- Powder metallurgy**
See Mechanical alloying
- Powder metallurgy parts, Alloy development**
Niobium-Alloyed High Speed Steel by Powder Metallurgy. 1395-1401A

Powder metallurgy parts

Powder metallurgy parts, Anisotropy

- Texture induced Magnetic Anisotropy in Fe—Nd—B Magnet Prepared via Rapid Solidification and Hot Extrusion Techniques. 3109-3112A

Powder metallurgy parts, Mechanical properties

- Microstructure Effects on Tensile Properties of Tungsten—Nickel—Iron Composites. 1523-1532A

Powder technology

- See Mechanical alloying

Powdering

- Formation of Ultra-Fine Amorphous Powders in Fe—M—B (M = Transition Metal) Systems by Chemical Reduction Method and Their Thermal and Magnetic Properties. 2315-2318A

Powders

- See Alloy powders
Metal powders

Precious metal alloys

- See Gold base alloys
Platinum metal alloys
Silver base alloys

Precious metal compounds

- See Platinum compounds
Ruthenium compounds

Precious metals

- See Gold
Palladium
Platinum
Silver

Precipitates

- Microstructure and Fracture Toughness of the Aged β -Ti Alloy Ti—10V—2Fe—3Al. 1037-1049A

Precipitates, Crystal growth

- Coarsening and Morphology of β' Particles in Fe—Ni—Al—Mo Ferritic Alloys. 1135-1146A

Precipitates, Crystal lattices

- Analytical Electron Microscopy of Internally Oxidized Low Si—Al Steel. 953-959A
On the Morphology of the Modulated Precipitation of Extended Multiplets and Fe₃C₄ Epsilon or Eta Carbide Obtained by Aging and Tempering in Fe—C Martensite. Structure and Deformation Behavior of T₁ Precipitate Plates in an Al—2Li—1Cu Alloy. 2901-2909A
2911-2920A

Precipitation

- See also Intergranular precipitation
Analysis of Nonisothermal Transformation Kinetics; Tempering of Iron—Carbon and Iron—Nitrogen Martensites. 925-932A
Dislocation Network Formation and Coherency Loss Around Gamma-Prime Precipitates in a Nickel-Base Superalloy. 2965-2973A

Precipitation, Composition effects

- The Partitioning of Alloying Elements in Vacuum Arc Remelted, Palladium-Modified PH 13-8 Molybdenum Alloys. 3063-3069A

Precipitation hardening

- See also Aging (artificial)
The Aging Characteristics of an Al—2% Li—3% Cu—0.12% Zr Alloy at 190°C. 51-66A
Phase Transformations and Modulated Microstructures in Ti—Al—Nb Alloys. 225-234A
Theoretical Investigation of the Precipitation of δ' in Al—Li. 249-258A
Investigation of Phase Transformation in an Al—0.58 wt.% Fe Alloy by Mossbauer Spectroscopy. 259-264A
Precipitation of the δ -Ni₃Nb Phase in Two Nickel Base Superalloys. 453-465A
Coarsening and Morphology of β' Particles in Fe—Ni—Al—Mo Ferritic Alloys. 1135-1146A
A Stress Relaxation Method for Following Carbonitride Precipitation in Austenite at Hot Working Temperatures. 1403-1413A
Ti(C,N) Precipitation in Microalloyed Austenite During Stress Relaxation. 1415-1424A
Orowan Strengthening by Mo₂C Fibers and Needle Interphase Precipitates in Fe—C—Mo Dual-Phase Steels. 1617-1620A
Spinodal Decomposition of a Co—Ti—Nb Alloy. 1703-1709A
Growth and Coarsening of G.P. Zones in Al—Zn Alloys. 1973-1980A
A New Model for Precipitation at Moving Interphase Boundaries. 2133-2138A

Precipitation hardening, Alloying effects

- The Prediction of Precipitation Strengthening in Microalloyed Steels. 1471-1480A
A Preliminary Study of the Influence of Separate and Combined Aluminum and Nickel Additions on the Properties of a Secondary Hardening Steel. 3103-3107A

Precipitation hardening, Cooling effects

- Effect of Melt Spinning on the Microstructure and Mechanical Properties of Three Nickel-Base Superalloys. 93-103A
Precipitation of Guinier—Preston Zones in Aluminum—Magnesium; a Calorimetric Analysis of Liquid-Quenched and Solid-Quenched Alloys. 2433-2443A

Precipitation hardening, Diffusion effects

- Inhibition of Cyclic Grain Boundary Migration Through Cellular Precipitation in Pb—5% Sn Alloy. 2355-2359A

Precipitation hardening, Heating effects

- Correlation Among Microstructure, Strength, and Electrical Conductivity of Cu—Ni—Be Alloy. 2279-2285A
On the Morphology of the Modulated Precipitation of Extended Multiplets and Fe₃C₄ Epsilon or Eta Carbide Obtained by Aging and Tempering in Fe—C Martensite. Structure and Deformation Behavior of T₁ Precipitate Plates in an Al—2Li—1Cu Alloy. 2901-2909A
2911-2920A

- Effects of SiC Whiskers and Particles on Precipitation in Aluminum Matrix Composites. 2945-2953A
Structure and Properties of a Near- α Titanium Alloy After β Solution Treatment and Aging at 625°C. 3025-3033A

Precipitation hardening, Temperature effects

- Application of a New Model to the Interphase Precipitation Reaction in Vanadium Steels. 2139-2151A

Precipitation hardening alloys, Alloy development

- Design and Development of an Experimental Wrought Aluminum Alloy for Use at Elevated Temperatures. 1027-1035A

Precipitation hardening alloys, Mechanical properties

- On Through Thickness Crystallographic Texture Gradient in Al—Li—Cu—Zr Alloy. 731-732A

Precipitation hardening steels

- See also Maraging steels

Precipitation hardening steels, Mechanical properties

- The Effect of Microstructure on the Fatigue Crack Growth Behavior of Age-Hardened High Strength Steels in a Corrosive Environment. 1461-1469A

Precipitation hardening steels, Melting

- The Partitioning of Alloying Elements in Vacuum Arc Remelted, Palladium-Modified PH 13-8 Molybdenum Alloys. 3063-3069A

Precipitation heat treatment

- See also Aging (artificial)
Precipitation hardening
The Precipitation Behavior of a Zr—2.5 wt.% Nb Alloy. 1153-1162A

Preferential attack (corrosion)

- See Intergranular corrosion

Press forming

- A Wrinkling Index for Press Forming. 2831-2837A

Press working

- See Press forming

Pressing

- See Hot isostatic pressing
Hot pressing
Press forming

Pressure

- See Vacuum
Vapor pressure

Pressure sintering

- See Hot pressing

Pressure welding

- See Diffusion welding
Projection welding

Pressureless sintering

- See Loose powder sintering

Primary displacements

- See Displacements (lattice)

Process control

- A Simple Fluid Mechanical Model for Planar Flow Casting Melt-Spinning. 571-579B
The Trajectories and Distribution of Particles in a Turbulent Axisymmetric Gas Jet Injected into a Flash Furnace Shaft. Characterization of Two-Phase Axisymmetric Plume in a Gas Stirred Liquid Bath—a Water Model Study. 871-884B
885-892B

Projection welding

- Consolidation of Metallic Glass Ribbons Using Electric Discharge Welding. 1634-1638A

Propagation

- See Crack propagation

Properzi process

- See Continuous casting

Protective atmospheres

- See Controlled atmospheres

Protective coatings

- Evaluation of High-Temperature Diffusion Barriers for the Pt—Mo System. 2163-2170A

Pulsation

- See Pulse plating

Pulse echo technique

- See Ultrasonic testing

Pulse plating

- Pulsed Electrodeposition of Layered Brass Structures. 1569-1573A

Pyrolysis, Heating effects

- Phase Transformation During Annealing of Rapidly Solidified Aluminum-Rich Al—Fe—Si Alloys. 2893-2900A

Pyrometallurgy

- The Reaction Between Spodumene and Tachyhydrite. 663-668B
Process Mineralogy of Suspended Particles From a Simulated Commercial Flash Smelter. 719-729B
Kinetics of Oxidation of MoS₂ by CaO in the Presence of Water Vapor. 973-975B

Quantitative analysis

- See Volumetric analysis

Quantitative metallography

- See also Areal analysis
Quantitative Fractography: a Modern Perspective. 961-971A

Quaternary systems, Phases (state of matter)

- Solidus and Solvus Isotherms for Quaternary Al—Li—Cu—Mg Alloys. 1631-1634A

- A Thermodynamic Evaluation of the C—Cr—Fe—W System. 2547-2554A
- Quench aging**
The Precipitation Behavior of a Zr—2.5 wt.% Nb Alloy. 1153-1162A
- Quench hardening**
See also Austempering
Observations on Void Nucleation and Growth in α/β Ti—Mn Alloys. 1311-1317A
- Quenching (cooling)**
See also Quench aging
Quench hardening
Rapid solidification
The Competition Between Martensite and Omega in Quenched Ti—Nb Alloys. 1677-1686A
Precipitation of Guinier—Preston Zones in Aluminum—Magnesium; a Calorimetric Analysis of Liquid-Quenched and Solid-Quenched Alloys. 2433-2443A
- Quenching stresses**
See Residual stress
- R H process**
See Vacuum degassing
- Radiant heating**
See Laser beam heating
- Radiation**
See Electron beams
- Radiation damage**
Creep Cavity Growth From Tritium-Induced Helium Bubbles in Nickel. 821-827A
- Radiocrystallography**
See Crystallography
- Radiography**
See Microradiography
- Raney nickel**
See Catalysts
- Rapid solidification**
Effect of Melt Spinning on the Microstructure and Mechanical Properties of Three Nickel-Base Superalloys. 93-103A
Thermal Considerations on the Recalescence of Alloy Powders. 687-697A
On the Formation of Dispersoids During Rapid Solidification of an Al—Fe—Ni Alloy. 1101-1107A
Characterization of the Aging Response of a Melt-Spun Al—Be—Li Alloy Ribbon. 1173-1178A
Use of Ion Scattering in Characterizing the Surface Oxide of P/M Aluminum Alloy 7091. 1372-1374A
Microstructural Characterization of the Dispersed Phases in Al—Ce—Fe System. 1645-1656A
Solidification Structures in Rapidly Quenched Cu—Ti—Zr Alloys. 1853-1860A
The Microstructure and Phase Relationships in Rapidly Solidified Type 304 Stainless Steel Powders. 2399-2405A
Effect of Rapid Solidification and Alloying Addition on Lattice Distortion and Atomic Ordering in $L1_0$ TiAl Alloys and Their Ternary Alloys. 2445-2455A
Processing Effects in Spray Casting of Steel Strip. 3077-3086A
- Rare earth alloys**
See Thulium base alloys
- Rare earth metals**
See also Cerium
- Rare earth metals, Alloying additive**
Influence of Rare Earth Metals on the Nucleation and Solidification Behavior of Iron and 1045 Steel. 383-395B
- Rare earth metals, Reactions (chemical)**
Equilibria Between the Rare Earth Elements, Oxygen and Sulfur, in Molten Iron. 409-418B
- Rare gases**
See Argon
Helium
- Reaction kinetics**
Reaction Mechanism for the CaO—Al and CaO—CaF_2 Desulfurization of Carbon-Saturated Iron. 261-268B
Kinetics of Manganous Oxide Sulfidization in Carbonyl Sulfide (COS) Contaminated Atmospheres. 303-310B
Hematite Single Crystal Reduction Into Magnetite With CO—CO_2 . 311-317B
Dissolution of Columbite and Tantalite in Acidic Fluoride Media. 355-363B
Dissolution Kinetics of Argentinian Plumbojarosite From Old Tailings of Sulfatizing Roasting Pyrites by HCl—CaCl_2 Leaching. 365-373B
Dissolution Kinetics of Particulate Graphite Injected Into Iron/Carbon Melts. 375-382B
On the Solubility of Aluminum in Cryolitic Melts. 449-457B
Analysis of Dissolution Rate of Metal Oxide in Acidic Chloride Solution in Terms of Water Activity. 505-507B
Possible Roles of Upper Slag Phases on the Fluid Dynamics of Gas Stirred Ladles. 507-511B
Discussion of "Physical Chemistry of Gas Liquid Solder Reactions" and Reply. 513-514B
Kinetics of Nonoxidative Leaching of Galena in Perchloric, Hydrobromic, and Hydrochloric Acid Solutions. 541-546B
Studies on Oxychlorination of MoS_2 in a Fluid Bed Reactor. 669-675B
The Effect of Alkali Salt Catalyst on the Carbothermic Reduction of Nickel Oxide. 685-686B
The Reaction Between Solid Iron and Liquid Al—Zn Baths. 1193-1203A
Observations on the Dynamics of Electromagnetically Levitated Liquid Metals and Alloys at Elevated Temperatures. 1939-1943A
- Isothermal Dendritic Growth—a Proposed Microgravity Experiment. 1945-1953A
Amorphous Cr_5Si_3 Thin Films—Morphology and Kinetics of Crystallization. 1991-2003A
Precipitation of Guinier—Preston Zones in Aluminum—Magnesium; a Calorimetric Analysis of Liquid-Quenched and Solid-Quenched Alloys. 2433-2443A
Rutherford Backscattering Study of High Temperature Oxidation of Melt-Spun Glassy Fe—22.5Al—10Zr. 2567-2573A
- Reactions (chemical)**
See also Carbothermic reactions
Chlorination
Deoxidizing
Desulfurizing
Hydrogen reduction
Hydrogenation
Interface reactions
Internal oxidation
Oxidation
Pyrolysis
Silicothermic reactions
Sulfation
Reactivity of Al—2.5% Li Alloy With Water as Studied by the Exploding Wire Technique. 255-259B
Water and Solute Activities of the Solution Systems of $\text{H}_2\text{SO}_4\text{—CuSO}_4\text{—H}_2\text{O}$ and $\text{HCl—CuCl}_2\text{—H}_2\text{O}$. 347-354B
Thermodynamics of Nitrogen in $\text{CaO—SiO}_2\text{—Al}_2\text{O}_3$ Slags and Its Reaction With Fe—C_{sat} Melts. 419-425B
Conditions Affecting the Formation of Chlorinated Carbon Compounds During Carbochlorination. 477-482B
- Reactions (nuclear)**
See Particle interactions
- Reactivity (chemical)**
See Activity (chemical)
- Reactor vessels (chemical)**
See Chemical reactors
- Reactors**
See Chemical reactors
- Recalescence**
Thermal Considerations on the Recalescence of Alloy Powders. 687-697A
Dendritic Growth of Undercooled Nickel—Tin. III. 1109-1119A
- Recovering, Composition effects**
Reducibility of Laterite Ores. 181-186B
- Recrystallization**
See also Grain refinement
Effects of Thermomechanical Processing on the Microstructure and Mechanical Properties of a Ti—V—N Steel. 1221-1234A
Effect of Annealing Temperature on Yield Anisotropy of Zircaloy-4 TRIP. 1243-1255A
Ostwald Ripening in a System With a High Volume Fraction of Coarsening Phase. 2713-2721A
The Absence of Steady-State Flow During Large Strain Plastic Deformation of Some FCC Metals at Low and Intermediate Temperatures. 3013-3024A
- Red hardness**
See Hardness
- Red shortness**
See Brittleness
- Reduction (chemical)**
See also Flash smelting
Hydrogen reduction
Vapor Phase Reduction of Chromic Oxide in an Ar—H₂ RF Plasma. 927-933B
Formation of Ultra-Fine Amorphous Powders in Fe—M—B (M = Transition Metal) Systems by Chemical Reduction Method and Their Thermal and Magnetic Properties. 2315-2318A
- Reduction (electrolytic)**
See Electrowinning
Hall Heroult process
- Reduction (metal working)**
See Finish rolling
Hot rolling
- Refining**
See Electrorefining
- Refractories**
Fluid Dynamics in Bubble Stirred Ladles. II. Mathematical Modeling. 755-764B
- Refractory alloys**
See Chromium base alloys
Molybdenum base alloys
Niobium base alloys
Tungsten base alloys
Vanadium base alloys
- Refractory materials**
See Refractories
- Refractory metal compounds**
See Chromium compounds
Molybdenum compounds
Niobium compounds
Tantalum compounds
Tungsten carbide
Vanadium compounds
- Refractory metals**
See Chromium
Molybdenum
Niobium

Refractory metals

- Tantalum
Tungsten
Vanadium
- Relaxation**
See Stress relaxation
- Research**
See also Technology transfer
An Emerging Role for the National Laboratories in Materials Research. 341-345B
An Emerging Role for the National Laboratories in Materials Research. 1379-1383A
- Residual stress, Deformation effects**
Characterization of Residual Stresses in Bent Incoloy-800 Tubing by Neutron Diffraction. 2207-2214A
- Resistance welding**
See Projection welding
- Resistance welds**
See Welded joints
- Resistivity**
Electrical Conductivity of Acidic Chloride Solutions. 53-58B
Ductile Al—Cu—V Amorphous Alloys Without Metalloid. 391-393A
Gibbs Free Energy of Formation of Cementite, Fe₃C. 2115-2117A
- Resistivity, Composition effects**
Correlations of Electrical Conductivity to Slag Composition and Temperature. 133-140B
Electrical Properties of High T_c EuBa₂Cu₃O_{7-x}. 738-743A
- Resistivity, Heating effects**
Amorphous Cr₂Si₂ Thin Films—Morphology and Kinetics of Crystallization. 1991-2003A
- Resistivity, Microstructural effects**
Correlation Among Microstructure, Strength, and Electrical Conductivity of Cu—Ni—Be Alloy. 2279-2285A
- Resonance testing**
See Ultrasonic testing
- Retained austenite, Alloying effects**
Tensile Deformation Behavior of Mechanically Stabilized Fe—Mn Austenite. 1563-1568A
- Revaporization**
See Vaporizing
- Reviews**
Literature Survey on Diffusivities of Oxygen, Aluminum, and Vanadium in Alpha Titanium, Beta Titanium, and in Rutile. Some Observations on the Matrix Microstructure of Aluminum—Silicon Alloy—Graphite Particle Composites. Coupled Growth Zone in Fe—18Cr—C Alloys. Formation of Metal—Metal Type Aluminum-Based Amorphous Alloys. 1121-1125A
1365-1367A
1367-1369A
1369-1371A
- Rheological properties**
See Viscosity
- Ribbons (metallic)**
See Tapes (metallic)
- Roasting**
See also Fluidized bed roasting
A Dynamic Mathematical Model of the Complete Grate/Kiln Iron-Ore Pellet Induration Process. 103-112B
Gas Flow and Pressure Balancing in Modeling Grate/Kiln Induration. 113-121B
Energy Cost Minimization in Grate/Kiln Induration. 123-132B
A Microscopic Study of the Transformation of Sphalerite Particles During the Roasting of Zinc Concentrate. 141-146B
- Rods, Casting**
Influence of Mold Length and Mold Heat Transfer on Horizontal Continuous Casting of Nonferrous Alloy Rods. 201-212B
- Rolling**
See Finish rolling
Hot rolling
- Rolling texture**
Microscopic Shear Localization in Nickel. 2041-2048A
- Rotary kilns**
See Kilns
- Rotating beam fatigue tests**
See Fatigue tests
- Rotating machines**
See Electric motors
- Roughing (rolling)**
See Hot rolling
- Rupture strength**
See Creep rupture strength
- Ruthenium compounds, Thermal properties**
Thermochemistry of the Intermetallic Compounds RuTi, RuZr, and RuHf. 1061-1066A
- Rutile, Diffusion**
Literature Survey on Diffusivities of Oxygen, Aluminum, and Vanadium in Alpha Titanium, Beta Titanium, and in Rutile. 1121-1125A
- Scale (corrosion), Heating effects**
Some Fundamental Aspects of Annealing and Pickling Stainless Steels. 1083-1100A
- Scale removal**
See Descaling
- Scattering**
Use of Ion Scattering in Characterizing the Surface Oxide of P/M Aluminum Alloy 7061. 1372-1374A
- Sea nodules, Reactions (chemical)**
Leaching of Manganese Nodule in Ammoniacal Medium Using Ferrous Sulfate as the Reductant. 331-334B
Studies on the Dry Chlorination of Deep Sea Manganese Nodules. 514-518B
- Seals (stoppers)**
See O ring seals
- Season cracking**
See Stress corrosion cracking
- Secondary displacements**
See Displacements (lattice)
- Seeding**
See Nucleation
- Segregations**
Grain Boundary Segregation in the Nickel-Base Alloy 182. Grain Boundary Segregation in Austenitic Stainless Steels and Its Effect on Intergranular Corrosion and Stress Corrosion Cracking. 137-143A
495-504A
Evaluation of the Effects of Segregation on Austenite Grain Boundary Energy in Fe—C—X Alloys. 1807-1818A
Channel Formation in Pb—Sn, Pb—Sb, and Pb—Sn—Sb Alloy Ingots and Comparison With the System NH₄Cl—H₂O. 1861-1871A
Grain Boundary Segregation of Sulfur and Antimony in Iron Alloys. 2005-2011A
Thermodynamics of Segregation in Alloys. 2091-2098A
Surface Segregation in MCrAlY Alloys. 2099-2108A
The Influence of Boron on the Grain Boundary Chemistry and Microstructure of Ni—16Cr—9Fe—0.03C. 2555-2566A
Dendritic Solidification of Alloys in Low Gravity. 2671-2676A
Directional Solidification of Lead—Copper Immiscible Alloys in a Cyclic Gravity Environment. 2677-2680A
- Segregations, Cooling effects**
Bulk Undercooling, Nucleation, and Macrosegregation of Pb—Sn Alloys. 2651-2658A
- Segregations, Field effects**
Gravitational Macrosegregation in Unidirectionally Solidified Lead—Tin Alloy. 2687-2694A
- Segregations, Heating effects**
Influence of Austenitizing Temperature on Stress Corrosion in 4330M Steel—the Role of Impurity Segregation in Stress Corrosion Cracking of High Strength Steel. 2225-2231A
- Segregations, Impurity effects**
The Nucleation of High Temperature Brittle Intergranular Fracture in 2.25Cr—1Mo Steel. 3005-3011A
- Self diffusion**
See Diffusion
- Semiconductors, Crystal growth**
A Proposal for Epitaxial Thin Film Growth in Outer Space. 2639-2643A
- Semicontinuous casting**
See Continuous casting
- Semikilling**
See Deoxidizing
- Sensitivity**
See Notch sensitivity
- Sensitizing, Heating effects**
Inhibition of Nitrogen Uptake by SiO₂ Surface Films Formed on Stainless Steel During Annealing in H/N Atmospheres. 3045-3055A
- Separation**
The Mechanism of Ferrite Formation From Iron Sulfides During Zinc Roasting. 777-785B
- Settlers (forehearth)**
See Holding furnaces
- Shaft kilns**
See Kilns
- Shape**
See Particle shape
- Shape memory**
X-Ray Study of the Premartensitic Phenomena in AuCd. 265-271A
The Effect of Aging on the Fracture Behavior of Cu—Al—Ni β Phase Alloys. 1761-1766A
- Shape memory alloys, Mechanical properties**
Some Stress—Strain—Temperature Relationships for Shape Memory Alloys. 2407-2413A
Preparation and Properties of Fine Grain β -CuAlNi Strain-Memory Alloys. 2921-2929A
- Shear properties**
See Shear strength
Shear stress
- Shear strength, Alloying effects**
Effects of Cobalt Concentration on the Relative Resistance to Octahedral and Cube Slip in Nickel-Base Superalloys. 2733-2739A
- Shear strength, Heating effects**
Mode III Fracture of 4340 Steel: Effects of Tempering Temperature and Fracture Surface Interference. 3035-3044A
- Shear strength, Microstructural effects**
An Analysis for the Effect of a Grain Size Gradient on Torsional and Tensile Properties. 329-335A
Biaxial Path Dependence of Deformation Substructure of Type 304 Stainless Steel. 1277-1293A
- Shear stress**
Orientation Dependence of $\beta_1 \rightarrow \beta'_1$ Stress-Induced Martensitic Transformation in a Cu—Al—Ni Alloy. 915-923A

- Shear stress, Microstructural effects**
Elastic Interaction Stresses. I. The Influence of Bicrystal Size on Stresses in [213] Iso-Axial 70-30 Alpha-Brass Bicrystals. 1727-1737A
- Sheet metal, Forming**
Effect of Geometrical Defects in Forming Sheet Steel by Biaxial Stretching. 2067-2074A
- Sheet metal, Mechanical properties**
Modeling of the Plastic Anisotropy of Textured Sheet. 105-120A
Effects of Work-Hardening and Rate Sensitivity on the Sheet Tensile Test. 293-300A
- Sheet steel**
See Strip steel
- Shielded arc welding**
See also Gas tungsten arc welding
Shielded metal arc welding
Environmental Cracking of Type 316 Austenitic Stainless Steel Weldments in High Temperature CO₂ Gas. 1445-1460A
A Model for the Strength of the As-Deposited Regions of Steel Weld Metals. 1597-1602A
- Shielded metal arc welding**
The Nonuniform Distribution of Inclusions in Low-Alloy Steel Weld Deposits. 669-674A
- Short range order**
Tweed Structures Associated With FCC—FCT Transformations in Fe—Pd Alloys. 803-810A
- Silica**
See Silicon dioxide
- Silicates, Solubility**
The Sulfur Partition Ratio and the Sulfide Capacity of Na₂O—SiO₂ Slags at 1400°C. 334-336B
- Silicides**
Amorphous Cr₅Si₃ Thin Films—Morphology and Kinetics of Crystallization. 1991-2003A
- Silicides, Deformation effects**
Effect of the Thermomechanical Treatments on Size and Distribution of Silicides and Tensile Properties of Alloy Ti—6Al—5Zr—0.5Mo—0.25Si. 389-391A
- Silicides, Mechanical properties**
Al₅ Compound Deformation and Secondary Slip in V₅Si. 1125-1127A
- Silicides, Phase transformations**
Low Temperature Electron Microscopy on the Cubic-Tetragonal Transformation of V₅Si. 797-801A
- Silicon, Alloying elements**
An Approach to Developing an Alternative Hot Work Die Steel. 1751-1760A
The Effect of Alloying Elements and Microstructure on the Strength and Fracture Resistance of Pearlitic Steel. 2819-2829A
- Silicon, Extraction**
An Intrinsic-Transport Model for Solid—Solid Reactions Involving a Gaseous Intermediate. 73-81B
Carbothermic Reduction of Silicon Dioxide—a Thermodynamic Investigation. 249-253B
Correction to "An Intrinsic-Transport Model for Solid—Solid Reactions Involving a Gaseous Intermediate". 519B
- Silicon, Ternary systems**
Enthalpies of Formation of the Ag—Au—Si, Ag—Au—Ge, and Ag—Au—Sn Ternary Liquid Alloys; Experimental Determinations and Application of the Hoch—Arpshofen Model. 2075-2089A
- Silicon base alloys, Thin films**
Radiation Induced Crystallization of Amorphous Si:H Alloy. 1345-1349A
- Silicon carbide, Composite materials**
Modeling of Infiltration Kinetics for Liquid Metal Processing of Composites. 95-101B
Columnar Dendritic Solidification in a Metal-Matrix Composite. 709-721A
Directional Solidification of Al—Ni/SiC Composites During Parabolic Trajectories. 1899-1904A
Correlation of Mechanical and Ultrasonic Properties of Al—SiC Metal-Matrix Composite. 2233-2246A
Behavior of Ceramic Particles at the Solid/Liquid Metal Interface in Metal Matrix Composites. 2847-2855A
Effects of SiC Whiskers and Particles on Precipitation in Aluminum Matrix Composites. 2945-2953A
A Method of Assessing the Reactivity Between SiC and Molten Aluminum. 3107-3109A
- Silicon compounds**
See also Silicon carbide
Silicon dioxide
- Silicon compounds, Microstructure**
Amorphous Cr₅Si₃ Thin Films—Morphology and Kinetics of Crystallization. 1991-2003A
- Silicon dioxide, Reduction (chemical)**
Carbothermic Reduction of Silicon Dioxide—a Thermodynamic Investigation. 249-253B
- Silicon steels**
See Electrical steels
- Silicone plastics**
See Silicone resins
- Silicone resins**
Containment of a Silicone Fluid Free Surface in Reduced Gravity. 1883-1888A
- Silicone resins, Physical properties**
Experimental Study of Thermocapillary Flows in a Thin Liquid Layer With Heat Fluxes Imposed on the Free Surface. 1895-1898A
- Silicones**
See Silicone resins
- Silicothermic reactions**
An Intrinsic-Transport Model for Solid—Solid Reactions Involving a Gaseous Intermediate. 73-81B
Correction to "An Intrinsic-Transport Model for Solid—Solid Reactions Involving a Gaseous Intermediate". 519B
- Silver, Bonding**
A Study of the Transient Liquid Phase Bonding Process Applied to a Ag/Cu/Ag Sandwich Joint. 675-686A
- Silver, Reactions (chemical)**
Speciation and Reduction Potentials of Metal Ions in Concentrated Chloride and Sulfate Solutions Relevant to Processing Base Metal Sulfides. 37-45B
- Silver, Recovering**
Mineralogical Characterization of Silver Flotation Concentrates Made From Zinc Neutral Leach Residues. 803-817B
- Silver, Ternary systems**
Phase Stability Relationships and Glass Formation in the System Cu—Ag—In. 13-21A
Experimental and Calculated Ag + Au + Ge Phase Diagram. 409-416A
Enthalpies of Formation of the Ag—Au—Si, Ag—Au—Ge, and Ag—Au—Sn Ternary Liquid Alloys; Experimental Determinations and Application of the Hoch—Arpshofen Model. 2075-2089A
- Silver base alloys, Microstructure**
Eutectic Structures of Ag—Cu After Melting and Solidification in Microgravity and on Earth. 2659-2664A
- Silver base alloys, Surface properties**
Surface Tension of Binary Metal—Surface Active Solute Systems Under Conditions Relevant to Welding Metallurgy. 483-491B
- Simulation**
See also Computer simulation
Creep Crack Growth Simulation Under Transient Stress Fields. 829-835A
Free Surface Flow and Heat Transfer in Conduction Mode Laser Welding. 851-858B
Eutectic Growth: Selection of Interlamellar Spacings. 2955-2964A
Dendritic Solidification in Binary Alloys. 3087-3096A
- Single crystals, Corrosion**
Transgranular Stress-Corrosion Cracking of Disordered Cu—25Au in Aqueous Chloride and Sulfate Media. 281-292A
- Single crystals, Crystal growth**
An Experimental Study on Process Variables in Crystal Growth by Ohno Continuous Casting. 1849-1852A
- Single crystals, Mechanical properties**
Hydrogen Effects in [001] Oriented Nickel-Base Superalloy Single Crystals. 73-82A
- Single crystals, Reduction (chemical)**
Hematite Single Crystal Reduction Into Magnetite With CO—CO₂. 311-317B
- Sintered compacts**
Gravity and Configurational Energy Induced Microstructural Changes in Liquid Phase Sintering. 1905-1913A
- Sintered compacts, Mechanical properties**
Sintering Atmosphere Effects on Tensile Properties of Heavy Alloys. 2467-2476A
Microstructural Refinement of W—Ni—Fe Heavy Alloys by Alloying Additions. 3100-3103A
- Sintered compacts, Melting**
Melting and Solidification in Microgravity of Sintered Aluminum Powder Alloys. 2695-2703A
- Sintering (powder metallurgy)**
See Liquid phase sintering
Loose powder sintering
- Slabs, Casting**
Flow Fields in Electromagnetic Stirring of Rectangular Strands With Linear Inductors. II. Computation of Flow Fields in Billets, Blooms, and Slabs of Steel. 595-602B
- Slag fuming**
Bubbling at High Flow Rates in Inviscid and Viscous Liquids (Slags). 83-94B
- Slags**
See also Blast furnace slags
Possible Roles of Upper Slag Phases on the Fluid Dynamics of Gas Stirred Ladles. 507-511B
- Slags, Electrical properties**
Correlations of Electrical Conductivity to Slag Composition and Temperature. 133-140B
- Slags, Reactions (chemical)**
Evaluation of the Activity and Molecular Form of Bismuth in Copper Smelting Slags. I. Ternary Silicate Slags. 627-641B
Thermodynamics of Ca—CaF₂ and Ca—CaCl₂ Systems for the Dephosphorization of Steel. 643-648B
- Slags, Solubility**
The Effect of Temperature on Nickel Solubility in Silica Saturated Fayalite Slags From 1523-1623K. 243-247B
The Sulfur Partition Ratio and the Sulfide Capacity of Na₂O—SiO₂ Slags at 1400°C. 334-336B

Slags

- Thermodynamics of Nitrogen in $\text{CaO-SiO}_2\text{-Al}_2\text{O}_3$ Slags and Its Reaction With Fe-C_{sat} Melts. 419-425B
- Slip**
See also Cross slip
Slip planes
- Slip, Alloying effects**
Fatigue Damage Accumulation in Nickel Modified by Ion Beam Surface Microalloying. 2775-2788A
- Slip planes**
Dislocation Structures in the Strain Localized Region in Fatigued 85/15 Brass. 1257-1262A
The Mechanism of Hydrogen Induced Cleavage in Fe-3% Si Alloy. 1335-1343A
Elastic Interaction Stresses. I. The Influence of Bicrystal Size on Stresses in [213] Iso-Axial 70-30 Alpha-Brass Bicrystals. 1727-1737A
A Finite Element Model of a Persistent Slip Band Based Upon Electron Microscopic Evidence. 2457-2465A
- Slip planes, Microstructural effects**
Slip Observations in 70-30 Alpha Brass. 1575-1581A
- Slip planes, Stress effects**
Growth of Slip Bands During Fatigue of 6061-T6 Aluminum. 83-91A
- Smelting**
See also Flash smelting
Saturation of Copper-Iron Mattes With Solid Magnetite. 935-941B
- Smelting furnaces**
Process Mineralogy of Suspended Particles From a Simulated Commercial Flash Smelter. 719-729B
- Sodium, Binary systems**
On the Slopes of Phase Boundaries. 1819-1825A
- Sodium aluminum fluoride**
See Cryolite
- Sodium compounds, Solubility**
The Sulfur Partition Ratio and the Sulfide Capacity of $\text{Na}_2\text{O-SiO}_2$ Slags at 1400°C. 334-336B
- Soft annealing**
See Annealing
- Soft solders**
See Solders
- Softening**
See Strain softening
- Solder coating**
See Alloy plating
- Solder plating**
See Alloy plating
- Solders, Mechanical properties**
Isothermal Fatigue of Low Tin Lead Based Solder. 1051-1059A
- Solders, Phases (state of matter)**
Densities of Pb-Sn Alloys During Solidification. 2349-2354A
- Solid phases**
The Competition Between the Alpha and Omega Phases in Aged Ti-Nb Alloys. 1687-1694A
- Solid solutions**
Measurement and Modeling of Alloy-Spinel-Corundum Equilibrium in the Ni-Mn-Al-O System at 1873K. 459-463B
Spinodal Decomposition of a Co-Ti-Nb Alloy. 1703-1709A
- Solidification**
See also Directional solidification
Rapid solidification
Flow Fields in Electromagnetic Stirring of Rectangular Strands With Linear Inductors. I. Theory and Experiments With Cold Models. 581-593B
Columnar Dendritic Solidification in a Metal-Matrix Composite. 709-721A
Some Observations on the Matrix Microstructure of Aluminum-Silicon Alloy-Graphite Particle Composites. 1365-1367A
Meteorites as Specimens for Microgravity Research. 1919-1923A
A Melting and Solidification Study of Alloy 625. 2319-2331A
Acoustic Levitation Technique for Containerless Processing at High Temperatures in Space. 2619-2623A
Melting and Solidification in Microgravity of Sintered Aluminum Powder Alloys. 2695-2703A
Enthalpies of a Binary Alloy During Solidification. 3057-3061A
The Partitioning of Alloying Elements in Vacuum Arc Remelted, Palladium-Modified PH 13-8 Molybdenum Alloys. 3063-3069A
Dendritic Solidification in Binary Alloys. 3087-3096A
- Solidification, Alloying effects**
Influence of Rare Earth Metals on the Nucleation and Solidification Behavior of Iron and 1045 Steel. 383-395B
Thermal Considerations on the Recalescence of Alloy Powders. 687-697A
- Solidification, Field effects**
Influence of Gravity Level and Interfacial Energies on Dispersion-Forming Tendencies in Hypermonotectic Cu-Pb-Al Alloys. 2645-2650A
Eutectic Structures of Ag-Cu After Melting and Solidification in Microgravity and on Earth. 2659-2664A
- Solidus**
Eutectic Growth: Selection of Interlamellar Spacings. 2955-2964A
- Solubility**
Thermodynamics of Nitrogen in $\text{CaO-SiO}_2\text{-Al}_2\text{O}_3$ Slags and Its Reaction With Fe-C_{sat} Melts. 419-425B
Activity of Carbon in Nickel-Rich Ni-Mo and Ni-W Alloys. 645-650A
- Hydrogen Permeation Through Coated and Uncoated Waspaloy. 1187-1192A
- Solubility, Composition effects**
Solubility and Diffusion of Hydrogen in Vanadium-Oxygen Alloys. 67-72A
On the Solubility of Aluminum Carbide in Cryolitic Melts. 441-447B
On the Solubility of Aluminum in Cryolitic Melts. 449-457B
- Solubility, High temperature effects**
Nitrogen Solubility in Solid Niobium. 613-616B
- Solubility, Temperature effects**
The Solubility of Hydrogen in Liquid Binary Al-Li Alloys. 227-232B
The Effect of Temperature on Nickel Solubility in Silica Saturated Fayalite Slags From 1523-1623K. 243-247B
- Solution entropy**
See Entropy of solution
- Solution heat treatment**
Structure and Properties of a Near- α Titanium Alloy After β Solution Treatment and Aging at 625°C. 3025-3033A
- Solvents**
Thermodynamic Consistency of the Interaction Parameter Formalism. 269-275B
- Sorption**
See Absorption (material)
Desorption
- Space environment**
Containment of a Silicone Fluid Free Surface in Reduced Gravity. 1883-1888A
Experimental Study of Thermocapillary Flows in a Thin Liquid Layer With Heat Fluxes Imposed on the Free Surface. 1895-1898A
Directional Solidification of Al-Ni/SiC Composites During Parabolic Trajectories. 1899-1904A
Ground-Based Microgravity Materials Science Research at NASA's Microgravity Materials Science Laboratory. 1915-1917A
Meteorites as Specimens for Microgravity Research. 1919-1923A
The Bubble, Drop, and Particle Unit (BDPU). 1925-1929A
Mixing Fuel Particles for Space Combustion Research Using Acoustics. 1931-1937A
Isothermal Dendritic Growth—a Proposed Microgravity Experiment. 1945-1953A
Acoustic Levitation Technique for Containerless Processing at High Temperatures in Space. 2619-2623A
Fluid Oscillation in the Drop Tower. 2625-2630A
Making Acceleration Data More Accessible and Useful to Microgravity Investigators. 2631-2637A
A Proposal for Epitaxial Thin Film Growth in Outer Space. 2639-2643A
Influence of Gravity Level and Interfacial Energies on Dispersion-Forming Tendencies in Hypermonotectic Cu-Pb-Al Alloys. 2645-2650A
Bulk Undercooling, Nucleation, and Macrosegregation of Pb-Sn Alloys. 2651-2658A
Eutectic Structures of Ag-Cu After Melting and Solidification in Microgravity and on Earth. 2659-2664A
The Influence of Interfacial Energies and Gravitational Levels on the Directionally Solidified Structures in Hypermonotectic Alloys. 2665-2669A
Dendritic Solidification of Alloys in Low Gravity. 2671-2676A
Directional Solidification of Lead-Copper Immiscible Alloys in a Cyclic Gravity Environment. 2677-2680A
Influence of Microgravity on the Morphology of the Directionally Solidified Front in an AlSi Alloy. 2681-2686A
Gravitational Macrosegregation in Unidirectionally Solidified Lead-Tin Alloy. 2687-2694A
Melting and Solidification in Microgravity of Sintered Aluminum Powder Alloys. 2695-2703A
Directional Solidification of Cu-Pb and Bi-Ga Monotectic Alloys Under Normal Gravity and During Parabolic Flight. 2839-2846A
- Space lattices**
See Crystal lattices
- Specific density**
See Density
- Specific gravity**
See Density
- Specific resistance**
See Resistivity
- Specific volume**
See Density
- Specific weight**
See Density
- Spectroscopy**
See Auger electron spectroscopy
- Speed**
See Velocity
- Spelter**
See Zinc
- Sphalerite, Reduction (chemical)**
Measurements of Dielectric Properties for Particulate Sphalerite Samples and Zinc Concentrates. 13-24B
Correlation Between Dielectric Properties and Aqueous Oxidation Rate for Pulverized Sphalerites and Zinc Concentrates. 25-36B
A Microscopic Study of the Transformation of Sphalerite Particles During the Roasting of Zinc Concentrate. 141-146B
- Spheroidal iron**
See Nodular iron
- Spinel**
Measurement and Modeling of Alloy-Spinel-Corundum Equilibrium in the Ni-Mn-Al-O System at 1873K. 459-463B

- Spinodal decomposition**
Spinodal Decomposition of a Co—Ti—Nb Alloy. 1703-1709A
- Spinodal decomposition, Heating effects**
A Theoretical Analysis of the Spinodal Decomposition in Fe—C Martensite During Aging Stage of Tempering. 2427-2432A
- Sponginess**
See Porosity
- Sputtering**
Formation of Amorphous and Metastable Extended Solid Solutions in Cu—Ti Alloys Using the Triode Sputtering Technique. 5-12A
- Stability**
See also Dimensional stability
Phase stability
Thermal stability
A Method of Assessing the Reactivity Between SiC and Molten Aluminum. 3107-3109A
- Stacking fault energy, Alloying effects**
Effects of Cobalt Concentration on the Relative Resistance to Octahedral and Cube Slip in Nickel-Base Superalloys. 2733-2739A
- Stainless steels**
See also Austenitic stainless steels
Duplex stainless steels
Ferritic stainless steels
- Stainless steels, Heat treatment**
Some Fundamental Aspects of Annealing and Pickling Stainless Steels. 1083-1100A
- Stainless steels, Reactions (chemical)**
Thermodynamics of Ca—CaF₂ and Ca—CaCl₂ Systems for the Dephosphorization of Steel. 643-648B
- Stamping**
A Wrinkling Index for Press Forming. 2831-2837A
- Static fatigue**
See Creep rupture strength
- Static tests**
See Creep tests
Hardness tests
- Statistical analysis**
Statistical Considerations on Uniform Grain Size. 2937-2944A
- Steel alloys**
See Alloy steels
- Steel constituents**
See Austenite
Bainite
Cementite
Ferrite
Martensite
Pearlite
Retained austenite
- Steel making**
See also Oxygen steel making
Possible Roles of Upper Slag Phases on the Fluid Dynamics of Gas Stirred Ladles. 507-511B
On the Flow Criteria for Suspending Solid Particles in Inductively Stirred Melts. I. Newtonian Behavior. 557-562B
Fluid Dynamics in Bubble Stirred Ladles. I. Experiments. 745-754B
Fluid Dynamics in Bubble Stirred Ladles. II. Mathematical Modeling. 755-764B
Characterization of Two-Phase Axisymmetric Plume in a Gas Stirred Liquid Bath—a Water Model Study. 885-892B
- Steels**
See also Alloy steels
Aluminum killed steels
Austenitic stainless steels
Carbon manganese steels
Carbon steels
Chromium molybdenum steels
Chromium molybdenum vanadium steels
Chromium steels
Die steels
Dual phase steels
Duplex stainless steels
Electrical steels
Ferritic stainless steels
Galvanized steels
High speed tool steels
High strength low alloy steels
High strength steels
Hot work tool steels
Killed steels
Low alloy steels
Manganese steels
Maraging steels
Molybdenum steels
Nickel chromium molybdenum steels
Nickel chromium steels
Nickel steels
Precipitation hardening steels
Stainless steels
Titanium steels
Vanadium steels
- Steels, Casting**
The Mathematical Modeling Revolution in Extractive Metallurgy. 525-540B
Flow Fields in Electromagnetic Stirring of Rectangular Strands With Linear Inductors. I. Theory and Experiments With Cold Models. 581-593B
- Flow Fields in Electromagnetic Stirring of Rectangular Strands With Linear Inductors. II. Computation of Flow Fields in Billets, Blooms, and Slabs of Steel. 595-602B
- Steels, Coating**
Scanning Auger Microprobe Study of Hot-Dipped Regular-Spangle Galvanized Steel. I. Surface Composition of As-Produced Sheet. 1603-1608A
Scanning Auger Microprobe Study of Hot-Dipped Regular-Spangle Galvanized Steel. II. Surface Composition of Chromated Sheet. 1609-1616A
- Steels, Mechanical properties**
Modeling of the Plastic Anisotropy of Textured Sheet. Effects of Work-Hardening and Rate Sensitivity on the Sheet Tensile Test. 105-120A
293-300A
- Steels, Microstructure**
Grain Shape and Its Influence on the Experimental Measurement of Grain Size. 933-940A
- Steels, Phase transformations**
The Kinetics of Ferrite Nucleation at Austenite Grain Boundaries in Fe—C Alloys. 427-440A
- Steels, Refining**
The Calcium—Phosphorus and the Simultaneous Calcium—Oxygen and Calcium—Sulfur Equilibria in Liquid Iron. 617-622B
- Steels, Structural hardening**
A New Model for Precipitation at Moving Interphase Boundaries. 2133-2138A
- Steels, Thermal properties**
Convective Heat-Transfer Measurements in Liquid Metals Under Different Fluid Flow Conditions. 859-870B
- Stick electrode arc welding**
See Shielded metal arc welding
- Stirring**
See also Electromagnetic stirring
Performance Analysis of the Aluminum Casting Furnace. Possible Roles of Upper Slag Phases on the Fluid Dynamics of Gas Stirred Ladles. 507-511B
Fluid Dynamics in Bubble Stirred Ladles. I. Experiments. 745-754B
Fluid Dynamics in Bubble Stirred Ladles. II. Mathematical Modeling. 755-764B
Experimental Investigation of Mixing Phenomena in a Gas Stirred Liquid Bath. 839-850B
Characterization of Two-Phase Axisymmetric Plume in a Gas Stirred Liquid Bath—a Water Model Study. 885-892B
- Stora Kald process**
See Oxygen steel making
- Strain**
See also True strain
- Strain, Deformation effects**
Biaxial Path Dependence of Deformation Substructure of Type 304 Stainless Steel. 1277-1293A
- Strain hardening**
The Law of Mixtures Applied to the Plastic Deformation of Two-Phase Alloys of Coarse Microstructures. 2027-2040A
- Strain hardening, Microstructural effects**
Slip Observations in 70-30 Alpha Brass. 1575-1581A
Tensile Fracture of Coarse-Grained Cast Austenitic Manganese Steels. 2269-2277A
- Strain rate**
Influence of Time and Temperature Dependent Processes on Strain Controlled Low Cycle Fatigue Behavior of Alloy 617. Test Temperature and Strain Rate Effects on the Properties of a Tungsten Heavy Alloy. 359-371A
487-494A
Determination of Parameters for Thermally Activated Glide From Stress—Strain Curves at Different Temperatures and Strain Rates. 2975-2978A
- Strain rate, Corrosion effects**
The Role of Dislocations During Transport of Hydrogen in Hydrogen Embrittlement of Iron. 2799-2803A
- Strain softening**
A Stress Relaxation Method for Following Carbonitride Precipitation in Austenite at Hot Working Temperatures. The Absence of Steady-State Flow During Large Strain Plastic Deformation of Some FCC Metals at Low and Intermediate Temperatures. 1403-1413A
3013-3024A
- Stress analysis**
Characterization of Residual Stresses in Bent Incoloy-800 Tubing by Neutron Diffraction. 2207-2214A
- Stress concentration, Deformation effects**
Characterization of Residual Stresses in Bent Incoloy-800 Tubing by Neutron Diffraction. 2207-2214A
- Stress corrosion cracking**
Cracking Kinetics of Two-Phase Stainless Steel Alloys in Hydrogen Gas. 145-152A
Transgranular Stress-Corrosion Cracking of Disordered Cu—25Au in Aqueous Chloride and Sulfate Media. 281-292A
- Stress corrosion cracking, Alloying effects**
Effects of Manganese, Phosphorus and Molybdenum on Sulfide Stress Cracking Resistance of High Strength Low Alloy Steels. 2171-2177A
- Stress corrosion cracking, Composition effects**
Discussion of "Sulfide Stress Cracking Susceptibility of Nickel Containing Steels" and Authors' Reply. 153A
- Stress corrosion cracking, Diffusion effects**
Grain Boundary Segregation in Austenitic Stainless Steels and Its Effect on Intergranular Corrosion and Stress Corrosion Cracking. 495-504A

Stress corrosion cracking

Stress corrosion cracking, impurity effects

- Clean Steels for Steam Turbine Rotors—Their Stress Corrosion Cracking Resistance. 1583-1596A
Influence of Austenitizing Temperature on Stress Corrosion in 4330M Steel—the Role of Impurity Segregation in Stress Corrosion Cracking of High Strength Steel. 2225-2231A

Stress corrosion cracking, microstructural effects

- Effect of Single Aging on Stress Corrosion Cracking Susceptibility of Inconel X-750 Under PWR Conditions. 1295-1304A

Stress corrosion cracking, welding effects

- Environmental Cracking of Type 316 Austenitic Stainless Steel Weldments in High Temperature CO₂ Gas. 1445-1460A

Stress corrosion resistance

See Corrosion resistance

Stress distribution

See Stress concentration

Stress intensity

- Application of the dc Potential Drop Technique in Investigating Crack Initiation and Propagation Under Sustained Load in Notched Rupture Tests. 863-871A

Stress relaxation

- A Stress Relaxation Method for Following Carbonitride Precipitation in Austenite at Hot Working Temperatures. Ti(C,N) Precipitation in Microalloyed Austenite During Stress Relaxation. 1403-1413A
Inelastic Deformation and Dislocation Structure of a Nickel Alloy: Effects of Deformation and Thermal Histories. 1415-1424A
2477-2486A

Stress relieving

See Grain refinement

Stress rupture strength

See Creep rupture strength

Stress strain curves

- Investigation of Panel Crack Formation in Steel Ingots. I. Mathematical Analysis and Mid-Face Panel Cracks. An Analysis for the Effect of a Grain Size Gradient on Torsional and Tensile Properties. 277-287B
The Influence of Mo₂C Morphology and Distribution on the Fatigue Crack Initiation and Propagation Behavior of Fe—C—Mo Dual-Phase Steels. 329-335A
Modeling Tensile Deformation of Dual-Phase Steel. 973-986A
The Flow Equation and Its Necking Criterion in Austenitic Cryogenic Fe—Mn—Al—X Steels. 1263-1268A
The Law of Mixtures Applied to the Plastic Deformation of Two-Phase Alloys of Coarse Microstructures. 1625-1626A
Some Stress—Strain—Temperature Relationships for Shape Memory Alloys. 2027-2040A
The Mechanical Properties of the Superplastic Al—33Cu Eutectic Alloy. 2407-2413A
2487-2496A

Stress strain curves, temperature effects

- Determination of Parameters for Thermally Activated Glide From Stress—Strain Curves at Different Temperatures and Strain Rates. 2975-2978A

Stresses

- See Residual stress
Shear stress
Stress intensity
Thermal stresses

Stretch forming

- Effect of Geometrical Defects in Forming Sheet Steel by Biaxial Stretching. 2067-2074A

Stretching

See Stretch forming

Strip

See Strip steel

Strip steel, Casting

- Processing Effects in Spray Casting of Steel Strip. 3077-3086A

Strip steel, Metal working

- A Wrinkling Index for Press Forming. 2831-2837A

Strontium, Binary systems

- On the Slopes of Phase Boundaries. 1819-1825A

Structural hardening

- See also Aging (artificial)
Precipitation hardening
Quench hardening
Strain hardening
Surface hardening
Microstructure and Fracture Toughness of the Aged β -Ti Alloy Ti—10V—2Fe—3Al. 1037-1049A

Structure (atomic)

See Atomic structure

Structures (crystalline)

- See Banded structure
Columnar structure
Crystal structure
Dendritic structure
Equiaxed structure
Grain structure
Intergranular structure
Lamellar structure
Microstructure
Unit cell
Widmanstätten structure

Submerged arc welds

See Welded joints

Suction

See Vacuum

Sulfates, Environment

- Transgranular Stress-Corrosion Cracking of Disordered Cu—25Au in Aqueous Chloride and Sulfate Media. 281-292A

Sulfates, Solubility

- Water and Solute Activities of the Solution Systems of H₂SO₄—CuSO₄—H₂O and HCl—CuCl₂—H₂O. 347-354B

Sulfation

- Dissolution Kinetics of Argentian Plumbogargite From Old Tailings of Sulfatizing Roasting Pyrites by HCl—CaCl₂ Leaching. 365-373B

Sulfidation (corrosion)

See Sulfurization

Sulfides, Reactions (chemical)

- Kinetics of Manganous Oxide Sulfidization in Carbonyl Sulfide (COS) Contaminated Atmospheres. 303-310B

Sulfides, Solubility

- Study by SEM-EDS of the In Situ Dynamic Leaching of Mercury Ores. 165-170B
The Sulfur Partition Ratio and the Sulfide Capacity of Na₂O—SiO₂ Slags at 1400°C. 334-336B

Sulfidizing (not diffusion)

- Kinetics of Manganous Oxide Sulfidization in Carbonyl Sulfide (COS) Contaminated Atmospheres. 303-310B

Sulfur

- Grain Boundary Segregation of Sulfur and Antimony in Iron Alloys. 2005-2011A

Sulfur, Alloying elements

- Surface Tension of Binary Metal—Surface Active Solute Systems Under Conditions Relevant to Welding Metallurgy. 483-491B

Sulfur, Binary systems

- The Cata- or Metatectic Reaction—Occurrence and Microstructural Development. 3097-3100A

Sulfur, Diffusion

- The Sulfur Partition Ratio and the Sulfide Capacity of Na₂O—SiO₂ Slags at 1400°C. 334-336B

Sulfur, Dopants

- Effects of Oxygen and Sulfur on Alloying Element Vaporization Rates During Laser Welding. 967-972B
Surface Segregation in MCRAIY Alloys. 2099-2108A

Sulfur, Impurities

- Influence of Austenitizing Temperature on Stress Corrosion in 4330M Steel—the Role of Impurity Segregation in Stress Corrosion Cracking of High Strength Steel. 2225-2231A
The Nucleation of High Temperature Brittle Intergranular Fracture in 2.25Cr—1Mo Steel. 3005-3011A

Sulfur, Recovering

- Direct Electrowinning of Lead From Suspension Galena Concentrate Anode in Different Electrolytes. 59-65B

Sulfur, Trace elements

- The Effects of Austenitization Temperature on the High Temperature Ductility of Fe—P—S Alloys. 887-892A

Sulfurization, Composition effects

- Discussion of "Sulfide Stress Cracking Susceptibility of Nickel Containing Steels" and Authors' Reply. 153A

Sulphur

See Sulfur

Superalloys, Casting

- Effect of Melt Spinning on the Microstructure and Mechanical Properties of Three Nickel-Base Superalloys. 93-103A

Superalloys, Cladding

- Microstructure of Laser Clad Ni—Cr—Al—Hf Alloy on a γ' Strengthened Nickel-Base Superalloy. 1981-1990A

Superalloys, Corrosion

- Fatigue Oxidation Interaction in IN 100 Superalloy. 2259-2268A

Superalloys, Directional solidification

- Study of Solidification Features of Nickel-Base Superalloys in Relation With Composition. 2333-2340A
Study of Microporosity Formation in Nickel-Base Superalloys. 2341-2348A
Dendritic Solidification of Alloys in Low Gravity. 2671-2676A

Superalloys, Heat treatment

- Effect of Single Aging on Stress Corrosion Cracking Susceptibility of Inconel X-750 Under PWR Conditions. 1295-1304A

Superalloys, Mechanical properties

- Hydrogen Effects in [001] Oriented Nickel-Base Superalloy Single Crystals. 73-82A
Crack Initiation and Near-Threshold Surface Fatigue Crack Propagation Behavior of the Iron-Base Superalloy A-286. 301-308A
Influence of Time and Temperature Dependent Processes on Strain Controlled Low Cycle Fatigue Behavior of Alloy 617. 359-371A
Creep—Fatigue Behavior of Directionally Solidified and Single Crystal Intermetallic Ni₃Al(B,Hf) at an Intermediate Temperature. 479-486A
Elevated Temperature Creep—Fatigue Crack Propagation in Nickel-Base Alloys and 1Cr—Mo—V Steel. 855-862A
Application of the dc Potential Drop Technique in Investigating Crack Initiation and Propagation Under Sustained Load in Notched Rupture Tests. 863-871A
Influence of Cyclic to Mean Load Ratio on Creep/Fatigue Crack Growth. 873-880A
Characterization of Residual Stresses in Bent Incoloy-800 Tubing by Neutron Diffraction. 2207-2214A

- Effects of Cobalt Concentration on the Relative Resistance to Octahedral and Cube Slip in Nickel-Base Superalloys. 2733-2739A
- Superalloys, Microstructure**
 Discussion of "Microdistribution of Cerium in Steel" and Author's Reply. 723A
 Assessment of Service Induced Microstructural Damage and Its Rejuvenation in Turbine Blades. 2049-2066A
 Inelastic Deformation and Dislocation Structure of a Nickel Alloy: Effects of Deformation and Thermal Histories. 2477-2486A
 The Influence of Boron on the Grain Boundary Chemistry and Microstructure of Ni-16Cr-9Fe-0.03C. 2555-2566A
 Dislocation Network Formation and Coherency Loss Around Gamma-Prime Precipitates in a Nickel-Base Superalloy. 2965-2973A
- Superalloys, Phase transformations**
 A Melting and Solidification Study of Alloy 625. 2319-2331A
- Superalloys, Phases (state of matter)**
 The Effect of Varying Aluminum, Titanium, and Niobium Content on the Phase Stability of Inconel 718. 1657-1666A
 Correction to "The Effects of Varying Aluminum, Titanium, and Niobium Content on the Phase Stability of Inconel 718". 1657-1666A
- Superalloys, Physical properties**
 Hydrogen Permeation Through Coated and Uncoated Waspaloy. 1187-1192A
 The Wetting Characteristics and Surface Tension of Some Nickel-Based Alloys on Yttria, Hafnia, Alumina, and Zirconia Substrates. 1833-1839A
- Superalloys, Structural hardening**
 Precipitation of the δ -Ni₃Nb Phase in Two Nickel Base Superalloys. 453-465A
- Superalloys, Welding**
 An Analytical Electron Microscope Investigation of the Phase Transformations in a Simulated Heat-Affected Zone in Alloy 800. 35-50A
 A Study of the Weldability and Weld Related Microstructure of Cabot Alloy 214. 657-667A
 The Kinetics of Intergranular Oxygen Penetration in Nickel and Its Relevance to Weldment Cracking. 2305-2313A
- Superconductors, Crystal growth**
 A Proposal for Epitaxial Thin Film Growth in Outer Space. 2639-2643A
- Superconductors, Electrical properties**
 Electrical Properties of High T_c EuBa₂Cu₃O_{7-x}. 738-743A
- Superconductors, Magnetic properties**
 Magnetic Properties of Rare Earth-Barium-Copper Oxides in the Normal and Superconducting States. 734-738A
- Superconductors, Powder technology**
 Densification of Oxide Superconductors by Hot Isostatic Pressing. 1841-1847A
- Supercooling**
 Dendritic Growth of Undercooled Nickel-Tin. III. Isothermal Dendritic Growth—a Proposed Microgravity Experiment. 1109-1119A
 Bulk Undercooling, Nucleation, and Macrosegregation of Pb-Sn Alloys. 1945-1953A
 Eutectic Growth: Selection of Interlamellar Spacings. 2651-2659A
 Dendritic Solidification in Binary Alloys. 2955-2964A
 3067-3096A
- Superplasticity**
 The Mechanical Properties of the Superplastic Al-33Cu Eutectic Alloy. 2487-2496A
- Superplasticity, Impurity effects**
 Superplastic Deformation Behavior in Commercial and High Purity Zn-22% Al. 2741-2752A
- Superplasticity, Microstructural effects**
 A Topological Study of Superplastic Deformation in an Al-Li Alloy With a Bimodal Grain Size Distribution. 1621-1624A
- Surface analysis (chemical)**
 Scanning Auger Microprobe Study of Hot-Dipped Regular-Spangle Galvanized Steel. I. Surface Composition of As-Produced Sheet. 1603-1608A
- Surface defects**
 A Computer Simulation on Tensile Strength of Surface-Damaged Fibers. 1499-1506A
 A Wrinkling Index for Press Forming. 2831-2837A
- Surface diffusion**
 See Diffusion
- Surface energy, Composition effects**
 Influence of Gravity Level and Interfacial Energies on Dispersion-Forming Tendencies in Hypermonotectic Cu-Pb-Al Alloys. 2645-2650A
 The Influence of Interfacial Energies and Gravitational Levels on the Directionally Solidified Structures in Hypermonotectic Alloys. 2665-2669A
- Surface finishing**
 See Descaling
- Surface hardening**
 See also Laser beam hardening
 Acoustic Emission Studies of Electron Beam Surface Modification of Aluminum. 493-503B
- Surface hardening, Alloying effects**
 Laser Transformation Hardening of Iron—Carbon and Iron—Carbon—Chromium Steels. 2013-2025A
- Surface hardening, Heating effects**
 Fatigue Strength Improvement of Age-Hardened 18Ni Maraging Steel by Stress-Laser Surface Treatment of Subsequent Aging. 2603-2606A
- Surface properties**
 See Emissivity
 Surface structure
 Surface tension
- Surface structure**
 Study by SEM-EDS of the In Situ Dynamic Leaching of Mercury Ores. 185-170B
- Surface structure, Alloying effects**
 Fatigue Damage Accumulation in Nickel Modified by Ion Beam Surface Microalloying. 2775-2788A
- Surface structure, Radiation effects**
 Laser Melting of Ti-High Speed Tool Steel. 377-382A
- Surface tension**
 The Wetting Characteristics and Surface Tension of Some Nickel-Based Alloys on Yttria, Hafnia, Alumina, and Zirconia Substrates. 1833-1839A
 Containment of a Silicone Fluid Free Surface in Reduced Gravity. 1883-1888A
- Surface tension, Composition effects**
 Surface Tension of Binary Metal—Surface Active Solute Systems Under Conditions Relevant to Welding Metallurgy. 483-491B
- Surface tension, Heating effects**
 Determination of Dihedral Angle Distributions in Polycrystals: Application to $\alpha + \beta$ Brass. 1147-1151A
- Susceptibility (magnetic)**
 See Magnetic permeability
- Suspensions**
 See Dispersions
- Synthetic resins**
 See Silicone resins
- Systems (metallurgical)**
 See Binary systems
 Quaternary systems
 Ternary systems
- Tailings, Reactions (chemical)**
 Dissolution Kinetics of Argentinian Plumbojarosite From Old Tailings of Sulfatizing Roasting Pyrites by HCl—CaCl₂ Leaching. 365-373B
- Tantalum, Alloying elements**
 Microstructural Refinement of W—Ni—Fe Heavy Alloys by Alloying Additions. 3100-3103A
- Tantalum compounds, Reactions (chemical)**
 Dissolution of Columbite and Tantalite in Acidic Fluoride Media. 355-363B
- Tapes (metallic), Mechanical properties**
 Ductile Al—Cu—V Amorphous Alloys Without Metalloid. 391-393A
- Tapes (metallic), Microstructure**
 On the Formation of Dispersoids During Rapid Solidification of an Al—Fe—Ni Alloy. 1101-1107A
- Tapes (metallic), Phase transformations**
 Beta-Eutectoid Decomposition in Rapidly Solidified Titanium—Nickel Alloys. 23-33A
- Technology transfer**
 An Emerging Role for the National Laboratories in Materials Research. 341-345B
 An Emerging Role for the National Laboratories in Materials Research. 1379-1383A
- Temper brittleness, Impurity effects**
 Clean Steels for Steam Turbine Rotors—Their Stress Corrosion Cracking Resistance. 1583-1596A
- Temperature**
 See Critical temperature
 Curie temperature
 Glass transition temperature
 High temperature
 Melting points
 Temperature distribution
- Temperature distribution**
 Initial Development of Thermal and Stress Fields in Continuously Cast Steel Billets. 2589-2602A
- Temperature distribution, Welding effects**
 Free Surface Flow and Heat Transfer in Conduction Mode Laser Welding. 851-858B
 Effects of Oxygen and Sulfur on Alloying Element Vaporization Rates During Laser Welding. 967-972B
- Temperature field**
 See Temperature distribution
- Temperature measuring instruments, Design**
 Measurement of Temperature and Emissivity of Specularly Reflecting Glowing Bodies. 1889-1894A
- Tempering**
 Analysis of Nonisothermal Transformation Kinetics; Tempering of Iron—Carbon and Iron—Nitrogen Martensites. 925-932A
 Crack Growth From Internal Hydrogen—Temperature and Microstructural Effects in 4340 Steel. 1319-1334A
 The Tempering of Iron—Carbon Martensite; Dilatometric and Calorimetric Analysis. 2415-2426A
 A Theoretical Analysis of the Spinodal Decomposition in Fe—C Martensite During Aging Stage of Tempering. 2427-2432A
 The Effect of Tempering Temperature on Near-Threshold Fatigue Crack Behavior in Quenched and Tempered 4140 Steel. 2497-2502A
 Mode III Fracture of 4340 Steel: Effects of Tempering Temperature and Fracture Surface Interference. 3035-3044A

Tenacity

Tenacity

See Tensile strength

Tensile modulus

See Modulus of elasticity

Tensile properties

See also Elongation

Tensile strength

Yield point

Yield strength

Design and Development of an Experimental Wrought Aluminum Alloy for Use at Elevated Temperatures. 1027-1035A

Correlation of Mechanical and Ultrasonic Properties of Al—SiC Metal-Matrix Composite. 2233-2246A

Tensile properties, Diffusion effects

Effect of Cathodic Charging on the Mechanical Properties of Aluminum. 2299-2304A

Tensile properties, Heating effects

The Effect of Austenitizing Temperature on the Fracture Initiation Toughness of As-Quenched HP9-4-20 Steel. 2989-3003A

Structure and Properties of a Near- α Titanium Alloy After β Solution Treatment and Aging at 625°C. 3025-3033A

Tensile properties, Microstructural effects

An Analysis for the Effect of a Grain Size Gradient on Torsional and Tensile Properties. 329-335A

The Law of Mixtures Applied to the Plastic Deformation of Two-Phase Alloys of Coarse Microstructures. 2027-2040A

The Effect of Grain Size on the Bulk Formability and Tensile Properties of Austenitic Stainless Steel Types 304 and 316. 2287-2298A

Sintering Atmosphere Effects on Tensile Properties of Heavy Alloys. 2467-2476A

Effect of Microstructure on Plane-Strain Fracture Toughness of AISI 4340 Steel. 2513-2521A

Microstructural Refinement of W—Ni—Fe Heavy Alloys by Alloying Additions. 3100-3103A

Tensile shear strength

See Shear strength

Tensile strength, Alloying effects

Aluminum—Lithium Powder Metallurgy Alloys With Improved Toughness. 603-615A

Tensile strength, Composition effects

Structure and Mechanical Properties of Unidirectionally Solidified Fe—Cr—C and Fe—Cr—X—C Alloys. 1235-1241A

Crack Growth From Internal Hydrogen—Temperature and Microstructural Effects in 4340 Steel. 1319-1334A

Tensile strength, Cooling effects

Effect of Melt Spinning on the Microstructure and Mechanical Properties of Three Nickel-Base Superalloys. 93-103A

Effects of Thermomechanical Processing on the Microstructure and Mechanical Properties of a Ti—V—N Steel. 1221-1234A

Tensile strength, Deformation effects

Effect of the Thermomechanical Treatments on Size and Distribution of Silicides and Tensile Properties of Alloy Ti—6Al—5Zr—0.5Mo—0.25Si. 389-391A

Modeling Tensile Deformation of Dual-Phase Steel. 1263-1268A

Tensile strength, Diffusion effects

Hydrogen Effects in [001] Oriented Nickel-Base Superalloy Single Crystals. 73-82A

Tensile strength, Environmental effects

Tensile and Impact Properties Changes of Hastelloy X After Exposure in High-Temperature Helium Environment. 1269-1275A

Tensile strength, Heating effects

Development of High Toughness in Austempered Type Ductile Cast Iron and Evaluation of Its Properties. 319-327A

The Effects of Heat Treatment and Cold Working on the Room-Temperature and Cryogenic Mechanical Properties of Fe—30Mn—9Al—0.9C Steel. 1873-1876A

Mode III Fracture of 4340 Steel: Effects of Tempering Temperature and Fracture Surface Interference. 3035-3044A

Tensile strength, Microstructural effects

The Strength of Ni₃Al Containing Titanium and Boron. 732-733A

A Computer Simulation on Tensile Strength of Metal Matrix Composites Reinforced With Surface-Damaged Fibers. 1491-1497A

A Computer Simulation on Tensile Strength of Surface-Damaged Fibers. 1499-1506A

Microstructure Effects on Tensile Properties of Tungsten—Nickel—Iron Composites. 1523-1532A

Tensile Deformation Behavior of Mechanically Stabilized Fe—Mn Austenite. 1563-1568A

Tensile Fracture of Coarse-Grained Cast Austenitic Manganese Steels. 2269-2277A

Preparation and Properties of Fine Grain β -CuAlNi Strain-Memory Alloys. 2921-2929A

Tensile strength, Temperature effects

The Effect of Triaxial Stress Field on Intermediate Temperature Embrittlement of Ferritic Spheroidal Graphite Cast Irons. 1213-1219A

The Flow Equation and Its Necking Criterion in Austenitic Cryogenic Fe—Mn—Al—X Steels. 1625-1626A

Tensile tests

See Tension tests

Tensile yield strength

See Yield strength

Tension

See Surface tension

Tension tests

Effects of Work-Hardening and Rate Sensitivity on the Sheet Tensile Test. 293-300A

Void Formation During Tensile Testing of Dual Phase Steels. 579-589A

The Effect of Matrix Strength on Void Nucleation and Growth in an Alpha—Beta Titanium Alloy, Corona-5. 591-601A

The Effect of Tin, Aluminum, and Nitrogen on the Hot Ductility of a Carbon—Manganese Steel Between 700-1200°C. 1305-1309A

Ternary systems

The Influence of the Ternary Interaction Parameter ϵ_{ij}^k on the Activity of Bismuth in Molten Copper. 427-432B

Ternary systems, Phases (state of matter)

Phase Stability Relationships and Glass Formation in the System Cu—Ag—In. 13-21A

Experimental and Calculated Ag + Au + Ge Phase Diagram. 409-416A

A Thermodynamic Evaluation of the Fe—Cr—C System. 627-636A

Phase Relationships in the Fe—Cr—Ni System at Solidification Temperatures. 899-908A

An Experimental Study and a Thermodynamic Evaluation of the Fe—Cr—Mo System. 1385-1394A

Solidification Structures in Rapidly Quenched Cu—Ti—Zr Alloys. 1853-1860A

An Experimental Study and a Thermodynamic Evaluation of the Cr—Fe—W System. 2531-2546A

Ternary systems, Thermal properties

Enthalpies of Formation of the Ag—Au—Si, Ag—Au—Ge, and Ag—Au—Sn Ternary Liquid Alloys; Experimental Determinations and Application of the Hoch—Arpshofen Model. 2075-2089A

Tertiary displacements

See Displacements (lattice)

Testing equipment, Design

Ground-Based Microgravity Materials Science Research at NASA's Microgravity Materials Science Laboratory. 1915-1917A

The Bubble, Drop, and Particle Unit (BDPU). 1925-1929A

Mixing Fuel Particles for Space Combustion Research Using Acoustics. 1931-1937A

Isothermal Dendritic Growth—a Proposed Microgravity Experiment. 1945-1953A

Texture

See also Rolling texture

Modeling of the Plastic Anisotropy of Textured Sheet. 105-120A

On Through Thickness Crystallographic Texture Gradient in Al—Li—Cu—Zr Alloy. 731-732A

Modeling the Texture Dependence of Environmentally Assisted Growth of Long and Short Cracks. 1009-1020A

Effect of Annealing Temperature on Yield Anisotropy of Zircaloy-4 TREX. 1243-1255A

Effect of Melt Spinning on Grain Size and Texture in Ni—Mo Alloys. 1711-1720A

Intercrystalline Structure Distribution in Polycrystalline Materials. 2611A

Texture, Alloying effects

Creep Crack Growth Behavior of Two Al—Li Alloys. 847-854A

Thallium, Alloying elements

Symmetry Aspects of Pretransformation Behavior in Metallic Alloys. 159-167A

Neutron Scattering Studies of Premartensitic Indium—Thallium Alloys. 193-198A

Premartensitic Anelasticity in Indium—Thallium Alloys. 789-792A

Thermal decomposition

See Pyrolysis

Thermal diffusion, Alloying effects

Change in Direction of Carbon Thermotransport in Nb—V System With Alloying. 1429-1435A

Thermal flux

See Heat transmission

Thermal properties

See Emissivity

Heat of activation

Heat of formation

Heat of mixing

Heat of reaction

Heat of solution

Melting points

Thermal stability

Vapor pressure

Thermal reduction

See Flash smelting

Thermal stability

The Generalized Lewis Acid-Base Titration of Palladium and Niobium. 893-917B

Modeling Tensile Deformation of Dual-Phase Steel. 1263-1268A

Thermal stresses

Initial Development of Thermal and Stress Fields in Continuously Cast Steel Billets. 2589-2602A

Thermodynamics

Carbothermic Reduction of Silicon Dioxide—a Thermodynamic Investigation. 249-253B

Thermodynamic Consistency of the Interaction Parameter Formalism. 269-275B

Thermodynamics of Nitrogen in CaO—SiO₂—Al₂O₃ Slags and Its Reaction With Fe—C_{sat} Melts. 419-425B

Determination of Standard Free Energies of Formation of Ca₃P₂ and Ca₂Sn at High Temperatures. 433-439B

Mass Spectrometric Study of the Activities of the Fe—Ge System at 1550°C. 511-513B

Thermodynamics for Arsenic and Antimony in Copper Matte Converting—Computer Simulation. 547-556B

- Evaluation of the Activity and Molecular Form of Bismuth in Copper Smelting Slags. I. Ternary Silicate Slags.**
Thermodynamics of Molten Li—Sn Alloys.
Thermodynamics of Ca—CaF₂ and Ca—CaCl₂ Systems for the Dephosphorization of Steel.
Thermodynamics of the Cr—Mn System Using an Isoopiestic Technique.
Thermodynamic Activity of Na₂O in Na₂O—CaO—SiO₂, Na₂O—MgO—SiO₂, and Na₂O—CaO—SiO₂—Al₂O₃ Melts at 1400°C.
Thermodynamics of Segregation in Alloys.
A Thermodynamic Evaluation of the C—Cr—Fe—W System.
Behavior of Ceramic Particles at the Solid/Liquid Metal Interface in Metal Matrix Composites.
A Method of Assessing the Reactivity Between SiC and Molten Aluminum.
- Thermoelastic properties**
 See also Internal friction
 Shape memory
 Some Stress—Strain—Temperature Relationships for Shape Memory Alloys.
- Thermomechanical properties**
 See Thermoelastic properties
- Thermomechanical treatment**
 Effect of the Thermomechanical Treatments on Size and Distribution of Silicides and Tensile Properties of Alloy Ti—6Al—5Zr—0.5Mo—0.25Si.
 Modeling of Thermomechanical Processing of Heat-Treatable Aluminum Alloys.
 Effects of Thermomechanical Processing on the Microstructure and Mechanical Properties of a Ti—V—N Steel.
 A Stress Relaxation Method for Following Carbonitride Precipitation in Austenite at Hot Working Temperatures.
- Thermostability**
 See Thermal stability
- Thickness measurements**
 Rutherford Backscattering Study of High Temperature Oxidation of Melt-Spun Glassy Fe—22.5Al—10Zr.
- Thin films, Casting**
 A Simple Fluid Mechanical Model for Planar Flow Casting Melt-Spinning.
- Thin films, Crystal growth**
 A Proposal for Epitaxial Thin Film Growth in Outer Space.
- Thin films, Phase transformations**
 Radiation Induced Crystallization of Amorphous Si:H Alloy.
- Thinners**
 See Solvents
- Thulium base alloys, Phase transformations**
 Nonlinear and Nonlocal Continuum Model of Transformation Precursors in Martensites.
- Tig arc welding**
 See Gas tungsten arc welding
- Tilting furnaces**
 See Converters
- Tin, Alloying elements**
 Dendritic Growth of Undercooled Nickel—Tin. III.
- Tin, Binary systems**
 Densities of Pb—Sn Alloys During Solidification.
 Enthalpies of a Binary Alloy During Solidification.
 The Cata- or Metatectic Reaction—Occurrence and Microstructural Development.
- Tin, Crystal growth**
 An Experimental Study on Process Variables in Crystal Growth by Ohno Continuous Casting.
- Tin, Ternary systems**
 Enthalpies of Formation of the Ag—Au—Si, Ag—Au—Ge, and Ag—Au—Sn Ternary Liquid Alloys: Experimental Determinations and Application of the Hoch—Arpshofen Model.
- Tin base alloys, Composite materials**
 Correlation of Mechanical Properties With Nondestructive Evaluation of Babbitt Metal/Bronze Composite Interface.
- Tin base alloys, Crystal growth**
 Bulk Undercooling, Nucleation, and Macroscopic Segregation of Pb—Sn Alloys.
 Ostwald Ripening in a System With a High Volume Fraction of Coarsening Phase.
- Tin base alloys, Directional solidification**
 Gravitational Macroscopic Segregation in Unidirectionally Solidified Lead—Tin Alloy.
- Tin base alloys, Reactions (chemical)**
 Discussion of "Physical Chemistry of Gas Liquid Solder Reactions" and Reply.
- Tin base alloys, Thermal properties**
 Thermodynamics of Molten Li—Sn Alloys.
- Tin compounds, Crystal growth**
 Determination of Standard Free Energies of Formation of Ca₃P₂ and Ca₂Sn at High Temperatures.
- Tin compounds, Mechanical properties**
 The Elastic Modulus and Flow Stress of Nb₃Sn at Elevated Temperatures.
- Tin nickel alloy plating**
 See Alloy plating
- Titanium, Alloying elements**
 Discussion of "The Role of Boron in the Grain Refinement of Aluminum With Titanium" and Authors' Reply.
 The Effect of Varying Aluminum, Titanium, and Niobium Content on the Phase Stability of Inconel 718.
 Correction to "The Effects of Varying Aluminum, Titanium, and Niobium Content on the Phase Stability of Inconel 718".
- Titanium, Binary systems**
 Formation of Amorphous and Metastable Extended Solid Solutions in Cu—Ti Alloys Using the Triode Sputtering Technique.
 Calculation of the Titanium—Aluminum Phase Diagram.
 The Stable and Metastable Ti—Nb Phase Diagrams.
- Titanium, Diffusion**
 Literature Survey on Diffusivities of Oxygen, Aluminum, and Vanadium in Alpha Titanium, Beta Titanium, and in Rutile.
- Titanium, Powder technology**
 Densification of Titanium Powder During Hot Isostatic Pressing.
- Titanium, Sorption**
 Kinetics of Hydrogen Absorption in Alpha Titanium.
- Titanium, Ternary systems**
 Solidification Structures in Rapidly Quenched Cu—Ti—Zr Alloys.
- Titanium base alloys, Crystal lattices**
 Effect of Rapid Solidification and Alloying Addition on Lattice Distortion and Atomic Ordering in L₁₀ TiAl Alloys and Their Ternary Alloys.
- Titanium base alloys, Heat treatment**
 Observations on Void Nucleation and Growth in α/β Ti—Mn Alloys.
- Titanium base alloys, Mechanical properties**
 Effect of the Thermomechanical Treatments on Size and Distribution of Silicides and Tensile Properties of Alloy Ti—6Al—5Zr—0.5Mo—0.25Si.
 Effects of Oxygen and Heat Treatment on the Mechanical Properties of Alpha and Beta Titanium Alloys.
 The Effect of Matrix Strength on Void Nucleation and Growth in an Alpha—Beta Titanium Alloy, Corona-5.
 Fatigue Crack Propagation Behavior of Titanium Alloys 6242S and 5621S at Elevated Temperature.
 Microstructure and Fracture Toughness of the Aged β -Ti Alloy Ti—10V—2Fe—3Al.
 The Effect of Matrix Strength on the Fracture Resistance of an Alpha—Beta Titanium Alloy, Corona-5.
- Titanium base alloys, Microstructure**
 The Effect of Matrix Strength on Void Nucleation and Growth in a Widmanstätten Alpha—Beta Titanium Alloy, Corona-5.
- Titanium base alloys, Phase transformations**
 Beta-Eutectoid Decomposition in Rapidly Solidified Titanium—Nickel Alloys.
 Simple Models for the Omega Phase Transformation.
 Phase Transformations and Modulated Microstructures in Ti—Al—Nb Alloys.
 Modulated Lattice Relaxation in β -Based Premartensitic Phase.
- Titanium base alloys, Phases (state of matter)**
 The Competition Between Martensite and Omega in Quenched Ti—Nb Alloys.
 The Competition Between the Alpha and Omega Phases in Aged Ti—Nb Alloys.
- Titanium base alloys, Structural hardening**
 Structure and Properties of a Near- α Titanium Alloy After β Solution Treatment and Aging at 625°C.
- Titanium base alloys, Thermal properties**
 The Generalized Lewis Acid-Base Titration of Palladium and Niobium.
- Titanium compounds**
 See also Titanium dioxide
- Titanium compounds, Thermal properties**
 Thermochemistry of the Intermetallic Compounds RuTi, RuZr, and RuHf.
 Standard Enthalpies of Formation of PtTi, PtZr, and PtHf.
- Titanium dioxide, Reactions (chemical)**
 Conditions Affecting the Formation of Chlorinated Carbon Compounds During Carbochlorination.
- Titanium ores**
 See Rutile
- Titanium steels, Structural hardening**
 A Stress Relaxation Method for Following Carbonitride Precipitation in Austenite at Hot Working Temperatures.
 Ti(CN) Precipitation in Microalloyed Austenite During Stress Relaxation.
- Titration**
 See Volumetric analysis
- Tool steels**
 See Die steels
 High speed tool steels
 Hot work tool steels
- Tools**
 See Cutting tools
- Topography, Welding effects**
 Free Surface Flow and Heat Transfer in Conduction Mode Laser Welding.

Torches

Torches

See Plasma arc torches

Torsional strength

See Shear strength

Toughness

See also Fracture toughness

Application of a New Model to the Interphase Precipitation Reaction in Vanadium Steels. 2139-2151A

Toughness, Microstructural effects

Tensile Fracture of Coarse-Grained Cast Austenitic Manganese Steels. 2269-2277A

Transferring

See Heat transfer
Mass transfer

Transformations (materials)

See Martensitic transformations
Phase transformations

Transformer steels

See Electrical steels

Transgranular fracture

The Effect of Tempering Temperature on Near-Threshold Fatigue Crack Behavior in Quenched and Tempered 4140 Steel. 2497-2502A

Transition metal alloys

See Cadmium base alloys
Chromium base alloys
Cobalt base alloys
Copper base alloys
Ferrous alloys
Gold base alloys
Hafnium base alloys
Manganese base alloys
Molybdenum base alloys
Nickel base alloys
Niobium base alloys
Platinum metal alloys
Silver base alloys
Titanium base alloys
Tungsten base alloys
Vanadium base alloys
Zinc base alloys
Zirconium base alloys

Transition metal compounds

See also Chromium compounds
Copper compounds
Hafnium compounds
Iron compounds
Iron oxides
Manganese compounds
Mercury compounds
Molybdenum compounds
Nickel compounds
Niobium compounds
Platinum compounds
Ruthenium compounds
Tantalum compounds
Titanium compounds
Titanium dioxide
Tungsten carbide
Vanadium compounds
Zinc compounds
Zirconium compounds

Transition metal compounds, Phase transformations

Quasi-One-Dimensional Model of Pretransitional Soft Mode Behavior. 811-818A

Transition metals

See also Chromium
Cobalt
Copper
Gold
Hafnium
Iron
Manganese
Mercury (metal)
Molybdenum
Nickel
Niobium
Palladium
Platinum
Silver
Tantalum
Titanium
Tungsten
Vanadium
Yttrium
Zinc
Zirconium

Transition metals, Alloying elements

Formation of Metal-Metal Type Aluminum-Based Amorphous Alloys. 1369-1371A

Transmission

See Heat transmission

Transmission electron microscopy

Tweed Structures Associated With FCC-FCT Transformations in Fe-Pd Alloys. 803-810A

Transuranium metal alloys

See Plutonium base alloys

Transuranium metal compounds

See Plutonium compounds

Transuranium metals

See Plutonium

True strain, Alloying effects

Observations on Void Nucleation and Growth in α/β Ti-Mn Alloys. 1311-1317A

TTT curves

The Effect of Varying Aluminum, Titanium, and Niobium Content on the Phase Stability of Inconel 718. 1657-1666A
Correction to "The Effects of Varying Aluminum, Titanium, and Niobium Content on the Phase Stability of Inconel 718". 1657-1666A

Tubes, Mechanical properties

Characterization of Residual Stresses in Bent Incoloy-800 Tubing by Neutron Diffraction. 2207-2214A

Tubular goods

See Tubes

Tungsten, Alloying elements

Activity of Carbon in Nickel-Rich Ni-Mo and Ni-W Alloys. 645-650A

Tungsten, Quaternary systems

A Thermodynamic Evaluation of the C-Cr-Fe-W System. 2547-2554A

Tungsten, Ternary systems

An Experimental Study and a Thermodynamic Evaluation of the Cr-Fe-W System. 2531-2546A

Tungsten arc welding

See Gas tungsten arc welding

Tungsten base alloys, Mechanical properties

Test Temperature and Strain Rate Effects on the Properties of a Tungsten Heavy Alloy. 487-494A
Microstructure Effects on Tensile Properties of Tungsten-Nickel-Iron Composites. 1523-1532A

Tungsten base alloys, Powder technology

Gravity and Configurational Energy Induced Microstructural Changes in Liquid Phase Sintering. 1905-1913A
Sintering Atmosphere Effects on Tensile Properties of Heavy Alloys. 2467-2476A
Microstructural Refinement of W-Ni-Fe Heavy Alloys by Alloying Additions. 3100-3103A

Tungsten carbide, Coatings

Coating of Graphite Fibers With Tungsten Carbide Using Solid and Liquid Copper as a Transfer Medium. 2109-2113A

Tungsten compounds

See Tungsten carbide

Turbine blades, Casting

A Melting and Solidification Study of Alloy 625. 2319-2331A
Study of Solidification Features of Nickel-Base Superalloys in Relation With Composition. 2333-2340A
Study of Microporosity Formation in Nickel-Base Superalloys. 2341-2348A

Turbine blades, Microstructure

Assessment of Service Induced Microstructural Damage and Its Rejuvenation in Turbine Blades. 2049-2066A

Turbine disks, Corrosion

Clean Steels for Steam Turbine Rotors—Their Stress Corrosion Cracking Resistance. 1583-1596A

Turbines

See Gas turbines

Turbulence

Experimental Measurement and Numerical Computation of Velocity and Turbulence Parameters in a Heated Liquid Metal System. 765-775B

Twinning

Low Temperature Electron Microscopy on the Cubic-Tetragonal Transformation of V_3Si . 797-801A
Electron Microscope Study on Martensitic Transformations in Fe-Pt Alloys: General Features of Internal Structure. 2723-2731A

Ultimate shear strength

See Shear strength

Ultimate tensile strength

See Tensile strength

Ultrasonic testing

Correlation of Mechanical Properties With Nondestructive Evaluation of Babbitt Metal/Bronze Composite Interface. 2215-2224A
Correlation of Mechanical and Ultrasonic Properties of Al-SiC Metal-Matrix Composite. 2233-2246A

Undercoatings, Materials selection

Evaluation of High-Temperature Diffusion Barriers for the Pt-Mo System. 2163-2170A

Undercooling

See Supercooling

Unit cell, Cooling effects

Effect of Melt Spinning on the Microstructure and Mechanical Properties of Three Nickel-Base Superalloys. 93-103A

Uranium, Mechanical properties

Elastic Properties of β -Uranium and the Martensitic α' -Phase in Uranium-Gallium Alloys. 909-913A

Uranium base alloys, Mechanical properties

Elastic Properties of β -Uranium and the Martensitic α' -Phase in Uranium-Gallium Alloys. 909-913A

Vacuum, Environment

Fatigue Crack Propagation Behavior of Titanium Alloys 6242S and 5621S at Elevated Temperature. 881-885A
Investigation of Microstructural Changes in a Ferritic Steel Caused by High Temperature Fatigue. 999-1007A

- Vacuum arc melting**
The Partitioning of Alloying Elements in Vacuum Arc Remelted, Palladium-Modified PH 13-8 Molybdenum Alloys. 3063-3069A
- Vacuum degassing**
Use of Ion Scattering in Characterizing the Surface Oxide of P/M Aluminum Alloy 7091. 1372-1374A
- Vacuum melting**
See Vacuum arc melting
- Vanadium, Alloying elements**
The Prediction of Precipitation Strengthening in Microalloyed Steels. 1471-1480A
An Approach to Developing an Alternative Hot Work Die Steel. 1751-1760A
- Vanadium, Diffusion**
Literature Survey on Diffusivities of Oxygen, Aluminum, and Vanadium in Alpha Titanium, Beta Titanium, and in Rutile. 1121-1125A
- Vanadium, Solubility**
Solubility and Diffusion of Hydrogen in Vanadium—Oxygen Alloys. 67-72A
- Vanadium base alloys, Diffusion**
Change in Direction of Carbon Thermotransport in Nb—V System With Alloying. 1429-1435A
- Vanadium base alloys, Thermal properties**
The Generalized Lewis Acid-Base Titration of Palladium and Niobium. 893-917B
- Vanadium compounds, Mechanical properties**
A15 Compound Deformation and Secondary Slip in V_3Si . 1125-1127A
- Vanadium compounds, Phase transformations**
Low Temperature Electron Microscopy on the Cubic-Tetragonal Transformation of V_3Si . 797-801A
- Vanadium steels**
See also Chromium molybdenum vanadium steels
- Vanadium steels, Structural hardening**
Application of a New Model to the Interphase Precipitation Reaction in Vanadium Steels. 2139-2151A
- Vapor pressure**
Chemical and Metallurgical Aspects of Environmentally Assisted Fatigue Crack Growth in 7075-T651 Aluminum Alloy. 1739-1750A
- Vaporizing, Welding effects**
Effects of Oxygen and Sulfur on Alloying Element Vaporization Rates During Laser Welding. 967-972B
- Vapors**
See Water vapor
- Velocity**
Experimental Measurement and Numerical Computation of Velocity and Turbulence Parameters in a Heated Liquid Metal System. 765-775B
- Vickers hardness**
See Diamond pyramid hardness
- Viscosity**
Fluid Oscillation in the Drop Tower. 2625-2630A
- Voids**
Void Formation During Tensile Testing of Dual Phase Steels. The Effect of Matrix Strength on Void Nucleation and Growth in an Alpha—Beta Titanium Alloy, Corona-5. 579-589A
The Effect of Matrix Strength on Void Nucleation and Growth in a Widmanstätten Alpha—Beta Titanium Alloy, Corona-5. 591-601A
Observations on Void Nucleation and Growth in α/β Ti—Mn Alloys. 1163-1171A
1311-1317A
- Volatilizing**
See Vaporizing
- Voltage**
See Electric potential
- Voltage drop**
See Electric potential
- Volumetric analysis**
The Generalized Lewis Acid-Base Titration of Palladium and Niobium. 893-917B
- Wastes**
See Tailings
- Water**
Thermal Explosions Resulting From Fuel—Coolant Interactions: Analysis of Single Bubble Hydrodynamics. 563-570B
- Water, Environment**
Corrosion Fatigue Crack Initiation in a Mode II Notch Specimen. 1067-1073A
- Water, Reactions (chemical)**
Reactivity of Al—2.5% Li Alloy With Water as Studied by the Exploding Wire Technique. 255-259B
- Water, Solubility**
Water and Solute Activities of the Solution Systems of H_2SO_4 — $CuSO_4$ — H_2O and HCl — $CuCl_2$ — H_2O . 347-354B
- Water vapor, Environment**
Chemical and Metallurgical Aspects of Environmentally Assisted Fatigue Crack Growth in 7075-T651 Aluminum Alloy. The Role of Hydrogen in Corrosion Fatigue of High Purity Al—Zn—Mg Exposed to Water Vapor. 1739-1750A
1775-1783A
- Wear**
See also Hot gas corrosion
Fluid Dynamics in Bubble Stirred Ladles. II. Mathematical Modeling. 755-764B
- Wear-Enhanced Hydrogen Evolution From Mild Steel. 1721-1726A
- Weld defects**
An Analytical Electron Microscope Investigation of the Phase Transformations in a Simulated Heat-Affected Zone in Alloy 800. 35-50A
A Study of the Weldability and Weld Related Microstructure of Cabot Alloy 214. 657-667A
- Weld metal, Mechanical properties**
A Model for the Strength of the As-Deposited Regions of Steel Weld Metals. 1597-1602A
- Weld metal, Microstructure**
The Nonuniform Distribution of Inclusions in Low-Alloy Steel Weld Deposits. 669-674A
Welding Parameters and the Grain Structure of Weld Metal—a Thermodynamic Consideration. 1075-1082A
- Weldability**
An Analytical Electron Microscope Investigation of the Phase Transformations in a Simulated Heat-Affected Zone in Alloy 800. 35-50A
On the Weldability, Composition, and Hardness of Pulsed and Continuous Nd:YAG Laser Welds in Aluminum Alloys 6061, 5456, and 5086. 319-329B
A Study of the Weldability and Weld Related Microstructure of Cabot Alloy 214. 657-667A
Design and Development of an Experimental Wrought Aluminum Alloy for Use at Elevated Temperatures. 1027-1035A
- Welded joints, Corrosion**
Environmental Cracking of Type 316 Austenitic Stainless Steel Weldments in High Temperature CO_2 Gas. 1445-1460A
- Welded joints, Mechanical properties**
On the Weldability, Composition, and Hardness of Pulsed and Continuous Nd:YAG Laser Welds in Aluminum Alloys 6061, 5456, and 5086. 319-329B
A Model for the Strength of the As-Deposited Regions of Steel Weld Metals. 1597-1602A
The Kinetics of Intergranular Oxygen Penetration in Nickel and Its Relevance to Weldment Cracking. 2305-2313A
- Welded joints, Microstructure**
A Study of the Weldability and Weld Related Microstructure of Cabot Alloy 214. 657-667A
- Welding**
See Arc welding
Diffusion welding
Gas tungsten arc welding
Laser beam welding
Projection welding
Shielded arc welding
Shielded metal arc welding
- Welding parameters**
Welding Parameters and the Grain Structure of Weld Metal—a Thermodynamic Consideration. 1075-1082A
- Welds**
See Welded joints
- Wetting**
The Wetting Characteristics and Surface Tension of Some Nickel-Based Alloys on Yttria, Hafnia, Alumina, and Zirconia Substrates. 1833-1839A
Fluid Oscillation in the Drop Tower. 2625-2630A
- Whisker composites, Nondestructive testing**
Correlation of Mechanical and Ultrasonic Properties of Al—SiC Metal-Matrix Composite. 2233-2246A
- Whisker composites, Structural hardening**
Effects of SiC Whiskers and Particles on Precipitation in Aluminum Matrix Composites. 2945-2953A
- Whiskers (metals)**
Materials for Advanced Studies and Devices. 155-164B
Materials for Advanced Studies and Devices. 749-758A
The Nucleation of Iron on Dense Wustite: a Morphological Study. 787-802B
- White iron, Phase transformations**
Competitive Growth of Stable and Metastable Fe—C—X Eutectics. I. Experiments. 1955-1963A
Competitive Growth of Stable and Metastable Fe—C—X Eutectics. II. Mechanisms. 1965-1971A
- Widmanstätten structure**
Meteorites as Specimens for Microgravity Research. 1919-1923A
The Effect of Matrix Strength on the Fracture Resistance of an Alpha—Beta Titanium Alloy, Corona-5. 2503-2512A
- Wire bar**
See Billets
- Wolfram**
See Tungsten
- Work hardening**
See Strain hardening
- Work softening**
See Strain softening
- Work strengthening**
See Strain hardening
- Workability**
See Formability
- Wustite**
Effect of Temperature on Magnetizing Reduction of Agbaja Iron Ore. 731-735B

Wustite

- The Nucleation of Iron on Dense Wustite: a Morphological Study. 787-802B
- X ray analysis**
See X ray diffraction
- X ray diffraction**
X-Ray and Neutron Diffraction Anomalies Preceding Martensitic Phase Transformation in AuCuZn_2 Alloys. 793-796A
- X ray diffractometer**
See X ray diffraction
- X ray micrographs**
See Microradiography
- Yield point, Microstructural effects**
Elastic Interaction Stresses. I. The Influence of Bicrystal Size on Stresses in [213] Iso-Axial 70-30 Alpha-Brass Bicrystals. 1727-1737A
- Yield strain**
See Strain
- Yield strength**
The Effect of Matrix Strength on Void Nucleation and Growth in an Alpha-Beta Titanium Alloy, Corona-5. 591-601A
The Effect of Matrix Strength on Void Nucleation and Growth in a Widmanstätten Alpha-Beta Titanium Alloy, Corona-5. Effects of Thermomechanical Processing on the Microstructure and Mechanical Properties of a Ti-V-N Steel. 1163-1171A
Application of a New Model to the Interphase Precipitation Reaction in Vanadium Steels. 1221-1234A
Yield Stress as Determined From Hardness Measurements for Mechanically Alloyed Aluminum Base Alloys. 2139-2151A
2363-2366A
- Yield strength, Alloying effects**
Aluminum-Lithium Powder Metallurgy Alloys With Improved Toughness. 603-615A
Effects of Cobalt Concentration on the Relative Resistance to Octahedral and Cube Slip in Nickel-Base Superalloys. 2733-2739A
- Yield strength, Composition effects**
High Temperature Strength and Ductility of Recrystallized $\text{Ni}_3\text{Al}-\text{Ni}_3\text{Mn}$ Alloys. 345-352A
Effects of Oxygen and Heat Treatment on the Mechanical Properties of Alpha and Beta Titanium Alloys. 527-542A
- Yield strength, Deformation effects**
Effect of the Thermomechanical Treatments on Size and Distribution of Silicides and Tensile Properties of Alloy Ti-6Al-5Zr-0.5Mo-0.25Si. 389-391A
- Yield strength, Diffusion effects**
Hydrogen Effects in [001] Oriented Nickel-Base Superalloy Single Crystals. 73-82A
- Yield strength, Heating effects**
Development of High Toughness in Austempered Type Ductile Cast Iron and Evaluation of Its Properties. 319-327A
The Effects of Heat Treatment and Cold Working on the Room-Temperature and Cryogenic Mechanical Properties of Fe-30Mn-9Al-0.9C Steel. 1873-1876A
Correlation Among Microstructure, Strength, and Electrical Conductivity of Cu-Ni-Be Alloy. 2279-2285A
Mode III Fracture of 4340 Steel: Effects of Tempering Temperature and Fracture Surface Interference. 3035-3044A
- Yield strength, High temperature effects**
The Elastic Modulus and Flow Stress of Nb_3Sn at Elevated Temperatures. 1127-1128A
The Effect of Tempering Temperature on Near-Threshold Fatigue Crack Behavior in Quenched and Tempered 4140 Steel. 2497-2502A
- Yield strength, Microstructural effects**
An Analysis for the Effect of a Grain Size Gradient on Torsional and Tensile Properties. 329-335A
On Through Thickness Crystallographic Texture Gradient in Al-Li-Cu-Zr Alloy. 731-732A
Crack Growth From Internal Hydrogen-Temperature and Microstructural Effects in 4340 Steel. 1319-1334A
Slip Observations in 70-30 Alpha Brass. 1575-1581A
Microstructure-Property Relationship in a 2XXX Aluminum Alloy With Magnesium Addition. 2523-2530A
Microstructural Refinement of W-Ni-Fe Heavy Alloys by Alloying Additions. 3100-3103A
- Yield stress**
See Yield strength
- Youngs modulus**
See Modulus of elasticity
- Yttrium, Diffusion**
Thermodynamics of Segregation in Alloys. 2091-2098A
- Yttrium, Dopants**
Surface Segregation in MCrAlY Alloys. 2099-2108A
- Zinc, Alloying elements**
Growth and Coarsening of G.P. Zones in Al-Zn Alloys. 1973-1980A
- Zinc, Beneficiation**
Mineralogical Characterization of Silver Flotation Concentrates Made From Zinc Neutral Leach Residues. 803-817B
- Zinc, Casting**
Influence of Mold Length and Mold Heat Transfer on Horizontal Continuous Casting of Nonferrous Alloy Rods. 201-212B
- Zinc, Coating**
Pulsed Electrodeposition of Layered Brass Structures. 1569-1573A
- Zinc, Diffusion**
Effect of High Pressure on Interdiffusion in Cu-Zn Alloys at Temperatures Near the Melting Point. 467-471A

Zinc, Extraction

- Determination of the Diffusion Coefficients of CuSO_4 , ZnSO_4 , and NiSO_4 in Aqueous Solution. 5-12B
Measurements of Dielectric Properties for Particulate Sphalerite Samples and Zinc Concentrates. 13-24B
Correlation Between Dielectric Properties and Aqueous Oxidation Rate for Pulverized Sphalerites and Zinc Concentrates. 25-36B
An Intrinsic-Transport Model for Solid-Solid Reactions Involving a Gaseous Intermediate. 73-81B
A Microscopic Study of the Transformation of Sphalerite Particles During the Roasting of Zinc Concentrate. 141-146B
The Behavior of Thiourea and Flotation Reagents in Zinc Electrowinning Circuits. 187-199B
Correction to "An Intrinsic-Transport Model for Solid-Solid Reactions Involving a Gaseous Intermediate". 519B
The Evidence for a Miscibility Gap in the Fe_3O_4 - ZnFe_2O_4 System—a Review. 919-925B

Zinc, Impurities

- The Effects of Mg^{2+} , Mn^{2+} , Zn^{2+} , and Al^{3+} on the Nickel Deposit During Electrowinning From Sulfate Bath. 823-830B

Zinc, Microstructure

- Grain Shape and Its Influence on the Experimental Measurement of Grain Size. 933-940A
Structure of a Small Angle Tilt Grain Boundary in Zinc. 2359-2363A
Statistical Considerations on Uniform Grain Size. 2937-2944A

Zinc, Reactions (chemical)

- Speciation and Reduction Potentials of Metal Ions in Concentrated Chloride and Sulfate Solutions Relevant to Processing Base Metal Sulfides. 37-45B

Zinc, Recovering

- The Mechanism of Ferrite Formation From Iron Sulfides During Zinc Roasting. 777-785B

Zinc base alloys, Mechanical properties

- Porosity and Tensile Ductility in Al-Zn Alloys. 517-526A
Superplastic Deformation Behavior in Commercial and High Purity Zn-22% Al. 2741-2752A

Zinc base alloys, Phase transformations

- X-Ray and Neutron Diffraction Anomalies Preceding Martensitic Phase Transformation in AuCuZn_2 Alloys. 793-796A

Zinc base alloys, Reactions (chemical)

- The Reaction Between Solid Iron and Liquid Al-Zn Baths. 1193-1203A

Zinc compounds

- The Mechanism of Ferrite Formation From Iron Sulfides During Zinc Roasting. 777-785B

Zinc ores

- See Sphalerite

Zinc plating

- See Hot dip galvanizing

Zirconium, Ternary systems

- Solidification Structures in Rapidly Quenched Cu-Ti-Zr Alloys. 1853-1860A

Zirconium base alloys, Corrosion

- The Influence of Hydride Size and Matrix Strength on Fracture Initiation at Hydrides in Zirconium Alloys. 1507-1522A
Determination of Fracture Initiation in Hydride Blisters Using Acoustic Emission. 2247-2257A

Zirconium base alloys, Heat treatment

- The Precipitation Behavior of a Zr-2.5 wt.% Nb Alloy. 1153-1162A
Effect of Annealing Temperature on Yield Anisotropy of Zircaloy-4 TREX. 1243-1255A

Zirconium base alloys, Mechanical properties

- Modeling the Texture Dependence of Environmentally Assisted Growth of Long and Short Cracks. 1009-1020A

Zirconium base alloys, Phase transformations

- Simple Models for the Omega Phase Transformation. 169-175A

Zirconium base alloys, Powder technology

- Mechanical Alloying of Brittle Materials. 2867-2874A

Zirconium base alloys, Thermal properties

- The Generalized Lewis Acid-Base Titration of Palladium and Niobium. 893-917B

Zirconium compounds, Reactions (chemical)

- Conditions Affecting the Formation of Chlorinated Carbon Compounds During Carbochlorination. 477-482B

Zirconium compounds, Thermal properties

- Thermochemistry of the Intermetallic Compounds RuTi , RuZr , and RuHf . 1061-1066A
Standard Enthalpies of Formation of PtTi , PtZr , and PtHf . 1827-1831A

